

**Non-lysosomal accumulation of
glucosylceramide alters cytoskeletal dynamics
causing globozoospermia**

Dissertation

**Zur
Erlangung des Doktorgrades (Dr. rer. nat.)
der
Mathematisch-Naturwissenschaftlichen Fakultät
der
Rheinischen Friedrich-Wilhelms-Universität Bonn**

vorgelegt von

Diana Nancy Raju

aus
Karaikudi

Bonn 2014

Angefertigt mit Genehmigung der Mathematisch-Naturwissenschaftlichen Fakultät der

Rheinischen Friedrich-Wilhelms-Universität Bonn

1. Gutachter: Prof. Dr. U. B. Kaupp

2. Gutachter: Prof. Dr. C. Thiele

Tag der Promotion: 22nd September 2014

Erscheinungsjahr: 2015

Glycosphingolipide sind wichtige Bestandteile der Zellmembran. Glucosylceramid (GlcCer) ist das einfachste Glycosphingolipid und dient als Baustein für die Synthese von komplexen Glycosphingolipiden. Defekte in der lysosomalen beta-Glucosidase 1 (GBA1), welche GlcCer zu Glucose und Ceramid spaltet, führt zu einer Anreicherung von GlcCer in den Lysosomen, wodurch das Gaucher-Syndrom, eine schwere Lipid-Speicherkrankheit, entsteht. Knockout-Mäuse, in denen das Gen für die non-lysosomale beta-Glucosidase 2 (GBA2) ausgeschaltet wurde, häufen GlcCer außerhalb der Lysosomen an. Dadurch entsteht eine schwere männliche Fertilitätsstörung, die als Globozoospermie bezeichnet wird. Die molekularen Mechanismen der Entstehung dieser Fertilitätsstörung sind jedoch unbekannt. In meiner Doktorarbeit habe ich zum einen untersucht, wo GBA2 in der Zelle lokalisiert ist und zum anderen, warum das Fehlen von GBA2 und damit die Anreicherung von GlcCer in GBA2 Knockout-Mäusen zu Globozoospermie führt. Meine Ergebnisse zeigen erstens, dass GBA2 an der zytosolischen Seite der Membranen des Golgi-Apparats und des Endoplasmatischen Retikulums (ER) assoziiert ist. Zweitens konnte ich zeigen, dass die Anreicherung von non-lysosomalen GlcCer mit der Funktion des Mikrotubuli-, als auch des Aktin-Zytoskeletts interferiert: die Lebensdauer der Mikrotubuli sowie die Rate der Aktin-Polymerisation sind in GBA2 Knockout-Mäuse erhöht. Das betrifft v.a. die Zytoskelett-Strukturen im Hoden, die für die Ausbildung des Spermienkopfs verantwortlich sind: Mikrotubuli in der Spermien-Manschette sind deutlich länger als in Wildtyp-Mäusen und die Organisation des filamentösen F-Aktins in der apikalen *ectoplasmic specialisation* (ES) ist gestört. Zusätzlich wird die Akrosombildung aufgrund eines Defekts in Vesikelfusionierung beeinträchtigt. In meiner Arbeit konnte ich zeigen, dass die Anreicherung von GlcCer außerhalb der Lysosomen die Lipidorganisation in der Plasmamembran erhöht, wodurch die Funktion von Proteinen in der Membran gestört wird. Dazu gehören vermutlich auch Proteine, die die Dynamik des Zytoskeletts regulieren. Meine Arbeit gibt zum einen Einblick darin, wie GlcCer Signalwege steuert. Zum anderen bieten die Ergebnisse meiner Doktorarbeit auch erste Erklärungsansätze dafür, wie eine Anreicherung von GlcCer die Spermienentwicklung beeinträchtigen und zu männlicher Unfruchtbarkeit führen kann.

Glycosphingolipids are important constituents of cellular membranes. Glucosylceramide (GlcCer) is the simplest glycosphingolipid and serves as a building block for the synthesis of higher-order glycosphingolipids. Defects in the lysosomal beta-glucosidase 1 (GBA1), which cleaves GlcCer to glucose and ceramide, causes accumulation of GlcCer in lysosomes and, thereby, the severe lipid-storage disorder *Gaucher disease*. Knockout-mice lacking the non-lysosomal beta-glucosidase 2 (GBA2) accumulate GlcCer outside the lysosomes, resulting in globozoospermia – a severe male fertility defect. The molecular mechanisms underlying this fertility defect are unknown. In my PhD thesis, I (1) investigated the subcellular localization of GBA2 and (2) analyzed how the lack of GBA2 causes globozoospermia in mice. First, I could demonstrate that GBA2 is attached to the cytosolic side of the endoplasmic reticulum (ER) and Golgi membranes. Second, my results revealed that accumulation of non-lysosomal GlcCer disrupts cytoskeletal dynamics, affecting both the microtubule and actin cytoskeleton: microtubule persistence and the rate of actin polymerization are increased in GBA2 knockout-mice. In particular, cytoskeletal structures in the testis that shape the sperm head are disturbed: the microtubule manchette in sperm of GBA2 knockout-mice persist longer and the F-actin organization in the apical ectoplasmic specialization (ES) is disrupted. In addition, acrosome formation is impaired due to a defect in vesicle fusion. My results indicate that accumulation of GlcCer outside the lysosomes increases lipid stacking in the plasma membrane, thereby, interfering with protein function, particularly with the function of proteins that control cytoskeletal dynamics. My work provides an insight into how GlcCer accumulation affects cellular signaling and, therefore, how the lack of GBA2 leads to a defect in male infertility.

1. Introduction	1
1.1. <i>Glycosphingolipids</i>	1
1.2. <i>GlcCer synthesis and function</i>	1
1.3. <i>GlcCer degradation</i>	2
1.4. <i>Beta-glucosidase 1 (GBA1)</i>	3
1.5. <i>Beta-glucosidase 2 (GBA2)</i>	3
1.6. <i>Spermatogenesis</i>	4
1.7. <i>Globozoospermia</i>	7
1.8. <i>The Cytoskeleton: machinery for sperm-head shaping</i>	9
1.9. <i>Aim of the thesis</i>	12
2. Materials	13
2.1. <i>Antibodies</i>	13
2.1.1. <i>Primary antibodies</i>	13
2.1.2. <i>Secondary antibodies</i>	13
2.1.3. <i>Dyes</i>	14
2.2. <i>Bacterial strains and Cell lines</i>	14
2.3. <i>Plasmids</i>	14
3. Methods	14
3.1. <i>Cell culture</i>	14
3.1.1. <i>Isolation of sperm and male germ cells</i>	14
3.1.2. <i>Isolation of P7 Sertoli cells</i>	15

Table of contents

3.1.3. Isolation of dermal fibroblasts	16
3.1.4. Immunocytochemistry (ICC).....	16
3.1.5. Immunohistochemistry (IHC).....	17
3.1.6. Unroofing of HEK293 cells	17
3.1.7. Fluorescence protease protection (FPP) assay	17
3.1.8. Transfection of mouse fibroblasts	17
3.1.9. Live-cell imaging	18
3.1.10. Analysis of microtubule dynamics	18
3.1.11. Measurement of microtubule manchette	18
3.1.12. Analysis of actin structures	18
3.1.13. Proliferation assay	19
3.1.14. Wound-healing assay.....	19
3.1.15. Isolation of giant plasma-membrane vesicles (GPMVs).....	19
3.1.16. Fluorescence spectroscopy	20
3.2. mRNA expression analysis	20
3.2.1. Quantitative real-time PCR	20
3.3. Biochemistry	22
3.3.1. Protein preparation.....	22
3.3.2. SDS-PAGE and Western-blot analysis	22
3.3.3. G-/F-Actin assay	23
3.3.4. Fluorescence-based GBA activity assays.....	23
3.4. Lipid analysis	23
3.4.1. Lipid analysis using thin-layer chromatography (TLC)	23
3.4.2. Extraction and quantification of sphingolipids using mass spectrometry.....	24

3.5. Identification of mGBA2 by mass spectrometry	25
4. Results	26
4.1. GBA2-specific antibodies.....	26
4.2. Subcellular localization of GBA2	29
4.3. GBA2 is expressed in Sertoli cells	34
4.4. GBA2 expression during sperm development.....	37
4.5. Lack of GBA2 leads to accumulation of GlcCer in testis and sperm	39
4.6. Loss of GBA2 causes cytoskeletal defects in testis	42
4.7. Cytoskeletal defects develop in the first spermatogenic wave	44
4.8. GBA2 knockout-spermatids contain longer microtubule manchettes	46
4.9. A defect in acrosome formation during the first spermatogenic wave results in globozoospermia in GBA2 knockout-mice	48
4.10. Dermal fibroblasts as a model system	50
4.11. GlcCer accumulation in the absence of GBA2 affects actin dynamics.....	52
4.12. GlcCer accumulation in the absence of GBA2 affects microtubule dynamics	55
4.13. GlcCer accumulation augments lipid stacking in the plasma membrane	57
4.14. GlcCer accumulation in the absence of GBA2 alters cellular behavior	59
4.15. NB-DNJ-mediated inhibition of GBA2 activity induces a similar cellular phenotype as observed in GBA2 knockout-fibroblasts.....	61
5. Discussion	64
5.1. Implications of the subcellular localization of GBA2 and GlcCer.....	64

Table of contents

5.2. <i>How does GlcCer accumulation in GBA2 knockout-mice lead to globozoospermia?</i>	66
5.3. <i>Novel role for GlcCer</i>	73
6. References	75
7. Appendix	89

1. Introduction

1.1. Glycosphingolipids

Glycosphingolipids are a class of lipids that can be found in all membranes from bacteria to men [1]. Glycosphingolipids control fundamental cellular processes such as growth, differentiation, cell-cell and cell-matrix interactions, migration, and morphogenesis [2]. They consist of a ceramide backbone and one or more carbohydrate head-groups. The ceramide consisting of a sphingosine and a fatty acid inserted into the membrane, while the sugar groups face the extracellular space [3]. Glucosylceramide (GlcCer) is the simplest glycosphingolipid and serves as a precursor for the synthesis of complex glycosphingolipids [4].

1.2. GlcCer synthesis and function

Ceramide is synthesized in the endoplasmic reticulum (ER) and transported to the *trans*-Golgi by the ceramide transport protein (CERT) [5]. At the cytosolic side of *trans*-Golgi, GlcCer synthase converts ceramide to GlcCer [6]. GlcCer is transported into the Golgi lumen, where it is converted to lactosylceramide (LacCer) by the LacCer synthase (Figure 1) [7]. GlcCer can also be transported from the Golgi to the ER by the glycolipid transfer protein (GLTP) and/or the phosphoinositol 4-phosphate adaptor protein-2 (FAPP2) [8] [9]. LacCer is further converted to complex glycosphingolipids in the inner leaflet of the Golgi membrane [1]. GlcCer that is not converted to LacCer, functions as an intracellular messenger and controls different cellular functions. It has been shown to maintain the skin barrier, control the differentiation of keratinocytes [10] [11] [12], and induce axonal growth in hippocampal neurons [13] either by controlling the activity of the basic fibroblast

growth factor and laminin [14] or by regulating protein transport to the axonal membrane [15]. GlcCer has also been proposed to induce cell growth either by accelerating DNA synthesis via stimulating thymidine kinase-activity or by augmenting the activity of protein kinase C [16] [17]. Last but not least, GlcCer has been shown to control vesicular transport of lipids to the cell surface in highly polarized cells and cells with tight junctions [18] and to regulate lipid sorting at the *trans*-Golgi [19].

1.3. GlcCer degradation

GlcCer is degraded to glucose and ceramide by beta-glucosidases [20]. Beta-glucosidases are glycosyl hydrolases that cleave the beta-1,4 glycosidic linkage between the terminal non-reducing residue (the glucose moiety) and the ceramide backbone [21]. Until now, three beta-glucosidases have been identified that degrade GlcCer: glucocerebrosidase 1 (GBA1), the non-lysosomal beta-glucosidase GBA2, and the cytosolic GBA3 (Figure 1) [22] [23] [24].

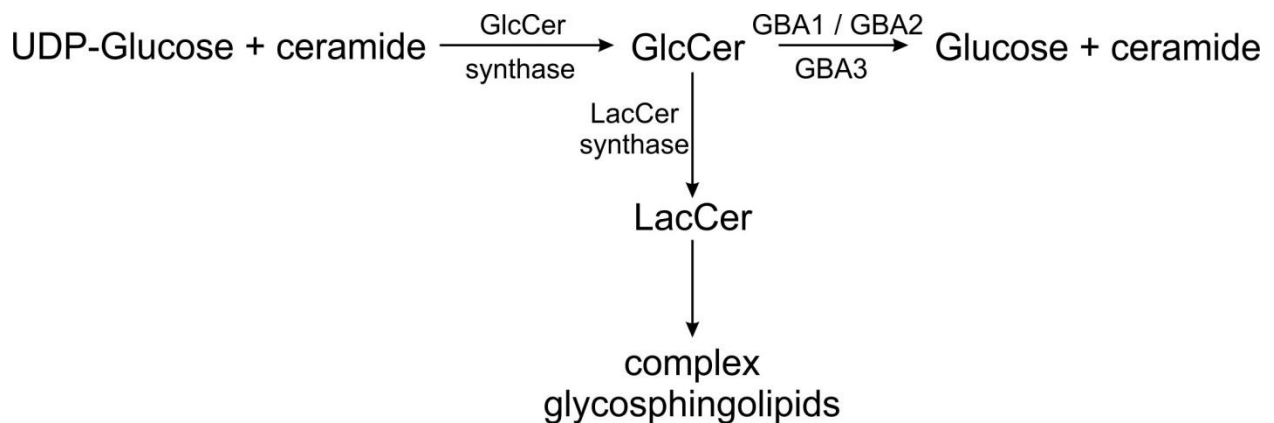


Figure 1. Synthesis and degradation of GlcCer. Ceramide is glycosylated by the GlcCer synthase to form GlcCer. GlcCer is converted to lactosylceramide (LacCer) by the LacCer synthase. LacCer is used as a building block to form higher order glycosphingolipids. GlcCer

is proteolytically cleaved to glucose and ceramide by the three beta-glucosidases: GBA1, GBA2, and GBA3.

1.4. Beta-glucosidase 1 (GBA1)

GBA1 is localized in the lysosomes and shows a maximum in enzymatic activity around pH 4.0, which can be completely blocked by conduritol B epoxide (CBE) [25] [26].

Macromolecules such as complex lipids are constitutively degraded in the endosomes and lysosomes. Defects in this pathway result in debilitating lysosomal storage disorders [27]. Deficiencies in GBA1 result in Gaucher disease, the most prominent lysosomal storage disorder [28]. Gaucher disease is characterized by accumulation of GlcCer in tissue macrophages. Patients suffer from liver and spleen enlargement and, in the most severe cases, impairment of the central nervous system. Gaucher disease is clinically heterogenous. However, there is no clear genotype-phenotype correlation that allows to predict the severity of Gaucher disease-pathology [29].

1.5. Beta-glucosidase 2 (GBA2)

GBA2 is a non-lysosomal beta-glucosidase that shares no sequence homology with GBA1 [30]. GBA2 shows a maximum in enzymatic activity around pH 6.0, which can be blocked by *N*-butyldeoxynojirimycin (NB-DNJ) [31] [26]. GBA2 has been proposed to be a transmembrane protein in the plasma membrane and the ER, with the N terminus and the catalytic domain being located on the extracellular side or in the lumen of the ER [32]. However, we have recently demonstrated that GBA2 is not a transmembrane protein but rather membrane-associated at the ER and Golgi

with both the N and the C termini facing the cytoplasm [26]. This implies that the site for GBA2-mediated degradation of non-lysosomal GlcCer is cytosolic.

GBA2 is ubiquitously expressed with highest expression levels in the testis and brain followed by liver, heart, spleen, and skin [30]. To study GBA2 function *in vivo*, a GBA2 knockout-mouse model was generated using a gene targeting approach that deleted exons 5–10 [30]. In the absence of GBA2, GlcCer accumulated predominantly in tissues with high GBA2 expression levels, e.g. testis and brain. While female GBA2 knockout-mice appeared to be phenotypically normal, male GBA2 knockout-mice were sub-fertile due to a defect during spermatogenesis called globozoospermia [30]. A detailed description of this defect is the subject of chapter 1.7.

Recently, it has been shown that GBA2 knockout-mice also display a liver phenotype: liver regeneration after partial hepatectomy was impaired and has been attributed to a defect in cytokine and growth factor-mediated signaling pathways [33]. Mutations in the *GBA2* gene in humans have been associated with autosomal recessive cerebellar ataxia (ARCA) and hereditary spastic paraplegia (HSP) due to cerebellar atrophy, which are both characterized by lack of limb coordination [34] [35].

Taken together, GBA2 seems to control different physiological functions. However, the underlying molecular mechanisms are ill defined.

1.6. Spermatogenesis

The primary phenotype of GBA2 knockout-mice is male sub-fertility [30]. Thus, it is important to investigate the role of GBA2 in spermatogenesis. The testis consists of seminiferous tubules, where spermatogenesis occurs in waves (Figure 2a). In the

mouse, each wave lasts for about 35 days and is characterized by a sequence of developmental stages (I to XIV) [36]. The blood-testis barrier (BTB) divides the seminiferous tubule into a basal and an adluminal part (Figure 2d). The BTB, also called basal ectoplasmic specialization, is a specialized junction formed by Sertoli cells close to the basal membrane. They are characterized by actin filaments arranged perpendicular to the plasma membrane, which are sandwiched by the ER cisternae on one side and the plasma membrane of the Sertoli cells on the other side [37]. The BTB restricts the flow of molecules from the basal into to the adluminal compartments, thereby, creating a microenvironment that is conducive for the development of germ cells [38]. Furthermore, the BTB also acts as an immunological barrier by preventing entry of antibodies generated against proteins expressed on developing germ cells [39]. The BTB confers cell polarity in the seminiferous epithelium via the recruitment of polarity-complex proteins to the BTB, which is crucial for spermatogenesis [40]. At birth, spermatogenesis starts at the basal lamina of the seminiferous epithelium with diploid spermatogonia. Spermatogonia undergo mitotic divisions to form primary spermatocytes, which cross the BTB in the preleptotene phase of meiosis I. Upon reaching the adluminal compartment, primary spermatocytes complete meiosis I and II to form secondary spermatocytes, which differentiate into round spermatids at puberty. During spermiogenesis, the round haploid spermatids undergo dramatic morphological rearrangements to form elongated sperm (Figure 2d) [41]. The sperm head is connected to the Sertoli cell via another testis-specific junction, the apical ectoplasmic specialization (ES) [42]. The function of the ES in sperm development is described in chapter 1.8.

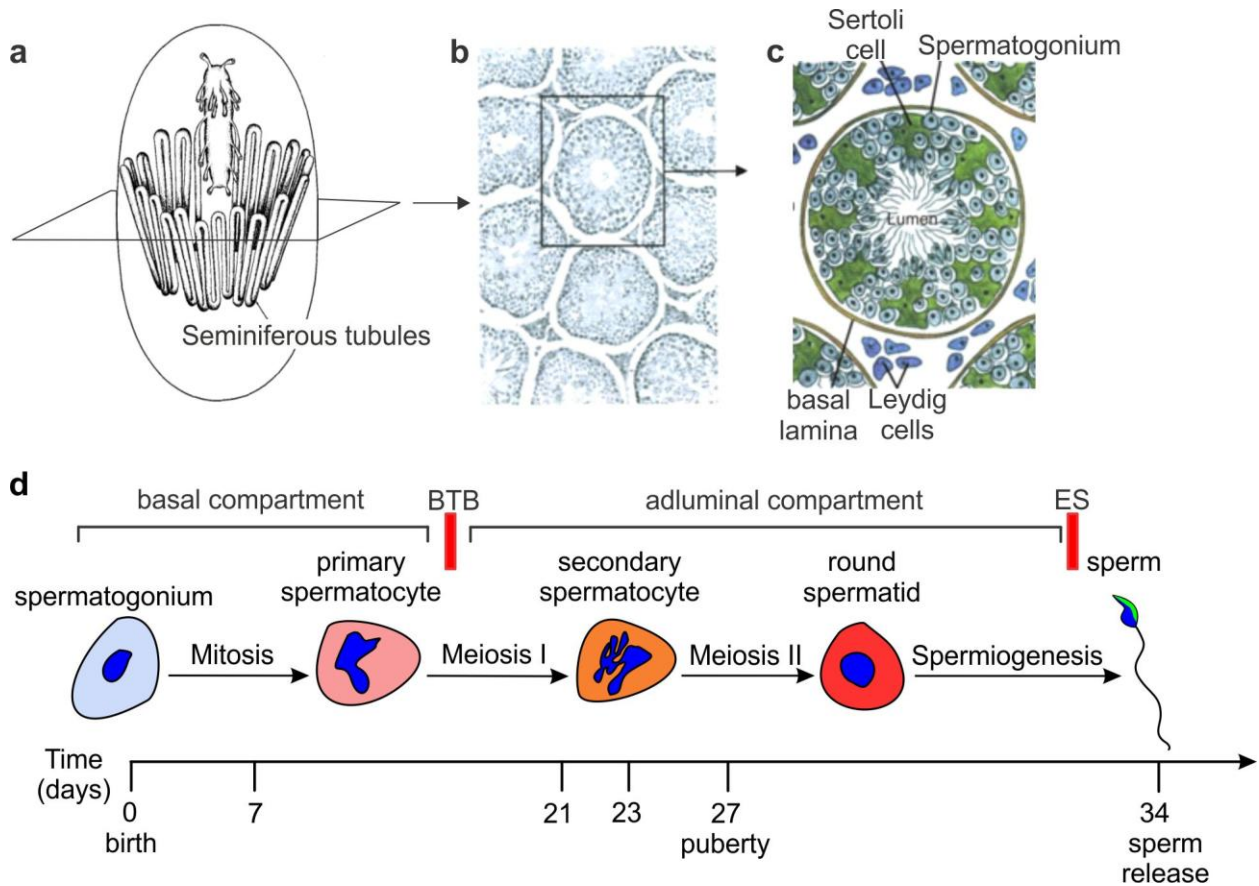


Figure 2. Spermatogenesis in the mouse. (a) Schematic representation of mouse testis with longitudinally arranged seminiferous tubules. (b) Light microscopic view of a cross section through the testis. (c) Schematic diagram of a cross section through a single tubule, showing Sertoli cells (green), different stages of developing spermatogonia (light blue), the basal lamina (brown), and Leydig cells (dark blue) [43]. (d) Schematic representation of the first wave of spermatogenesis. It starts at birth (P0) and ends with the release of mature sperm (P34). At P5, diploid spermatogonia (light blue) undergo mitotic divisions to form primary spermatocytes (pink) followed by meiosis I to form secondary spermatocytes (orange). At puberty (P27 – P29), secondary spermatocytes undergo meiosis II to form round haploid spermatids (red). During spermiogenesis, round spermatids dramatically change their morphology to form elongated sperm. The position of the blood-testis barrier (BTB) and the apical ectoplasmic specialization (ES) is shown in red.

1.7. Globozoospermia

Globozoospermia results from a defect during sperm development and is characterized by round-headed sperm with a severely deformed acrosome [44]. As mentioned above, *GBA2* knockout-males are sub-fertile due to globozoospermia: the heads of wild-type sperm are sickle-shaped with a well-formed acrosome, whereas heads of *GBA2* knockout-sperm are round, contain no or a malformed acrosome, and the mitochondria in the sperm flagellum are displaced (Figure 3) [30]. Recently, men with mutations in the *GBA2* gene have been diagnosed with bilateral testicular hypotrophy and their sperm displayed severe head and acrosome deformation [35]. However, the molecular mechanisms underlying the defects in sperm development in the absence of *GBA2* are not known.

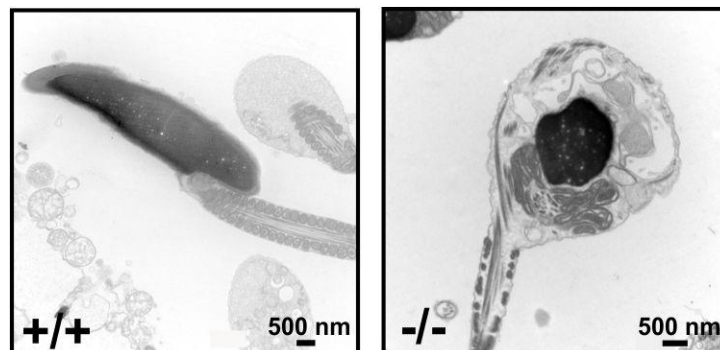


Figure 3. Wild-type and *GBA2* knockout-sperm head morphology. Left: electron micrograph of sperm from a wild-type (+/+) mouse with a normal, sickle-shaped head. Right: electron micrograph of a *GBA2* knockout-sperm (-/-) with a round-shaped head. The electron-dense region represents the sperm nucleus. Scale bars: 500 nm [30].

The prominent feature of globozoospermia is a defect in acrosome formation [45]. The acrosome is derived from the Golgi [46]. Vesicles emanate from the *trans*-Golgi and fuse with the nuclear membrane to form the acrosome at the anterior end of the sperm head [47]. A number of proteins have been identified that regulate

acrosome formation. They mainly control vesicle trafficking and fusion or anchoring of the acrosome to the nuclear membrane [46] [47] [48] [49] [50] [51]. Knockout mice for the underlying genes all display globozoospermia.

The DPY19L2 protein is a transmembrane protein in the nuclear envelope. In DPY19L2 knockout-mice, the acrosome detaches from the nuclear membrane, whereby, shaping of the sperm head is abolished and acrosomal vesicles are eliminated [52].

Hrb (HIV-1 Rev binding protein) is associated with the outer membrane of the proacrosomal vesicles emanating from the Golgi. In Hrb knockout-mice, vesicle fusion leading to acrosome formation is abolished, indicating that Hrb is important for vesicle docking and/or fusion [46].

GOPC (Golgi-associated PDZ and coiled coil motif containing protein) is localized at the *trans*-Golgi of developing sperm. GOPC knockout-sperm display a defect in proacrosomal vesicle fusion, nuclear shaping, and in the alignment of mitochondria along the flagellum [48]. A similar phenotype is observed in PICK1 (protein interacting with C-kinase) knockout-mice [49]. PICK1 has been proposed to interact with GOPC and together, they seem to coordinate the formation of proacrosomal vesicles from the *trans*-Golgi [49].

Vps54 is a vesicular protein that controls vesicular sorting [53]. Together with GARP (Golgi associated retrograde protein), it is involved in vesicle transport from the endosomes to the *trans*-Golgi [54]. Mutations in the Vps54 gene render proacrosomal vesicles incapable of fusing to form the acrosome [50].

ZBP1 (zona pellucida binding protein 1) is a protein associated with the inner acrosomal membrane that binds to the zona pellucida, the egg coat, during fertilization [55]. Mice lacking ZBP1 fail to form a compact acrosomal structure,

resulting in a dilated acrosome overlying the sperm head. The dilated acrosome is fragmented and ingested by the Sertoli cells [51]. Thus, sperm heads are round, lack an acrosome, and are therefore, incapable of fertilizing an oocyte.

1.8. The Cytoskeleton: machinery for sperm-head shaping

Globozoospermia not only involves a defect in acrosome formation. In many cases, the shaping of the sperm head is also affected, indicating that the two processes are linked. During spermatid elongation, the sperm head is shaped at the posterior end by a manchette of microtubules and at the anterior end by the apical ES (Figure 4) [56] [57]. The microtubule manchette consists of a perinuclear ring that is supported by numerous vertically arranged microtubules. The constrictive downward movement of the manchette shapes the postacrosomal region of the sperm head [58] [59]. The other cytoskeletal structure that shapes the sperm head is the apical ES, a testis-specific adherence junction between the developing spermatid head and the Sertoli cell (Figure 4). Similar to the BTB, this ES consists of F-actin supported by the endoplasmic reticulum and plasma membrane of the Sertoli cells [37]. F-actin at the ES forms bundles or hoops around the sperm head. Since F-actin in the ES is devoid of myosin, the ES cannot generate contractile forces [60]. However, the polymerization and depolymerization of F-actin, initiated by actin severing proteins like gelsolin [61] and proteins that facilitate polymerization like profilin-3 [62], causes tread milling of the F-actin containing hoops. Thereby, constriction forces are generated that shape the acrosomal region of the sperm head [57]. These forces are transduced to the spermatid head via the acrosplaxome, an F-actin/keratin 5 containing cytoskeletal plate that anchors the acrosome to the spermatid head [57]. Together, the microtubule manchette and the apical ES act as endogenous constrictors that steer spermatid elongation and shape the sperm head (Figure 4).

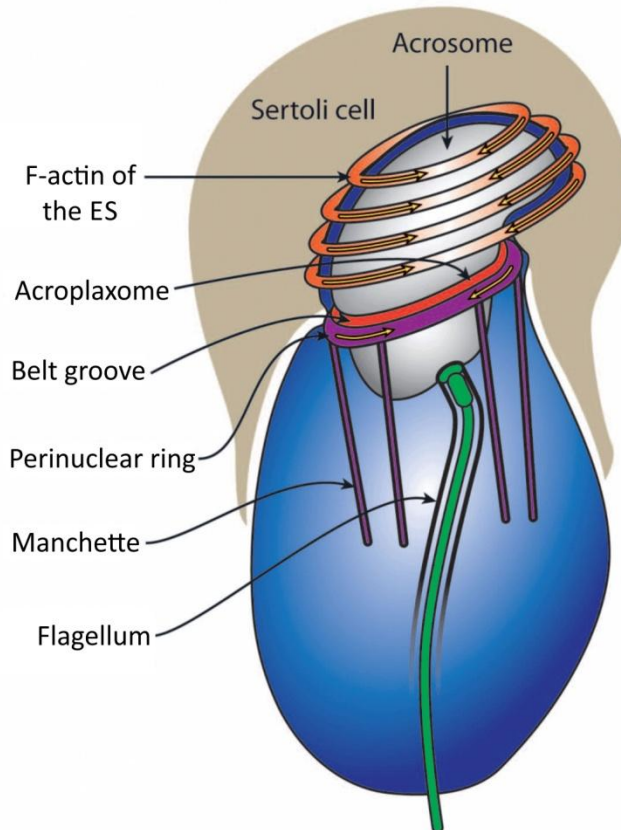


Figure 4. Schematic representation of the structural components that shape the sperm head. The elongated spermatid (*blue*) is attached to the Sertoli cell (*brown*) via the apical ectoplasmic specialization (ES). The F-actin hoops (*orange*) that form the ES act as a scaffold and contribute to the shaping of the acrosomal region of the spermatid head. The microtubules (*purple*) form a manchette, consisting of a perinuclear ring supported by longitudinal microtubules around the spermatid neck that shape the postacrosomal region of the sperm head. The acroplaxome (*red*) anchors the acrosome to the spermatid nucleus. The perinuclear ring of the manchette is separated from the acroplaxome by the belt groove. The spermatid flagellum is shown in *green*. Diagram adapted from [63] and [64].

Defects in the assembly and removal of the microtubule manchette have been shown to affect the morphology of the sperm head [63]. The p80 subunit of katanin, a microtubule-severing protein, controls the removal of the microtubule manchette. In katanin p80 knockout-mice, removal of the microtubule manchette is abolished, resulting in abnormal sperm-head morphology [63].

Clip 170 is a microtubule plus-tip binding protein that is localized to the perinuclear ring of the microtubule manchette and maintains the structural integrity of the manchette [65]. In the absence of Clip 170, the microtubule manchette is misaligned, leading to a defect in sperm-head formation [65].

Mutations in genes that control microtubule dynamics have also been shown to disrupt the microtubule network in Sertoli cells. A mutation in the *KATNAL1* gene, which encodes a microtubule-severing protein, disrupts the microtubule dynamics in Sertoli cells, resulting in infertility due to premature release of spermatids from the seminiferous epithelium [66].

The apical ES contributes to the shaping of the spermatid head, but also assists in positioning and moving the developing sperm across the seminiferous epithelium, which prevents premature release of immature sperm [67]. Extensive research on the molecular composition of the ES has identified several actin binding and regulatory proteins.

Chemical disruption of the actin cytoskeleton in the ES by cytochalasin D treatment has been shown to cause premature release of immature sperm, resulting in infertility [68].

The junctional adhesion molecule-C (JAM-C) is a transmembrane protein expressed in spermatogenic cells. JAM-C interacts with JAM-B at the ES in Sertoli cells, thereby, controlling the communication between Sertoli and germ cells. JAM-C

is also responsible for recruiting the cell-polarity complex, Par6-Cdc-42-PKC λ , to the ES [69]. Spermatids from JAM-C knockout-mice lack cellular polarity, which is required for spermatid differentiation. As a consequence, these mice fail to produce mature sperm [69].

Abnormal bundling of actin fibers at the apical ES has been shown to cause infertility due to malformations in the sperm head. Nectin-2 is exclusively expressed in Sertoli cells and is localized at the junctions between Sertoli cells and between Sertoli and germ cells. Nectin-2 recruits and/or maintains F-actin bundles at the ES. In the absence of nectin-2, the ES fails to form due to the lack of actin bundling. Consequently, sperm heads are deformed and are unable to fertilize the oocyte [70].

1.9. Aim of the thesis

The physiological function of the GBA2, a non-lysosomal beta-glucosidase, is ill-defined. Accumulation of GlcCer in GBA2 knockout-mice causes globozoospermia and, thereby, male infertility. However, the underlying molecular mechanism is not known. Thus, the aim of my PhD thesis is to investigate the molecular mechanisms underlying the development of globozoospermia in GBA2 knockout-mice.

2. Materials

2.1. Antibodies

2.1.1. Primary antibodies

ANTIBODY	ORIGIN	DILUTION		MANUFACTURER
		ICC	WB	
Calnexin	rb	1:100	1:20000	abcam
GBA2-4A12	rt	1:50	1:20	E. Kremmer (HZ München)
GBA2-4D7	rt	1:50	1:20	E. Kremmer (HZ München)
GBA2-2F8	rt	1:50	1:20	E. Kremmer (HZ München)
GBA2-5A8	rt	1:50	1:20	E. Kremmer (HZ München)
Polyclonal GBA2	rb	1:1000	1:2000	Y. Yildiz (Yildiz et al., 2006)
beta-tubulin-CY3	ms	1:500	-	Sigma #C4585
HA		1:1000	1:10,000	Roche #11867431001
beta-tubulin III	rb	1:500	1:1000	Covance #MRB-435P
BrdU	ms	1:200	-	Invitrogen #MP35128
GM-130	ms	1:100	-	BD Transduction Labs #610822
Giantin	rb	1:1000	-	Abcam #ab24586
Lamp1	rb	1:200	-	Abcam #ab24170
Sox9	rb	1:1000	-	Millipore #AB5535
Cdc-42	rb	-	1:1000	Abcam #ab64533
Rac1	ms	-	1:1000	Abcam #ab33186

2.1.2. Secondary antibodies

ANTIBODY	ORIGIN	DILUTION		MANUFACTURER
		ICC	WB	
d α rb Cy3	d	1:250	-	Dianova
d-α- rtCy3	d	1:250	-	Dianova
gt α ms Dylight 488	gt	1:100	-	abcam
d α rb IRDye680	d	-	1:20000	LI-COR Bioscience
gt α rt IRDye800	gt	-	1:20000	LI-COR Bioscience
d α ms IRDye800	d	-	1:20000	LI-COR Bioscience

2.1.3. Dyes

DYE	DILUTION		MANUFACTURER
	ICC	WB	
Phalloidin	1:500	-	Molecular Probes #A12379
MitoTracker	0.5 μ M	-	Molecular Probes #M22426
Peanut lectin	1:100	-	Sigma #7381
DAPI	1:10,000	1:10,000	Molecular Probes #D1306

2.2. Bacterial strains and Cell lines

The *Escherichia coli* XL1-Blue (Bullock et al. 1987) was used to amplify plasmid DNA.

2.3. Plasmids

Lifect-GFP and EB3-mCherry were kindly provided by Dr. Roland Wedlich-Söldner and Dr. J.Victor Small, respectively.

3. Methods

GBA2 knockout-mice were generated as mentioned in [30]. All experiments performed with animals were in accordance with the relevant guidelines and regulations. The generation of antibodies and stable HEK293 cell lines is described in [26].

3.1. Cell culture

3.1.1. Isolation of sperm and male germ cells

Sperm were isolated by incision of the cauda epididymis in modified TYH medium containing 138 mM NaCl, 4.8 mM KCl, 2 mM CaCl₂, 1.2 mM KH₂PO₄, 1 mM MgSO₄, 5.6 mM glucose, 0.5 mM sodium pyruvate, 10 mM L-lactate, pH 7.4.

For isolation of germ cells, testes were decapsulated and incubated in 1 ml Hank's Balanced Salt Solution (HBSS) (20 mM HEPES, 137 mM NaCl, 5.4 mM KCl, 0.3 mM Na₂HPO₄, 0.4 mM KH₂PO₄, 1.2 mM MgSO₄, 1.3 mM CaCl₂, 6.6 mM sodium pyruvate, 0.05% lactate, 5.6 mM glucose, pH 7.2) containing 0.5 mg/ml Collagenase type IA (Sigma) for 30 min at 32 °C. The dissociated interstitial cells were removed by two washing steps with HBSS. The seminiferous tubules were then incubated in 1 ml HBSS containing 0.5 mg/ml Trypsin type XIII (Sigma) and 1 µg/ml DNaseI (Applichem) for 10 min at 32 °C. Cell aggregates were sheared gently with a Pasteur pipette. The dispersed seminiferous cells were washed twice by centrifugation at 200 x g for 5 min at room temperature. The final cell pellet was resuspended in HBSS and filtered through a Nylon mesh (40 µm pore size).

3.1.2. Isolation of P7 Sertoli cells

Seminiferous tubules were isolated from testis of 7 days old mice (P7) by removal of the tunica albuginea. The tubules were treated with 1 mg/ml collagenase (Sigma) at 37°C in a shaker for 8 min. The digestion was stopped by addition of DMEM/GlutaMax medium (Invitrogen) containing 10% FCS (Biochrom). The cell suspension was centrifuged at 400 x g for 8 min, the pellet was re-suspended in DMEM/GlutaMax medium containing 10% FCS and 0.5 mg/ml trypsin (Sigma) and 0.22 mg/ml EDTA (Sigma), and incubated in a shaker at 37°C for 5 min. The reaction was stopped by adding medium. The cell suspension was then treated with 1 µg/ml DNase I (Applichem) in a shaker at 37°C for 5 min. Afterwards, cells were centrifuged at 600 x g for 10 min, and re-suspended in medium containing 70 IU/ml penicillin, 70 µg/ml streptomycin, 100 mM sodium pyruvate, and 200 mM L-glutamine (all Life technologies). Cells were seeded at a density of 5 x 10⁴ cells/5 cm cell culture plate (Greiner bio-one) and used on the 5th day for experiments.

In order to maintain the intercellular junctions of the isolate, the seminiferous tubules were treated with 1 mg/ml dispase (Stem cell technologies, #07923) instead of collagenase and trypsin in a shaker at 37°C for 30 min. After treatment the cells were centrifuged, re-suspended in fibroblast growth medium (see 3.1.3) and plated on poly-L-lysine coated glass coverslips.

3.1.3. Isolation of dermal fibroblasts

Dermal fibroblasts were isolated from mouse tails using collagenase digestion. Tail pieces were incubated in fibroblast growth medium containing 0.1 mg/ml collagenase (Sigma) for 3h, 37 °C, and 5% CO₂. After digestion, the supernatant was centrifuged for 5 min, 600 x g at room temperature. The cell pellet was re-suspended in fibroblast growth medium; cells were plated on cell culture plates, and cultured at 37°C, 5% CO₂. After 24 h, the medium was changed.

Fibroblast growth medium	DMEM/GlutaMax containing 10% FCS, 100 mM sodium pyruvate, 200 mM L-glutamine, 70 IU/ml penicillin, 70 µg/ml streptomycin.
--------------------------	---

3.1.4. Immunocytochemistry (ICC)

Cells were fixed in 4% paraformaldehyde at room temperature for 10 min. To preserve the cytoskeleton, cells were fixed with PHEM for 15 min at RT. After washing with PBS (1.5 mM KH₂PO₄, 2.7 mM KCl, 6.5 mM Na₂HPO₄, 137 mM NaCl, pH 7.4), a quenching step was introduced by incubating the cells for 10 min in 25% glutaraldehyde and 50 mM NH₄Cl in PBS at room temperature. Sperm were immobilized on microscope slides and fixed with 4% paraformaldehyde at room temperature for 10 min. Before blocking, all cells were washed 3 x with PBS. To block unspecific binding sites, cells were incubated for 1 h with blocking buffer (0.5% Triton X 100 and 5% ChemiBLOCKER (Millipore) in 0.1 M phosphate buffer, pH 7.4). Primary antibodies were diluted in blocking buffer and incubated 1 h at room temperature. Fluorescent secondary antibodies were diluted in blocking buffer containing 0.5 µg/µl DAPI (Invitrogen) and incubated for 1 h in the dark. Pictures were taken on a confocal microscope (Olympus FV1000). For the analysis of cytoskeletal structures in dermal fibroblasts, cells were seeded on multi-pattern fibronectin coated CYTOO chips (#10-900-13-06, CYTOO Cell Architects).

PHEM BUFFER STOCK (PH 7.0)	1X PHEM
2 mM MgCl ₂	1x PHEM buffer
10 mM EGTA	0.1 % (v/v) Triton X-100 (Roth)
25 mM HEPES	0.25 % (w/v) glutaraldehyde (Sigma)
60 mM PIPES	3.7 % (w/v) PFA/sucrose

3.1.5. Immunohistochemistry (IHC)

Testes were fixed overnight with 4% paraformaldehyde/PBS, cryo-protected in 10% and 30% sucrose, and afterwards embedded in TissueTec (Sakura Finetek). Thin cross-sections of (16 μm) thickness were made in a cryotome (Microm HM 560). Immunofluorescent labeling was performed as described above except that the primary antibody was incubated overnight in a humidified chamber at room temperature.

3.1.6. Unroofing of HEK293 cells

HEK293 cells were transfected with a membrane-anchored GFP (CAAX). For unroofing 1 ml of stabilization buffer (30 mM HEPES pH 7.4, 70 mM KCl, 5 mM MgCl_2 , 3 mM EGTA, 1 mM DTT) was added and cells were sonicated once for 0.1 sec with a pulse amplitude of 5% in a sonifier (Branson sonifier 450). Afterwards, cells were gently washed to remove debris and stained with antibodies.

3.1.7. Fluorescence protease protection (FPP) assay

The assay was performed as described in [71].

3.1.8. Transfection of mouse fibroblasts

1×10^6 mouse fibroblasts were resuspended in 100 μl transfection buffer (Neon transfection system, Life technologies) and 4 μg of plasmid DNA was added. Using a microporator mini (Digital Bio Technology, MP-100), 10 μl of the cell suspension were subjected to two pulses (20 ms each) of 1000 V and afterwards transferred to poly-L-Lysine-coated glass-bottom dishes (Mat Tek, #P35G-1.5-20-C). A total of 30 μl of cells were electroporated. The cells were allowed to grow overnight at 37°C and 5% CO_2 in medium.

3.1.9. Live-cell imaging

Cells were imaged 24 h after transfection using the DeltaVision Core microscope (Applied Precision, Inc.). Images were acquired every 3 s with 200-500 ms exposure time over 5 min.

3.1.10. Analysis of microtubule dynamics

Image analysis was performed using the track-points function of Metamorph (version 7.0, Molecular Devices Corporation). A microtubule track was followed from the first frame an EB3-labelled microtubule plus-tip appeared until the last frame, when the plus-tip was no longer visible. Data for velocity (microtubule advance-rate) and distance (microtubule persistence) were calculated. Per cell, a minimum of 10 microtubule tracks and 7 cells per cell line were analyzed. In total, for each genotype, cells from 3 animals were analyzed.

3.1.11. Measurement of microtubule manchette

Isolated germ and Sertoli cells were labeled with a beta-tubulin antibody to visualize the manchette and DAPI to label the DNA in the sperm head. Images were taken using an Olympus FV1000 confocal microscope and the length of individual sperm manchettes was measured using ImageJ (version 1.46m). A minimum of 7 cells and three animals per genotype were analyzed.

3.1.12. Analysis of actin structures

Mouse fibroblasts were plated on CYTOO chips (CYTOO Cell Architects, #10 900-13-06) placed in a 35 mm cell culture plate and labeled with Phalloidin and DAPI. Images were taken using an Olympus FV1000 confocal microscope. Filopodia (slender actin-protrusions) and lamellipodia (wave-like actin extensions) structures were manually counted and expressed as number of filopodia or lamellipodia per cell.

3.1.13. Proliferation assay

Fibroblasts were seeded at a density of 4×10^4 cells/well and allowed to grow overnight. Cells were labelled with BrdU (Invitrogen #00-0103, diluted 1:100 from concentrate of 10:1 5-bromo-2'-deoxyuridine and 5-fluoro-2'-deoxyuridine) in fibroblasts growth medium for 8 hours at 37°C, 5% CO₂, and fixed with 70% ethanol for 10 min at room temperature. Before performing ICC using an anti-BrdU antibody cells were treated with 1.5 M HCl for 30 min. BrdU labeled nuclei were counted using the ImageJ (version 1.46m) cell counter plug-in. The proliferation rate was calculated by determining the ratio of proliferated cells to the total number of cells. Seven animals per genotype were analyzed.

3.1.14. Wound-healing assay

Silicone cell culture-inserts (Ibidi, #80209) with a defined cell-free gap (width = 500 µm) were placed in 35 mm cell culture dishes. 4×10^4 cells were transferred into each of the culture inserts and incubated at 37°C, 5% CO₂ for 2 h. Afterwards, inserts were removed and cells were washed with PBS (1.5 mM KH₂PO₄, 2.7 mM KCl, 6.5 mM Na₂HPO₄, 137 mM NaCl, pH 7.4). Fresh medium was added and a phase contrast image was taken (t = 0 h) using the Nikon eclipse (TE 2000-S) microscope. An image of the same region was taken every 2 h (t = 2, 4, 6, 8 h). The area of the cell-free gap was measured using ImageJ (version 1.46m) and the speed of migration was calculated.

3.1.15. Isolation of giant plasma-membrane vesicles (GPMVs)

Giant plasma-membrane vesicles (GPMVs) have been isolated as described elsewhere [72]. In brief, dermal fibroblasts were incubated with GPMV buffer (10 mM HEPES, 150 mM NaCl, 2 mM CaCl₂, pH 7.4) containing 2 mM NEM for 1-2 h at 37°C, 5% CO₂. The supernatant was centrifuged for 10 min at 2,000 x g and room temperature to pellet cell debris and intact cells. The resulting supernatant was subjected to high-speed centrifugation for 1 h at 45,000 x g and 4 °C to pellet the vesicles. The pellet was re-suspended in GPMV buffer.

3.1.16. Fluorescence spectroscopy

Measurements were performed in a quartz cuvette using the FluoroMax-3 Spectrofluorometer (Horiba Jobin yvon). The emission spectrum was recorded from 400 nm to 500 nm at 385 nm excitation to detect the lipid resonance-peak at 425 nm. All samples were normalized to the lipid resonance-peak for the GPMV buffer. GPMVs were labeled with 5 μM laurdan (6-Dodecanoyl-2-Dimethylaminonaphthalene, Molecular Probes, #D250) for 20 min at 23 °C. Measurements were performed at 350 nm excitation and fluorescence emission was recorded from 400 to 600 nm. All measurements were done at 23 °C. GP value was calculated according to the following equation where I_x is the intensity of emitted light at wavelength x.

$$GP = \frac{\frac{460}{420} I_x - \frac{510}{470} I_x}{\frac{460}{420} I_x + \frac{510}{470} I_x}$$

3.2. mRNA expression analysis

Total RNA isolation and reverse transcription to obtain cDNA was performed according to the manufacturer’s instructions (Nucleo-Spin RNA II: Macherey & Nagel, Düren, Germany; Superscript III: Invitrogen).

3.2.1. Quantitative real-time PCR

For qRT-PCR, two master mixes were prepared:

MIX I	MIX II
<ul style="list-style-type: none">• 1 μl of a 5 μM dilution of each primer of one primer pair• 12.5 μl SYBR Green Supermix (Biorad)	<ul style="list-style-type: none">• 1 μl of the 1:5 cDNA dilution• 10.5 μl H₂O

Materials and Methods

qRT-PCR was performed for *Cdc-42*, *Rac1*, *RhoA*, *Nectin2*, and *Vinculin*, and for the housekeeping genes *Tfrc* and *Gusb*. Primers for qRT-PCR were tested for efficiency before use. Efficiency tests include dilution of template cDNA from 1:1 up to 1:1000. The slope obtained from plotting the individual CT values is used to calculate primer efficiency ($E = 10^{-1/\text{slope}}$). Primers used for real-time PCR showed at least 90% efficiency. Different annealing temperatures were used for the primers.

PRIMER	FORWARD PRIMER	REVERSE PRIMER	PRIMER NUMBER	ANNEALING TEMPERATURE (°C)
Cdc-42	ACCCAACCATGC GTCCCC	GTCCTCAGCTTC TCCGCC	C2076/C 2077	62
Rac1	TTTCCCAGCTT TGGGTGG	TCCCACCACCAC ACACTTG	C2080/C 2081	51
RhoA	CGTGGATGCGT TCTTGAGC	ATGGAGAGAACC GACGGAG	C2078/C 2079	59
Nectin2	GAGAGGCCAAA GATACTCAG	CCAAGGTACCAG TTGTCATC	C1877/C 1878	59
Vinculin	TGTTTCAGACCAC TGAGGATC	TCAGCCTCATCG AAGGTAAG	C2082/C 2083	59

The reaction was set up in duplets for each gene and each template (mouse GBA2 wild-type and knockout testis cDNA). Additionally, a non-template control was set up for each primer pair. All qRT-PCR experiments were performed in the BioRad I-cycler with an IQ5 optical system. Data was analyzed using the BioRad IQ5 optical system software and calculated according to the delta-delta-CT method [73].

The following PCR program was used:

CYCLE	STEP	TEMPERATURE (°C)	TIME (SEC)
Denaturation	Step I	95	180
Denaturation Annealing Extension (35X)	Step I	95	10
	Step II	see above	30
	Step III	72	30
Denaturation	Step I	95	60
Melt curve	Step I	55	60
	Step I	55	30

After running the cycles, a melt-curve analysis was performed to detect non-specifically amplified products. mRNA expression-levels for wild-type and knockout were normalized to the housekeeping genes.

3.3. Biochemistry

3.3.1. Protein preparation

All steps were performed at 4 °C in the presence of mammalian protease inhibitor cocktail (mPIC, Sigma Aldrich). Tissues or cells were homogenized in a 10-fold surplus (v/w) of hypotonic buffer (10 mM HEPES, 0.5 mM EDTA, pH 7.4) using an Ultra-thurrax (IKA) and three pulses (20 s each) of sonification (Branson sonifier). The suspension (total lysate) was centrifuged for 10 min at 1,000 × g. The supernatant (PNS, post-nuclear supernatant) was used for activity assays. For Western-blot analysis the tissue was homogenized in detergent containing buffer (10 mM Tris/HCl pH 7.6, 140 mM NaCl, 1 mM EDTA, 1 % Triton X-100). After 30 min of incubation on ice, the suspension was centrifuged for 5 min at 10,000xg. The supernatant was used for experiments. The protein concentration was estimated using the bicinchoninic acid (BCA) test. Aa protein standard gamma-globulin protein was used. The absorbance of the protein of interest and the standards was measured at 570 nm in the Packrad Fusion Instrument plate reader. The protein concentration of the sample was calculated using the linear regression of the protein standard.

3.3.2. SDS-PAGE and Western-blot analysis

SDS-sample buffer (4x; 200 mM Tris/HCL pH 6.8, 0.04 % bromophenol blue, 4 % beta-mercaptoethanol, 8 % SDS, 50 % glycerine) was added to all samples (final 1x) and heated for 5 min at 95 °C prior to loading onto SDS-PAGE (sodium dodecyl sulfate polyacrylamide gel electrophoresis). The SDS-PAGE was performed in running buffer (final 1x; 10x: 250 mM Tris, 1.92 M glycine, 1 % SDS) at 180 V and 120 mA. As protein standard the Novex prestained protein ladder (Invitrogen; 3.5–

260 kDa) was used. For Western-blot analysis, proteins were transferred onto PVDF membranes (Immobilon-FL, Millipore), probed with antibodies, and analyzed using the Odyssey Imaging System (LI-COR). Quantification of the Western blots was done using ImageJ (version 1.46m).

3.3.3. G-/F-Actin assay

The assay was performed according to the manufacturer's protocol (#BK037, Cytoskeleton).

3.3.4. Fluorescence-based GBA activity assays

The assay has been performed as described previously [26]. Briefly, cleavage of 4-MU-beta-D-glucopyranoside (Sigma Aldrich) was monitored in real-time in a Fluostar Omega reader (BMG labtech) at 29 °C using the filter pair 355 nm/460 nm for excitation and emission, respectively. The assays were performed in 384-well plates (Greiner) in the plate mode. Per well, 25 µl of lysate containing 20 µg of total protein were used. To discriminate between GBA1 and GBA2 activity, 30 µM CBE (Conduritol B epoxide, Sigma Aldrich), an inhibitor for GBA1, or 10 µM NB-DNJ (N-butyldeoxynojirimycin, Sigma Aldrich), an inhibitor for GBA2, were included. The pH of the protein lysates and the 4-MU-beta-D-glucopyranoside solution were adjusted by diluting with McIlvaine buffer (0.1 M citric acid and 0.2 M Na₂HPO₄). The assay was initiated by adding 5 µl of 4-MU-beta-D-glucopyranoside (10 mM) resulting in a final concentration of 1.67 mM. The hydrolysis of 4-MU-beta-D-glucopyranoside was monitored and recorded as a change of relative fluorescence units (rfu) per minute. Each analysis was performed as a quadruplicate in parallel. Per genotype, tissues or cells from three animals were analyzed if not otherwise stated.

3.4. Lipid analysis

3.4.1. Lipid analysis using thin-layer chromatography (TLC)

For lipid extraction, dermal fibroblasts from GBA2 wild-type (+/+) and knockout-mice (-/-) were grown until confluency, washed with PBS (1.5 mM KH₂PO₄,

2.7 mM KCl, 6.5 mM Na₂HPO₄, 137 mM NaCl, pH 7.4), and harvested using trypsin/EDTA in medium. Cells were pelleted for 7 min at 700 x g and room temperature. Afterwards, cells were lysed in 1 ml distilled water with three pulses (30 s each) of sonification (Branson sonifier). Lipids were extracted for 24 h at 37 °C in chloroform/methanol/water (10/5/1, v/v/v). For a better analysis of glucosylceramide, glycerophospholipids were degraded by alkaline hydrolysis with 125 mM sodium hydroxide for 2 h at 37 °C. After neutralization with acetic acid, lipid extracts were desalted by reversed-phase chromatography and separated into acidic and neutral glycosphingolipids as described previously [74] [75].

For separation of neutral lipids by thin layer chromatography (TLC), 1 mg of total protein was applied to prewashed thin layer Silica Gel 60 (Merck, Darmstadt, Germany) and chromatograms were developed and quantified as described previously [75].

3.4.2. Extraction and quantification of sphingolipids using mass spectrometry

Sperm cells, testis, and Sertoli cells were frozen in liquid nitrogen and ground to a fine powder using the Precellys24 tissue homogenizer (PeqLab). Lipids were extracted and fractionated using solid-phase-extraction on silica columns [76]. Long chain bases, ceramides, and hexosylceramides were eluted with acetone/2-propanol (9:1, v/v) and sphingomyelin was eluted with methanol. The purified sphingolipids were analyzed via direct infusion nanospray mass-spectrometry using an Agilent 6530 Accurate-Mass Q-TOF LC/MS device [76]. Sphingolipids were quantified after collision-induced dissociation by scanning for specific fragment ions: long chain bases, NL of 18. 0106; ceramides, EIC m/z 264. 2686 or m/z 262. 2493; hexosylceramides, EIC m/z 264.2686; sphingomyelin, 184. 0739. Internal standards were added for each sphingolipid class [77].

3.5. Identification of mGBA2 by mass spectrometry

For LCMS, proteins of Sertoli cells, testis, and sperm were separated on SDS gels and stained with Coomassie. Per lane, 14-17 gel slices were excised, proteins were in-gel digested with trypsin (Promega), peptides were separated in a 90 or 180 min gradient by a nanoAcquity LC System equipped with a HSS T3 analytical column (1.8 μm particle, 75 μm x 150 mm) (Waters), and analyzed by ESI-LC-MS/MS using an LTQ Orbitrap Elite mass spectrometer (Thermo Scientific). All database searches were performed using SEQUEST as well as MS Amanda (Mechothler lab, Vienna, Austria) algorithm, embedded in Proteome DiscovererTM (Rev. 1.4, Thermo Electron[©] 2008-2011), with a NCBI protein database (mouse, accession number NP_766280.2, accessed June 13, 2013). Only fully tryptic peptides with up to two missed cleavages were accepted. Oxidation of methionine was permitted as variable modification. The mass tolerance for precursor ions was set to 10 ppm; the mass tolerance for fragment ions was set to 0.4 amu. To filter the results, a peptide FDR threshold of 0.01 (q-value) according to Percolator was set in Proteome Discoverer, two peptides per protein and peptides with search result rank 1 were required.

4. Results

4.1. GBA2-specific antibodies

To investigate the intracellular localization of GBA2, monoclonal antibodies directed against four different peptide epitopes were generated (Table 1).

<i>Peptide (epitope)</i>	<i>Amino acids</i>	<i>Antibody label</i>	<i>Species</i>
1	36 – 50	4A12	Rat
2	358 – 377	4D7	Rat
3	505 – 529	2F8	Rat
4	720 – 744	5A8	Rat

Table 1. Monoclonal GBA2-specific antibodies. The position of the peptide epitope, the antibody label, and the species, in which the antibody has been generated are indicated.

The peptides were chosen based on their antigenicity and position in the mouse GBA2 protein-sequence. In particular, epitopes located in the N and C terminus were chosen to reveal the subcellular localization of GBA2 and, thereby, solve the discrepancy in the literature about the subcellular localization of GBA2. Peptide 1 is located in the N terminus and peptide 4 in the C terminus. Peptide 2 is located in the catalytic beta-glucocerebrosidase domain, while peptide 3 is located downstream outside the catalytic domain (Figure 5a, 25). Furthermore, antibodies against peptides 2, 3, and 4 will allow to confirm the absence of GBA2 protein in GBA2-knockout mice.

The specificity of the antibodies was evaluated using Western-blot analysis and immunocytochemistry. The monoclonal antibodies 4A12, 4D7, 2F8, and 5A8 detected the heterologously expressed GBA2 protein in HEK293 cells at 110 kDa, which is also detected by the HA antibody (Figure 5b). Furthermore, the 4A12, 2F8, and 5A8 antibodies detected the endogenously expressed GBA2 in protein lysates from wild-type testis and did not show a specific band at the corresponding height in lysates from GBA2 knockout-testis (Figure 5b). The 4A12 antibody additionally recognized a band of larger molecular weight in both wild-type and GBA2 knockout-testis (Figure 5b). Only the 4D7 antibody did not detect the endogenously expressed GBA2 protein, but the heterologously expressed protein in HEK293 cells. The specificity of the antibodies was confirmed by immunocytochemistry (Figure 5c). HEK293 cells were transfected with GFP-tagged GBA2 and the antibody staining co-localized with the GFP fluorescence. In line with the results from Western-blot analysis, the 4D7 antibody did not show GBA2-specific labelling (Figure 5c).

In conclusion, the newly generated monoclonal peptide antibodies against GBA2 are a reliable tool to detect GBA2 using Western blot and immunocytochemistry [26].

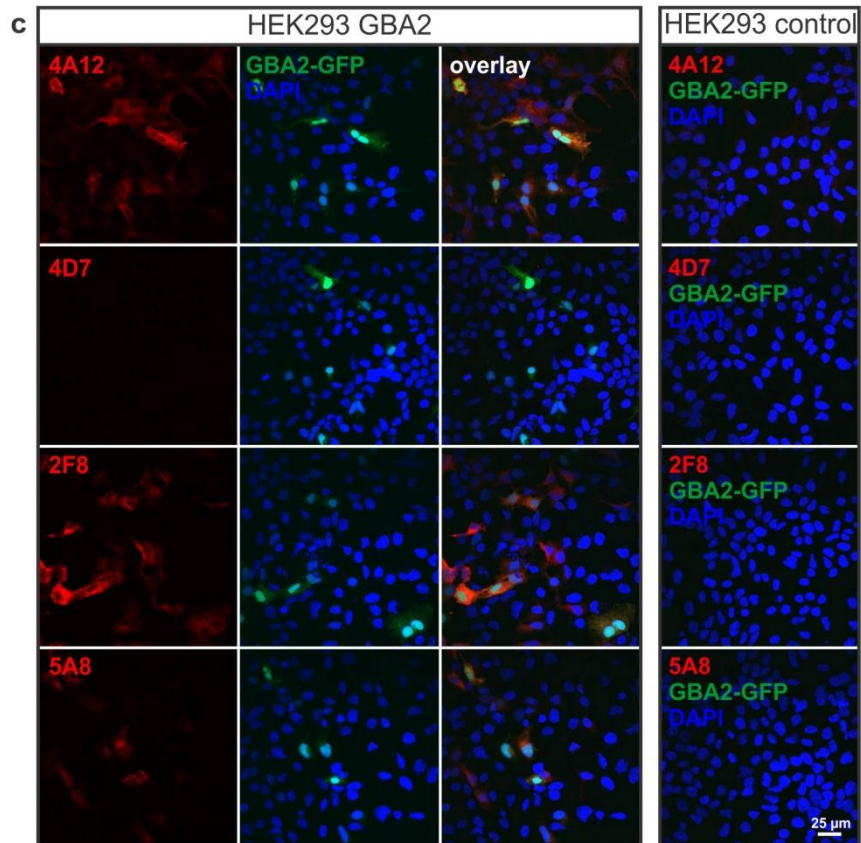
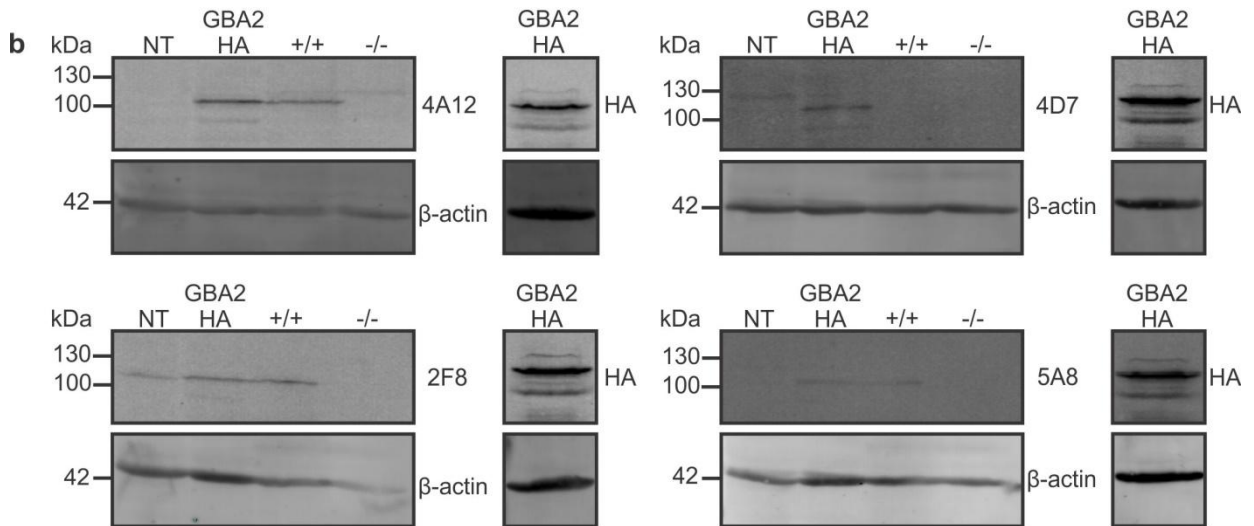
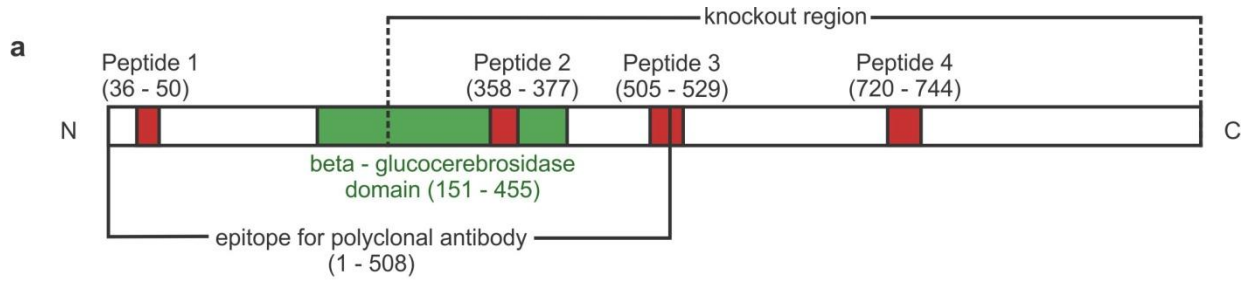


Figure 5. GBA2-specific antibodies. (a) Schematic representation of the mouse GBA2 protein-sequence showing the position of the different peptide epitopes (*red*). The region against which a polyclonal antibody was generated is indicated [30]. The catalytic domain (beta-glucocerebrosidase, *green*) and the region that is deleted in GBA2 knockout-mice are also shown. Amino-acid positions for the different regions are shown in brackets. (b) Western-blot analysis of total protein lysates from HEK293 wild-type (*NT*, *control*) cells, GBA2-HA over-expressing cells, and wild-type (+/+) and GBA2 knockout-testis (-/-). The blot was labeled with a HA antibody and the GBA2-specific antibodies 4A12 (*top left*), 4D7 (*top right*), 2F8 (*bottom left*), and 5A8 (*bottom right*). β -actin was used as a loading control. (c) Immunocytochemical analysis of HEK293 cells expressing GBA2-GFP (*green*) labeled with the 4A12, 4D7, 2F8, and 5A8 (*red*) antibodies along with DAPI (*blue*) to stain the DNA. Non-transfected HEK293 cells are shown on the right. Scale bar: 25 μ m.

4.2. Subcellular localization of GBA2

To understand the function of GBA2, its subcellular localization was elucidated. Earlier reports proposed that GBA2 is an integral plasma-membrane protein with one transmembrane domain and the N terminus containing the catalytic domain facing the extracellular space [32]. However, GlcCer is incorporated in the inner leaflet of the plasma membrane [1] and would, therefore, not be accessible as a substrate for GBA2. To resolve this discrepancy, the subcellular localization of GBA2 was studied using different techniques. First, it was tested whether the N terminus of GBA2 indeed faces the extracellular space. HEK293 cells over-expressing GBA2 were labeled with the 4A12 antibody (against peptide 1 at the N terminus) with and without permeabilization of the cells by Triton X-100. As a control, cells were co-transfected with GFP. Labelling of GBA2 was only observed when cells had been permeabilized, indicating that the N terminus of GBA2 does not face the extracellular space (Figure 6a).

This result was corroborated with a fluorescence protease-protection (FPP) assay. The assay is based on the accessibility of proteases versus their inaccessibility to polypeptides that are located in the lumen of organelles [71]. To determine the topology, the protein of interest is fused to a fluorescent protein. Trypsin treatment of permeabilized or non-permeabilized cells allows to determine the localization of the fluorescent tag relative to the membrane [71]. HEK293 cells expressing a N-terminally eGFP-tagged GBA2 were imaged before and after treatment with 4 mM trypsin (Figure 6b). As a control, HEK293 cells were transfected with a YFP-tagged GPI-anchored prion protein (YFP-PrP) with the YFP facing the extracellular space [78]. After trypsin treatment, the fluorescence of YFP-PrP was diminished, whereas the fluorescence in cells expressing the eGFP-tagged GBA2 remained unchanged (Figure 6b). Thus, the N terminus of GBA2 is not accessible from the extracellular side.

Experiments performed by Dr. Heinz-Gerd Körschen revealed that GBA2 is not a transmembrane but rather a membrane-associated protein [26]. To determine if GBA2 is associated with the plasma membrane, GBA2-expressing HEK293 cells were co-transfected with a GFP-tagged CAAX membrane anchor, which is incorporated into the plasma membrane via its lipid anchor. Transfected cells were subjected to unroofing by ultrasonification. This technique generates plasma-membrane sheets exposing the cytosolic side of the cell [79]. Membrane sheets were labeled with a GBA2-specific antibody and identified by GFP fluorescence (Figure 6c). However, GBA2 expression was absent in the membrane sheets, indicating that in HEK293 cells, GBA2 is not associated with the plasma membrane (Figure 6c).

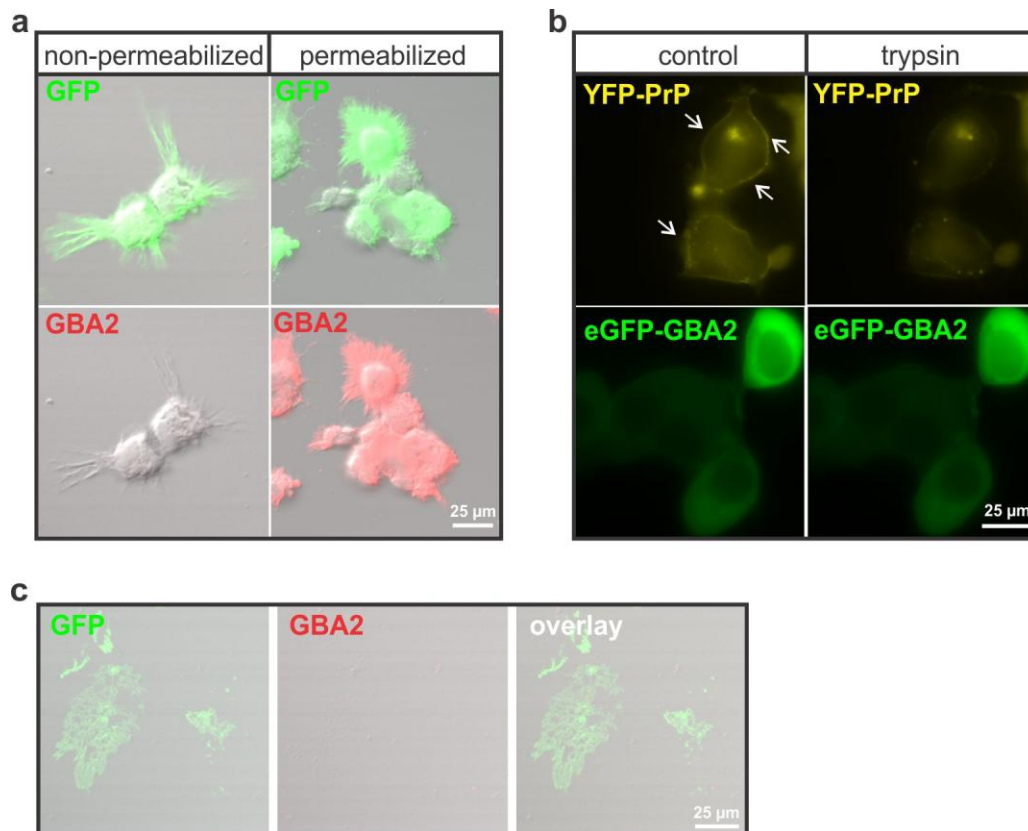


Figure 6. GBA2 topology. **(a)** Non-permeabilized (*left*) and Triton X-100 permeabilized (*right*) HEK293 cells over-expressing GBA2 labeled with the 4A12 antibody (*red*). As a control, cells were transfected with CAAX-GFP (*green*). **(b)** HEK293 cells transfected with YFP-PrP (positive control; *yellow*; indicated by arrows) or eGFP-GBA2 (*green*). Cells were imaged before (*control, left*) and after treatment with 4 mM trypsin for 1 min (*right*). The YFP-PrP signals (*yellow*) at the membrane of control cells vanished after trypsin treatment, indicating proteolysis of extracellular proteins. However, the eGFP fluorescence (*green*) in GBA2-expressing HEK293 cells did not change, demonstrating that the N terminus is not facing the extracellular space. **(c)** GFP labeled-membrane sheets (*green*) of HEK293 cells over-expressing GBA2. Cells were transfected with GFP-tagged CAAX membrane anchor and unroofed by ultrasonification. GBA2 was detected by the 4A12 antibody (*red*). Scale bars: 25 μm .

To reveal where GBA2 is localized in the cell, the FPP assay was performed under permeabilizing conditions. Before trypsin treatment, cells were permeabilized with digitonin (20 μ M) for 1 min, which allows trypsin to enter the cell. Thus, fluorescent moieties facing the cytoplasmic side will be degraded [71]. Cells were transfected with GBA2 with eGFP fused to either the N or C terminus and imaged before and after treatment with digitonin and trypsin (Figure 7a). As a control, HEK293 cells were co-transfected with CD3 δ containing either a cytoplasmic C-terminal CFP-tag or a luminal N-terminal YFP-tag [71]. After trypsin treatment, the YFP signal in CD3 δ transfected cells remained unchanged, whereas the CFP signal in CD3 δ transfected cells was diminished, demonstrating cytosolic protein degradation (Figure 7a). In eGFP-tagged GBA2-expressing HEK293 cells, the fluorescence was diminished for both constructs (Figure 7a). Thus, both the N and C terminus of GBA2 are accessible from the cytoplasmic side.

To determine whether GBA2 is localized at specific organelles in the cell, co-localization studies using marker antibodies for the endoplasmic reticulum (ER), the Golgi, and the lysosomes were performed. GBA2 is mainly expressed in the cytoplasm (Figure 7b). However, GBA2 expression also overlapped with calnexin, a marker for the ER, GM-130, a marker for the *cis*-Golgi, and giantin, a marker for the Golgi cisternae (Figure 7b), but not with Lamp 1, a marker for lysosomes. Since the localization of the over-expressed protein in HEK293 cells might differ from the endogenously expressed GBA2 protein, co-localization experiments were also performed in hippocampal neurons. GBA2 expression displayed a similar expression pattern in these cells, demonstrating that indeed GBA2 is localized at the ER and the Golgi [26].

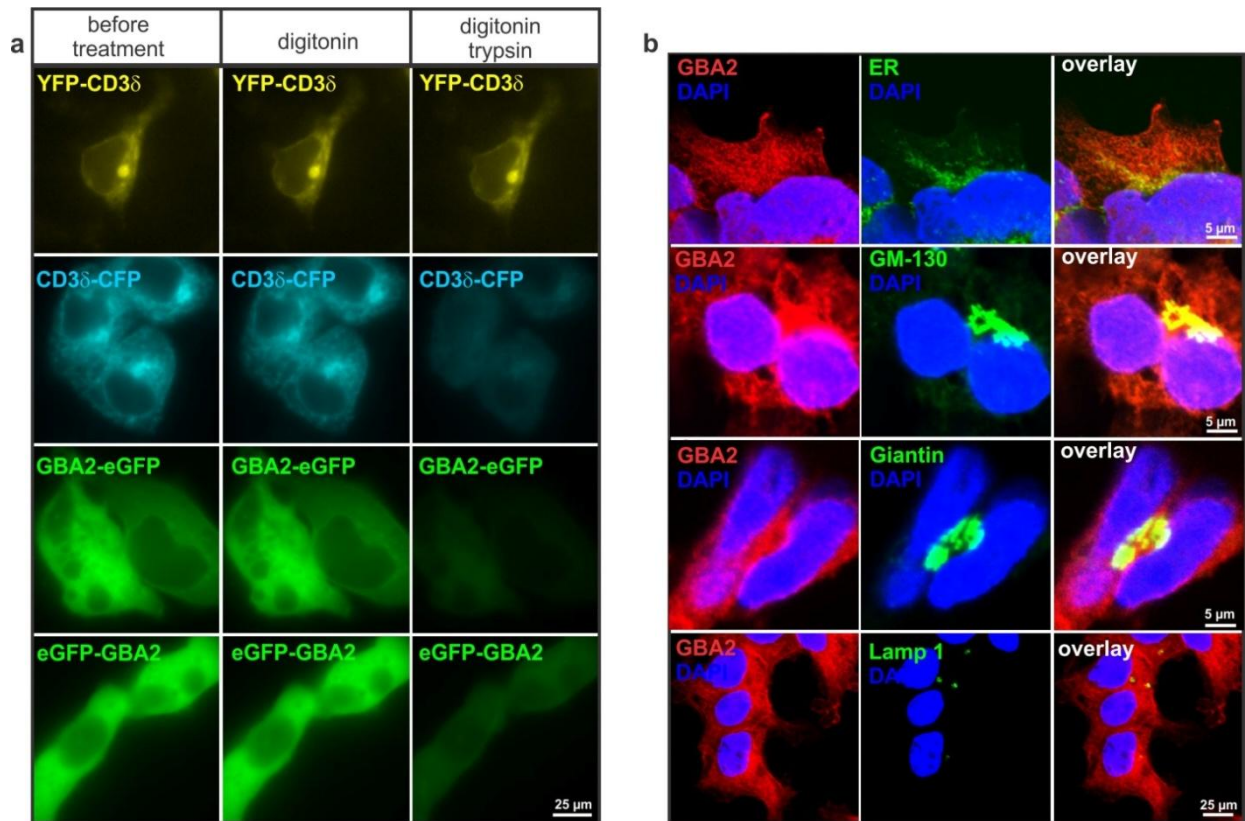


Figure 7. GBA2 is localized at the ER and Golgi with both N and C terminus facing the cytosol. (a) HEK293 cells were transfected with eGFP-GBA2 or GBA2-eGFP (green). YFP-CD3δ (YFP facing the ER lumen; yellow) and CD3δ-CFP (CFP facing the cytosol; cyan) were used as controls. Cells were imaged before (left) and after treatment with 20 μm digitonin (middle) and 4 mM trypsin (right) for 1 min each. After trypsin treatment, the YFP-CD3δ signal remained unchanged, whereas the CFP-CD3δ signal decreased, indicating proteolysis of cytosolic proteins. However, in GBA2-expressing HEK293 cells, eGFP fluorescence (green) was diminished for both constructs, demonstrating that both the N and C terminus of GBA2 are accessible from the cytoplasmic side. Scale bar: 25 μm. (b) HEK293 cells over-expressing GBA2 were labeled with the 4A12 (GBA2-specific; red), calnexin (ER; green), GM-130 (cis-Golgi; green), giantin (Golgi cisternae; green), and Lamp 1 (lysosomes; green) antibodies. DAPI was used to label the DNA (blue). Scale bar: 5 μm.

Taken together, GBA2 is a non-integral, membrane-associated protein at the ER and the Golgi with both the N and the C terminus facing the cytoplasm (Figure 8).

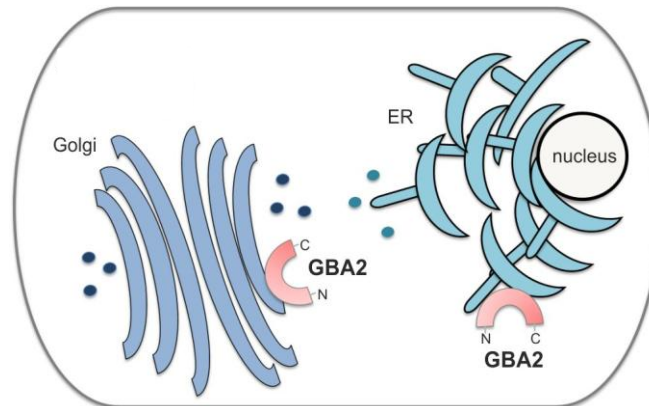


Figure 8. Schematic representation of the topology and localization of GBA2. GBA2 (red) is present at the ER (cyan) and the *cis*-Golgi (blue) with both the N and the C terminus facing the cytoplasm [26].

4.3. GBA2 is expressed in Sertoli cells

GBA2 is highly expressed in the testis [30]; however, its precise localization within the testis is ill-defined. GBA2 has been proposed to be expressed in Sertoli cells [30], which are the only somatic cells in the seminiferous tubules and are important for spermatogenesis [43]. To investigate the expression pattern of GBA2 in the testis in more detail, testis cross-sections were labeled with GBA2-specific antibodies and an anti-tubulin III antibody, a marker for Sertoli cells [80] (Figure 9a). Indeed, GBA2 expression overlapped with tubulin III, demonstrating that GBA2 is expressed in Sertoli cells (Figure 9a). To verify this result, germ and Sertoli cells were isolated and the expression of GBA2 was analyzed by immunocytochemistry. Again, the expression pattern of GBA2 and tubulin III overlapped (Figure 9b), confirming that GBA2 is predominantly expressed in Sertoli cells. In adult testis, Sertoli cells only

account for 5-10% of the total cells [81]. However, 7 days after birth (P7), the majority of cells in the testis are Sertoli cells [82]. Thus, I isolated Sertoli cells at P7 and analyzed the expression of GBA2 by Western blot (Figure 9c). Indeed, GBA2 was expressed in Sertoli cells at P7. So far, there was no indication of GBA2 expression in germ cells. Therefore, I analyzed whether GBA2 is expressed in mature sperm. Labelling of mouse sperm with GBA2-specific antibodies did not reveal a specific staining for GBA2 (data not shown). In Western-blot analysis, a weak band at 110 kDa was detected in total lysates from mouse sperm that was absent in lysates from GBA2 knockout-sperm (Figure 9d). To unequivocally reveal whether GBA2 is only expressed in Sertoli cells or also in sperm, mass spectrometric analysis of proteins from testis, Sertoli cells, and sperm was performed (Figure 24 in appendix). Unique peptides for GBA2 were only identified in testis and Sertoli cells, but not in sperm, demonstrating that GBA2 is only expressed in Sertoli cells.

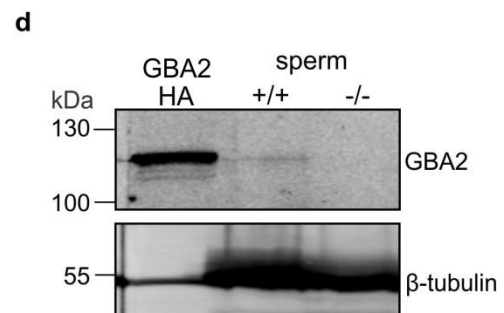
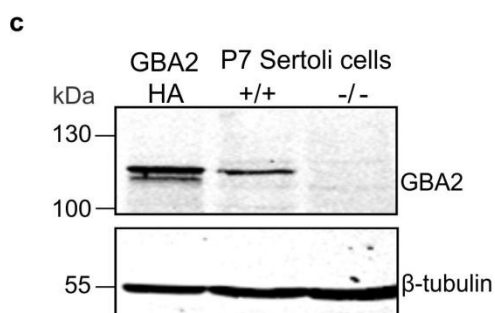
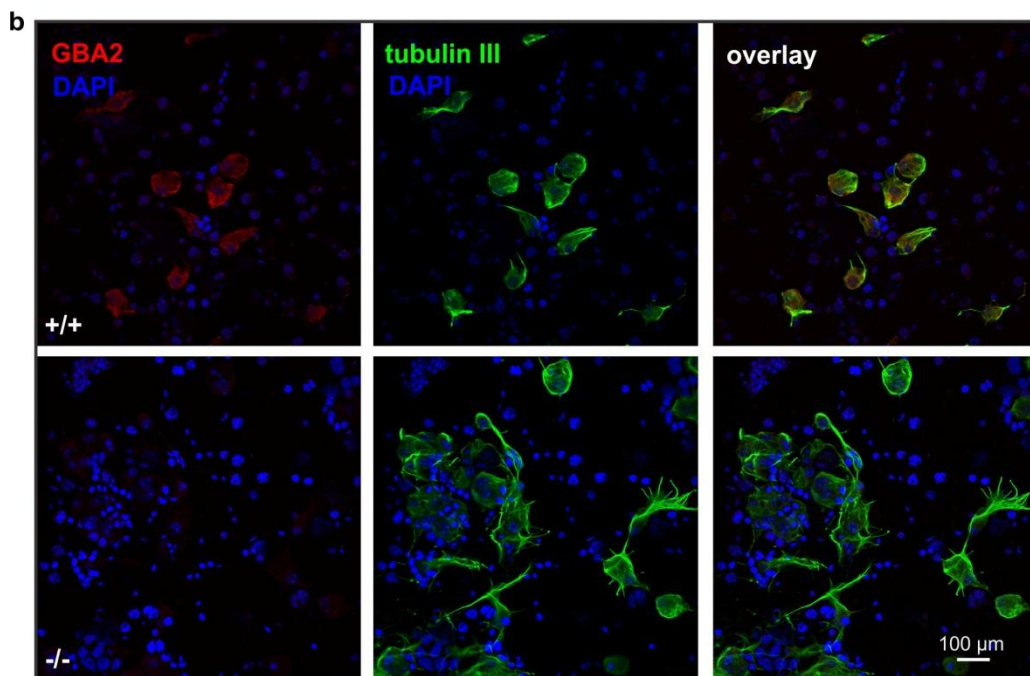
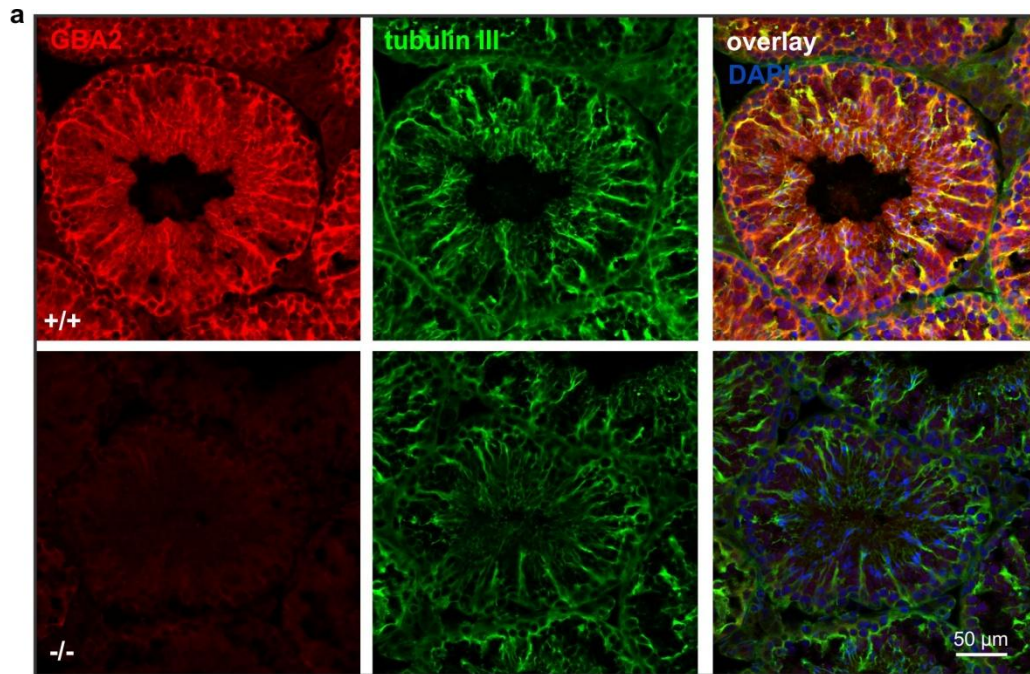


Figure 9. GBA2 is expressed in Sertoli cells. (a) Testis cross-sections were labeled with the polyclonal anti-GBA2 antibody (*red*) and an anti-tubulin III antibody (*green*). DAPI was (*blue*) used as a DNA marker to label the nuclei. Top: wild-type, +/+; bottom: GBA2 knockout, -/-. Scale bar: 50 μ m. **(b)** See (a) for isolated and labeled germ and Sertoli cells. Scale bar: 100 μ m. **(c)** Western-blot analysis using total protein lysates from P7 Sertoli cells. The blot has been labeled with the GBA2-specific 2F8 antibody; beta-tubulin has been used as a loading control. Wild-type: +/+, GBA2 knockout: -/-, HEK293 cells expressing GBA2-HA: GBA2-HA. **(d)** See (c) for mature sperm.

4.4. GBA2 expression during sperm development

To unravel the function of GBA2 during spermatogenesis, its expression and enzymatic activity was analyzed during the first spermatogenic wave. Only the first wave is synchronized and allows correlating protein expression and activity with specific stages during sperm development. In the adult testis, spermatogenic waves are no longer synchronized, making it difficult to investigate protein function at a particular developmental stage. I focused on two different time points in the first wave: pre-puberty (P7) and early puberty (P21), and compared them to adult animals (≥ 25 weeks old).

During the first spermatogenic wave, GBA2 followed the expression pattern of the Sertoli cell marker tubulin III (Figure 10a). Normalizing GBA2 expression to the expression level of tubulin III using Western-blot analysis revealed that GBA2 expression increased from P7 to P21 and decreased in the adult state (Figure 10b, c). Similarly, GBA2 activity increased from P7 to P21 and decreased from P21 to adult (Figure 10d) (enzyme activity measurements were performed by Sophie Schonauer, caesar). These results suggest that GBA2 function is particularly important at the onset of puberty in the first spermatogenic wave.

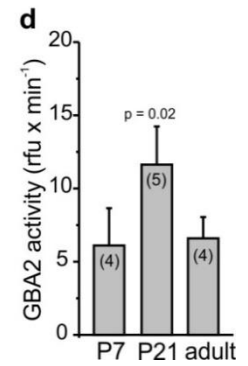
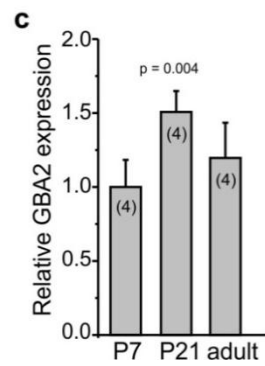
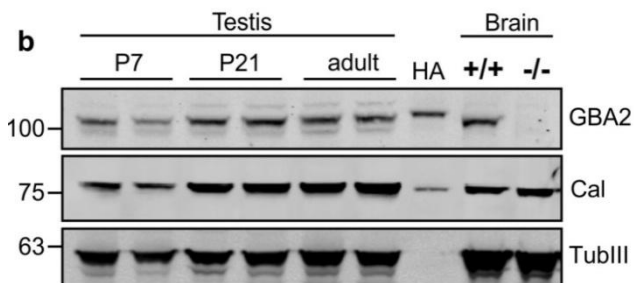
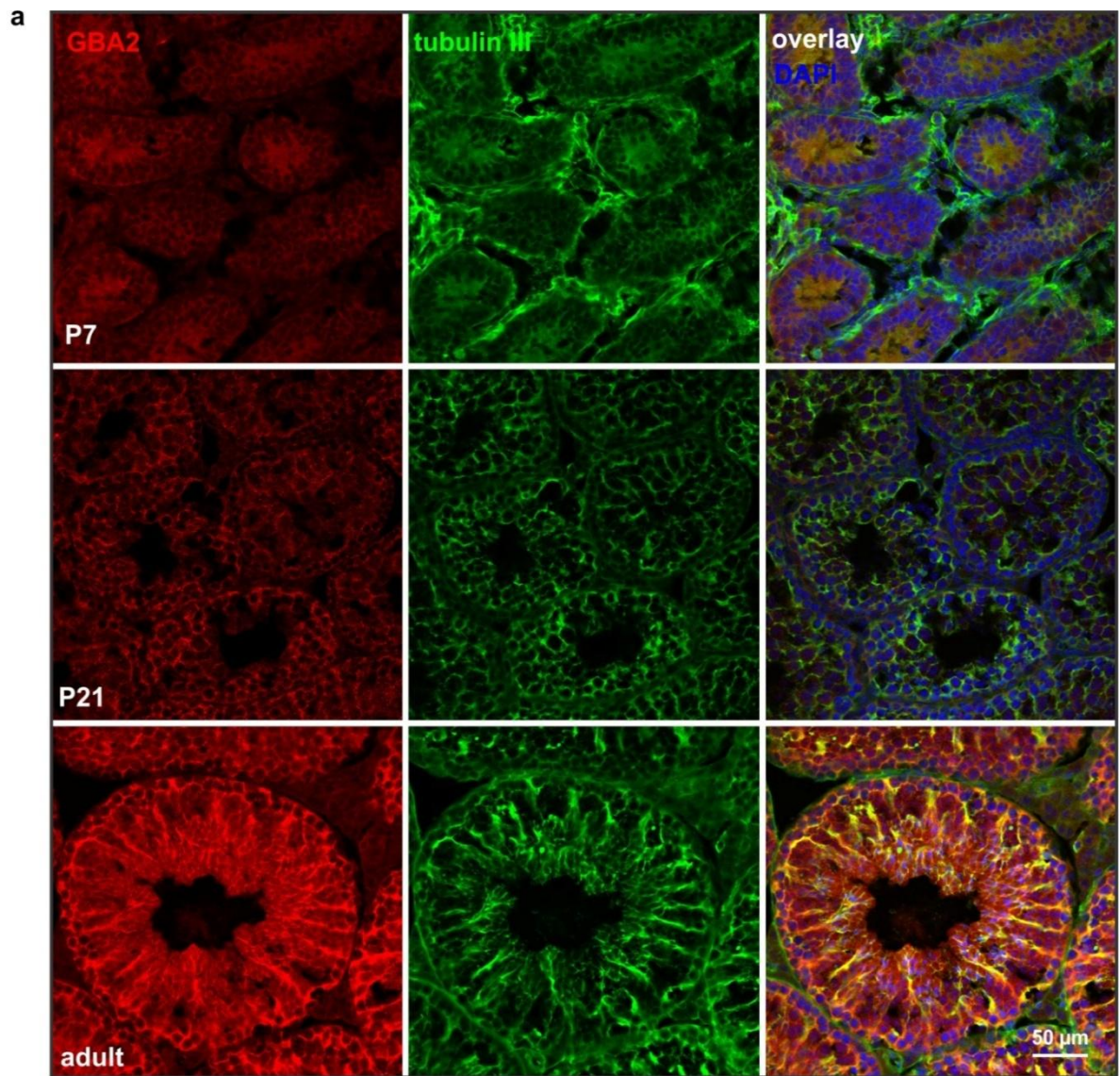


Figure 10. GBA2 expression and activity during the first spermatogenic wave. **(a)** Testis cross-sections from P7 (*top*), P21 (*middle*), and adult (*bottom*) testis were labeled with the polyclonal anti-GBA2 (*red*), and the tubulin III (*green*) antibody. DAPI (*blue*) was used to visualize DNA. Scale bar: 50 μ m. **(b)** Western-blot analysis using total protein lysates from P7, P21, and adult testis. Protein lysates of HEK293 cells expressing GBA2-HA (HA) were used as a positive control. The blot has been labeled with the GBA2-specific 2F8 antibody and tubulin III (TubIII) as a marker for Sertoli cells. Calnexin (Cal) served as a loading control. Protein lysates from wild-type (+/+) and GBA2 knockout-brain (-/-) have been used as controls. **(c)** Quantification of GBA2 protein expression. GBA2 expression levels have been normalized to the expression level of tubulin III. **(d)** Fluorescence-based beta-glucosidase activity measured at pH 6 in protein lysates from P7, P21, and adult wild-type testes. Data are presented as mean \pm S.D.; n numbers and p values determined using One-way ANOVA are indicated.

4.5. Lack of GBA2 leads to accumulation of GlcCer in testis and sperm

Sertoli cells and germ cells contain a different repertoire of glycosphingolipids. While Sertoli cells mainly contain sphingolipids with saturated long-chain fatty acids ($\geq C_{18}$), germ cells show a stage-specific increase in neutral fucosylated glycosphingolipids during spermatogenesis [83] [84] [85]. Developing germ cells have been shown to contain very long-chain (C_{28} , C_{30} , and C_{32}) polyunsaturated fatty acids [86]. Also associated with differentiating germ cells are ceramides, sphingomyelins, and gangliosides [85]. We set out to determine, which glycosphingolipids accumulate in the different cell types during spermatogenesis.

Quantitative analysis of sphingolipid content in adult testis, P7 Sertoli cells, and sperm was performed using mass spectrometry (in collaboration with the group of Prof. Peter Dörmann, Molecular Biotechnology, University of Bonn). In detail, we determined the total mass of long chain bases (LCB; C_{18}), saturated and unsaturated

ceramides (Cer; C₁₆ – C₂₆), hexacylceramides (HexCer; C₁₄ – C₂₄; both GlcCer and galactosylceramide (GalCer)), and sphingomyelin (SM; C₁₄ – C₂₆). In GBA2 knockout-testis, LCB, Cer, and SM levels did not change, whereas HexCer levels were dramatically increased (Figure 11a). Similarly, GBA2 knockout-sperm showed an increase in HexCer levels, but levels of LCB, Cer, and SM remained unchanged (Figure 11b). In both GBA2 knockout-testis and sperm, levels of saturated C₁₆, C₁₈, C₂₂, and C₂₄ HexCer were increased. However, the levels of C₂₈ HexCer were elevated only in GBA2 knockout-testis, but not in GBA2 knockout-sperm (Figure 11d, e). Since it is not possible to distinguish between GlcCer and GalCer using mass spectrometry, we performed thin-layer chromatography (TLC). GalCer levels did not change in GBA2 knockout-testis (data not shown), indicating that the changes observed in the HexCer levels represent changes in GlcCer levels. In P7 Sertoli cells, no change in any of the lipids was observed between wild-type and GBA2 knockout-mice (Figure 11c).

Thus, in the absence of GBA2, a plethora of GlcCer species with different chain lengths accumulate in testis and sperm, but not in P7 Sertoli cells. In adult testis, it is not possible to quantitatively separate Sertoli cells from germ cells, which makes it difficult to analyze glycosphingolipid levels exclusively in Sertoli cells. However, increased levels of saturated long chain GlcCer (C₂₈) in GBA2 knockout-testis, but not sperm, might indicate accumulation of GlcCer in adult Sertoli cells, which predominantly contain saturated long-chain sphingolipids. These results demonstrate that the lack of GBA2 also alters the levels of GlcCer in germ cells and sperm, although GBA2 is not expressed in these cell types, at least not in detectable amounts.

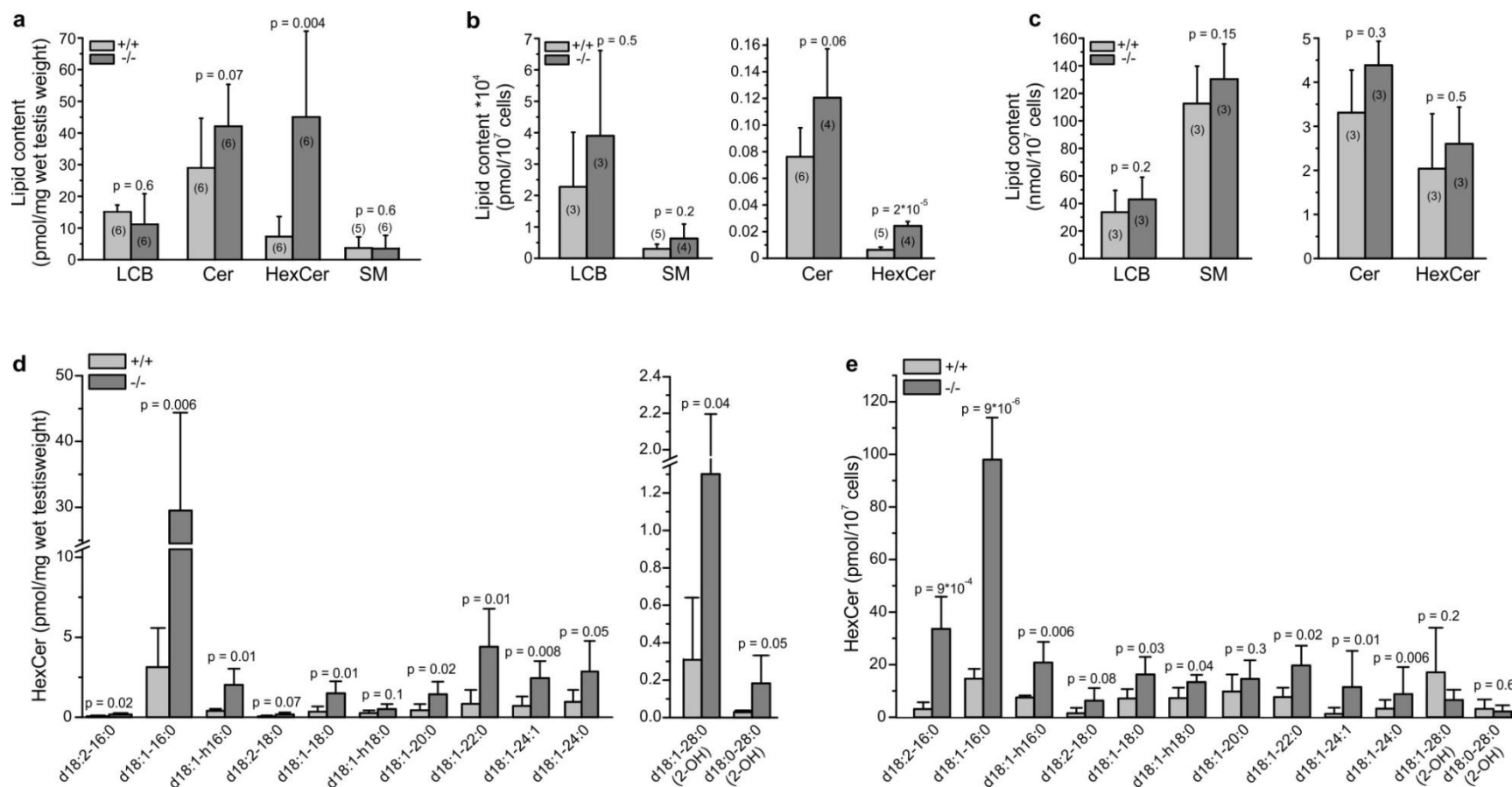


Figure 11. Quantitative analysis of lipid content. (a) Quantitative mass spectrometric analysis of long-chain bases (LCB), ceramides (Cer), hexosylceramides (HexCer), and sphingomyelin (SM) in wild-type (+/+) and GBA2 knockout (-/-) testis. (b) See (a) for sperm. (c) See (a) for P7 Sertoli cells. (d) Quantitative lipid profiles of HexCer with different chain lengths from wild-type (+/+) and GBA2 knockout-testis (-/-). (e) See (d) for sperm. Data are presented as mean \pm S.D.; n numbers and p values determined using One-way ANOVA are indicated.

4.6. Loss of GBA2 causes cytoskeletal defects in testis

Sperm from GBA2 knockout-mice display globozoospermia [30]. However, the molecular mechanism underlying this defect is not known. Shaping of the sperm head depends on cytoskeletal rearrangements in Sertoli cells and developing spermatids [64]. To investigate whether defects in the cytoskeleton underlie defects in sperm-head formation, I analyzed the actin and tubulin cytoskeleton in wild-type and GBA2 knockout-testis using fluorescently-tagged phalloidin and an anti-tubulin antibody (Figure 12a). While the organization of actin bundles around the sperm heads in wild-type testis followed a clear sickle shape, the F-actin labeling in GBA2 knockout-testis appeared augmented and the actin bundles around sperm heads were severely disorganized (Figure 12a).

To determine the cellular origin of this defect, germ and Sertoli cells were isolated from adult wild-type and GBA2 knockout-testis. To distinguish between Sertoli cells and germ cells, the Sertoli cell-specific marker tubulin III was used. Immunocytochemistry revealed that both the actin and tubulin network was more extensive in Sertoli cells from GBA2 knockout-testis (Figure 12b).

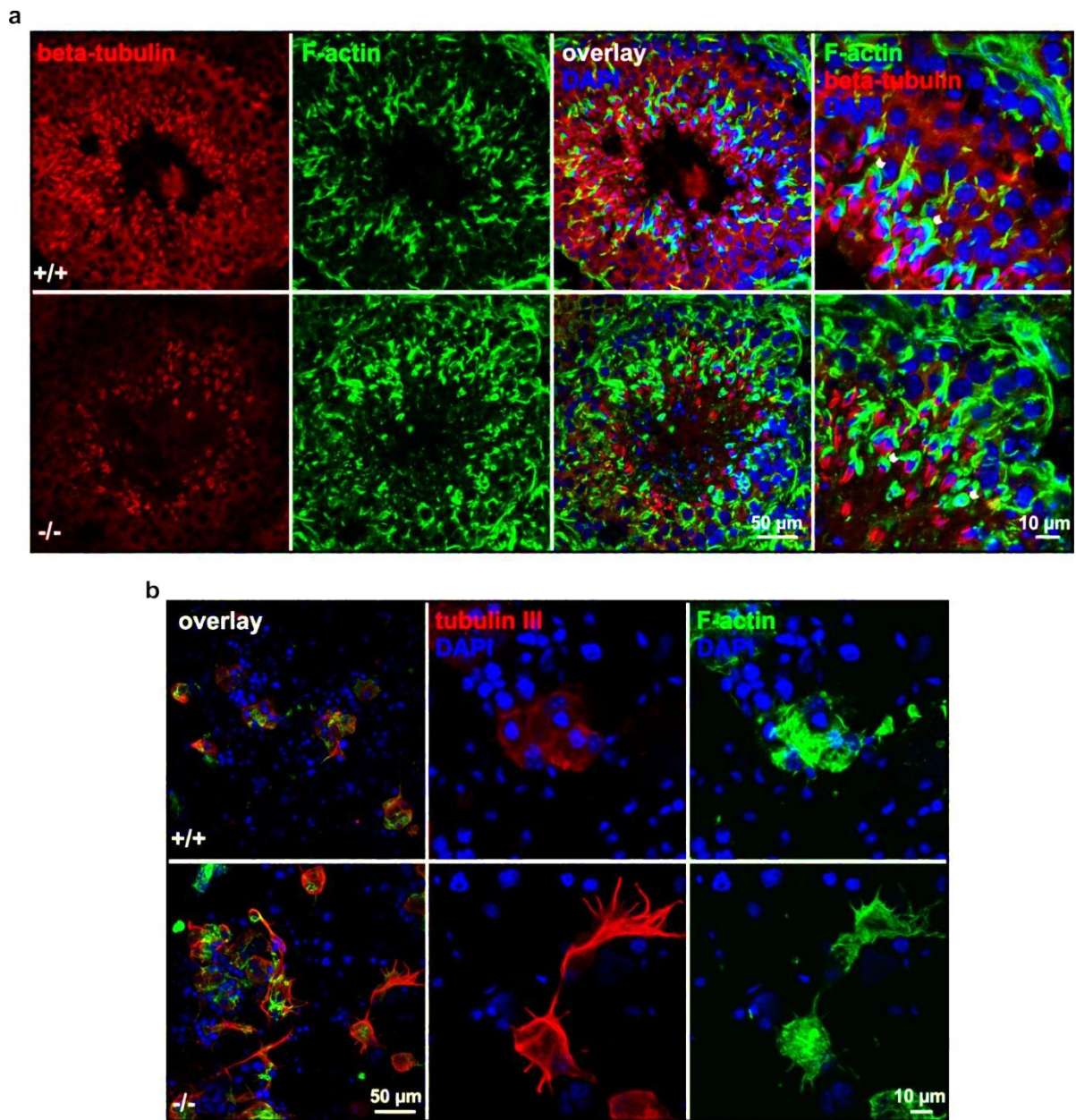


Figure 12. Cytoskeletal defects in adult GBA2 knockout-testis. (a) Testis cross-sections of adult wild-type (+/+) and GBA2 knockout-mice (-/-) labeled with a beta-tubulin antibody (*red*), phalloidin (*green*) to visualize F-actin, and DAPI (*blue*) to label the DNA. The ES is indicated by arrows. Scale bars: overview: 50 μm , zoom-in: 10 μm . **(b)** Germ and Sertoli cells isolated from wild-type (+/+) and GBA2 knockout-mice (-/-) labeled with an anti-tubulin III (*red*) antibody, phalloidin (*green*), and DAPI (*blue*). Scale bars: overview: 50 μm , zoom-in: 10 μm .

4.7. Cytoskeletal defects develop in the first spermatogenic wave

According to its expression and activity, GBA2 is particularly important during the first spermatogenic wave (Figure 10). Thus, I analyzed whether the cytoskeletal defects already develop in the first spermatogenic wave. To compare the first spermatogenic wave between wild-type and GBA2 knockout-mice, four different time points were analyzed: P7, P21, P23, and P34 (Figure 13).

Immunohistochemical analysis of F-actin and microtubules in testis cross-sections did not show a difference between wild-type and GBA2 knockout-testis at P7 (P7, Figure 13). At P21, in wild-type testis, F-actin was mainly present at the blood-testis barrier and at the junctions between Sertoli cells and germ cells (P21, Figure 13). However, in GBA2 knockout-testis, only the F-actin structures lining the blood-testis barrier were formed, but those around the junctions appeared disturbed (P21, Figure 13). This defect was even more pronounced at P23 (P23, Figure 13). At P34, in wild-type testis, F-actin forms the ectoplasmic specialization (ES) embracing the sickle-shaped sperm heads. However, in GBA2 knockout-testis, distinct F-actin-based structures surrounding the sperm heads were absent and the sperm heads appeared deformed (P34, Figure 13).

These results show that during the first spermatogenic wave, defects in the actin cytoskeleton first appear at P21, which correlates with the peak in GBA2 expression and activity around puberty (Figure 10c, d).

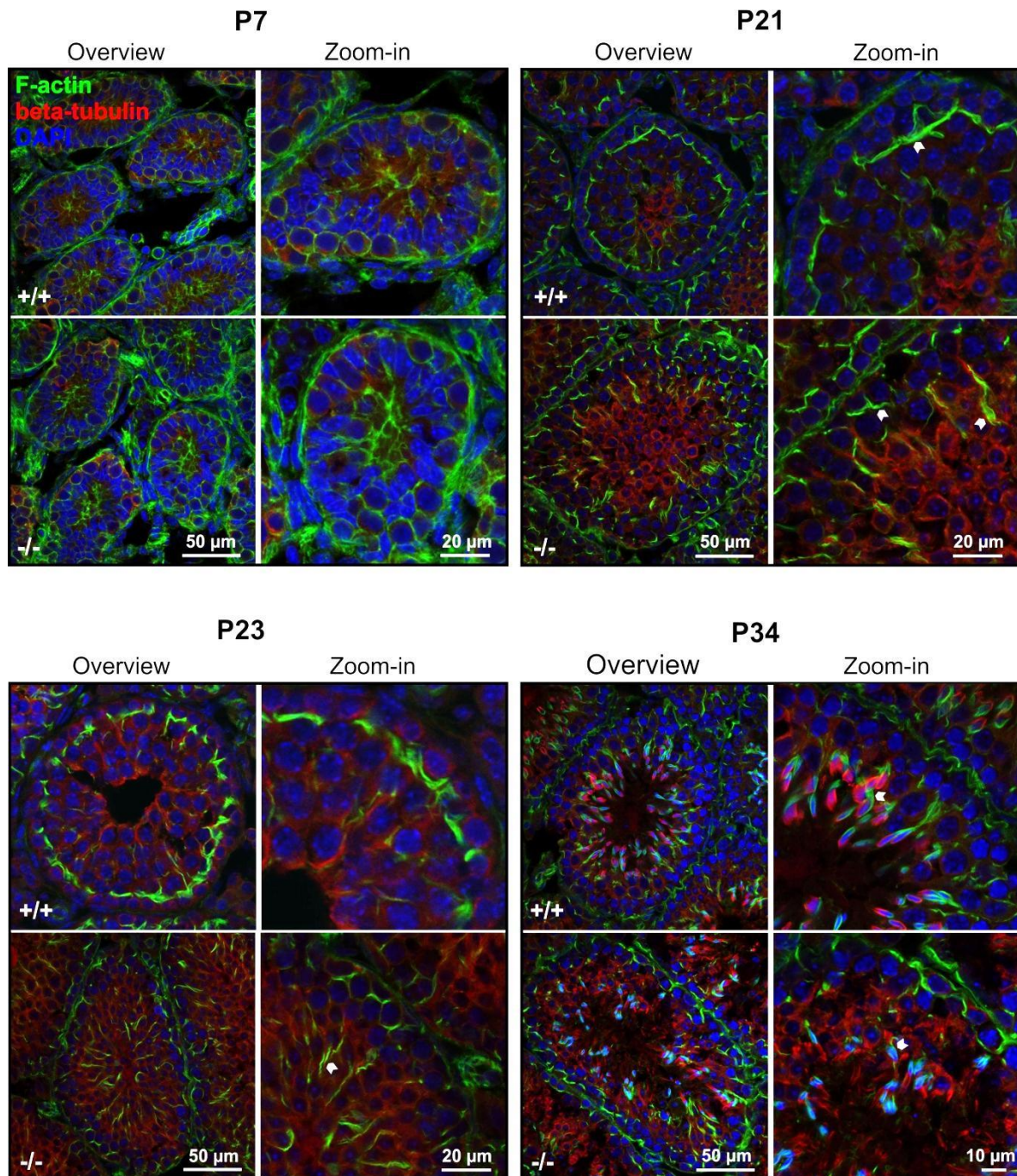


Figure 13. Analysis of cytoskeletal defects in the first wave of spermatogenesis. Testis cross-sections from P7, P21, P23, and P34 wild-type (+/+) and GBA2 knockout-mice (-/-) stained with phalloidin to visualize F-actin (*green*), a beta-tubulin antibody (*red*), and DAPI to label the DNA (*blue*). F-actin at the blood-testis barrier, junctions between Sertoli-Sertoli and Sertoli-germ cells, and the ectoplasmic specialization (ES) are indicated by arrows. Scale bar: overview: 50 μm ; zoom-in: 20 μm .

4.8. GBA2 knockout-spermatids contain longer microtubule manchettes

Immunohistochemical analysis of individual spermatid microtubule structures in testis-sections is difficult, because the developing sperm are tightly packed within seminiferous tubules (Figure 13). To analyze microtubule structures in more detail, germ cells were isolated and microtubules were immunocytochemically analyzed (Figure 14b). During spermatid elongation, the microtubule cytoskeleton forms a manchette around the neck of the sperm head just below the acrosome [56] [64]. Movement of the manchette towards the flagellum generates forces sufficient to shape the post-acrosomal region of the sperm head (Figure 14a) [58] [59]. Thus, I compared the development of the manchette in wild-type and GBA2 knockout-mice (Figure 14b). Wild-type spermatids developed a symmetric, conical-shaped manchette that regressed with the progression of spermatogenesis (Figure 14b). However, in GBA2-knockout spermatids, microtubules of the manchette persisted and did not regress even at stage XIV of spermatogenesis (Figure 14b). When the length of the microtubule manchettes between stages IX – XIV of spermatogenesis was measured, GBA2-knockout spermatids displayed significantly longer manchettes than wild-type spermatids (wild-type: $5.2 \pm 0.6 \mu\text{m}$ vs. GBA2 knockout: $11.2 \pm 0.9 \mu\text{m}$; Figure 14c). Thus, accumulation of GlcCer in the absence of GBA2 seems to affect the actin cytoskeleton in Sertoli cells and the microtubule cytoskeleton in germ cells.

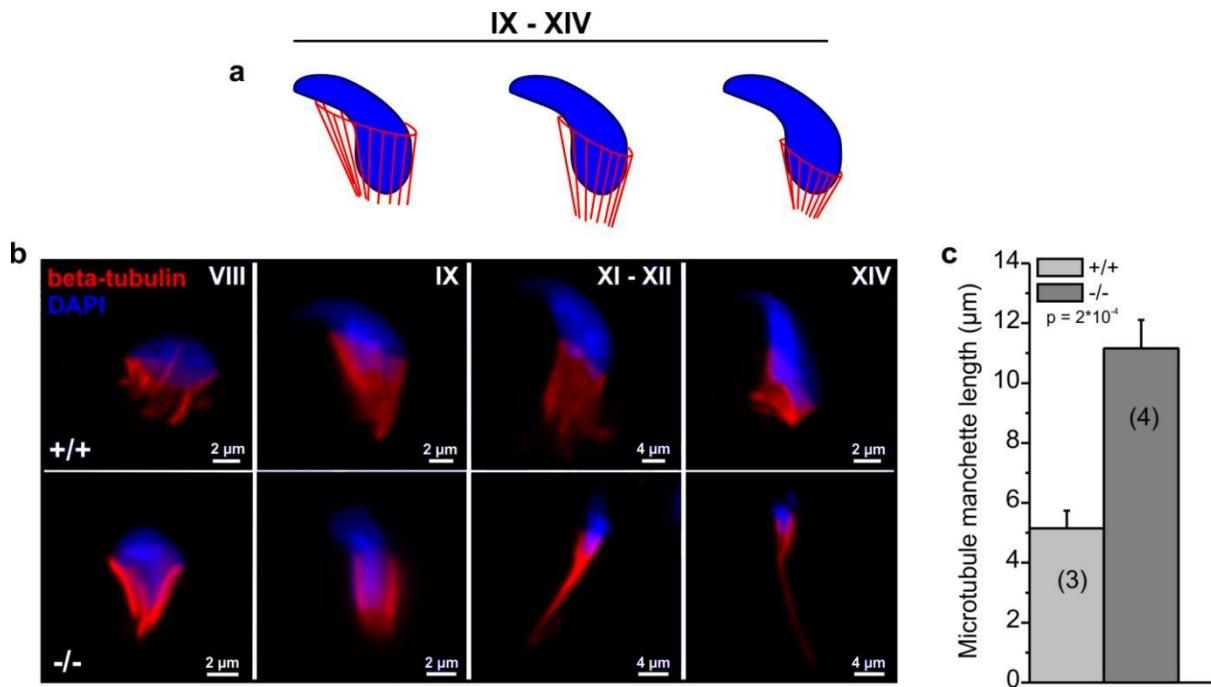


Figure 14. Development of the sperm manchette in wild-type and GBA2 knockout-mice. (a) The manchette consists of a perinuclear ring attached to several vertical microtubules (red) around the spermatid head (blue). The downward motion of the manchette is responsible for shaping the post-acrosomal region of the sperm head [59]. A schematic representation of the sperm manchette is shown for stages IX to XIV of spermatogenesis. (b) Germ cells isolated from wild-type (+/+) and GBA2 knockout-mice (-/-) were stained with an anti-beta tubulin antibody (red) and DAPI to label the DNA (blue). Stages VIII, IX, XI-XII, and XIV of spermatogenesis are shown. Scale bars are indicated. (c) Mean length of microtubule manchettes measured in wild-type (+/+) and GBA2 knockout-spermatids (-/-). Data is presented as mean \pm S.D.; n numbers and the p value determined using One-way ANOVA is indicated.

4.9. A defect in acrosome formation during the first spermatogenic wave results in globozoospermia in GBA2 knockout-mice

Globozoospermia is the main phenotypic defect in GBA2 knockout-mice [30]. The hallmark of globozoospermia is a malformed acrosome [45]. To test whether sperm of the first spermatogenic wave from GBA2 knockout-mice already display a defect in acrosome formation, I analyzed sperm from wild-type and GBA2 knockout-mice at P34 using immunocytochemistry. Indeed, GBA2 knockout-sperm showed a severely deformed acrosome (Figure 15a).

To test whether the defect in acrosome formation develops due to the cytoskeletal, I analyzed acrosome formation in wild-type and GBA2 knockout-mice during the first spermatogenic wave (Figure 15c). Acrosome formation is characterized by three major phases: the Golgi phase, the cap phase, and the acrosome phase (Figure 15b).

I followed acrosome formation immunohistochemically using fluorescently-tagged lectin from peanut. Peanut lectin binds carbohydrate moieties on the outer membrane of the acrosome [87]. In the Golgi phase of wild-type testis, proacrosomal vesicles had already fused to form the acrosomal vesicle. However, in GBA2 knockout-testis, proacrosomal vesicles remained dispersed (P21, Figure 15c). Furthermore, in the cap phase of wild-type testis, the acrosomal vesicle formed a cap-like structure around the nucleus. However, in GBA2 knockout-testis, formation of the cap-like structure was incomplete (P23, Figure 15c). Finally, in the acrosome phase, well defined, sickle-shaped acrosomes were formed around the spermatid heads in wild-type testis, whereas in GBA2 knockout-testis, many spermatids lacked an acrosome and only a few contained acrosome-like structures (P34, Figure 15c). Thus, the defects in acrosome formation and the cytoskeleton in GBA2 knockout-mice are evident at the same time-point during the first spermatogenic wave and correlate with the peak in GBA2 expression and activity in wild-type mice.

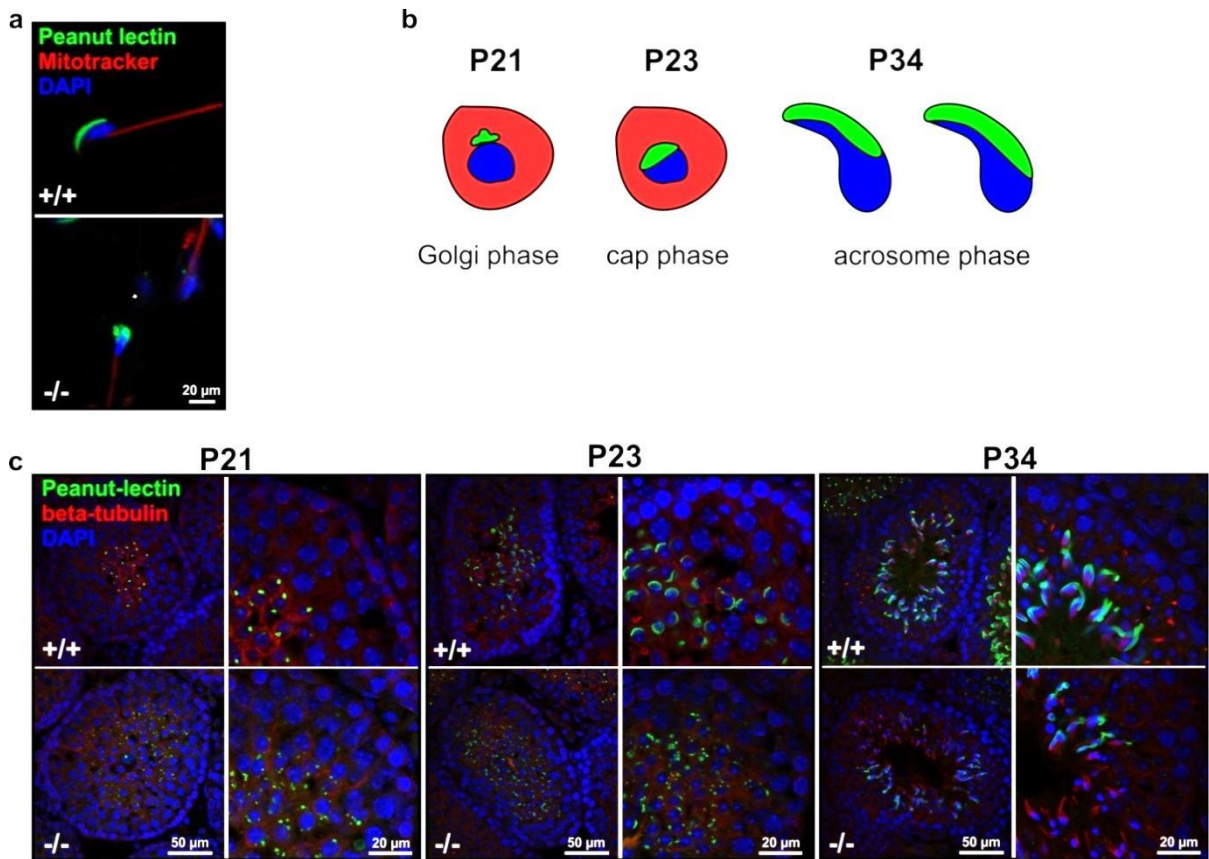


Figure 15. Acrosome formation. (a) P34 Wild-type (+/+) and GBA2 knockout-sperm (-/-) isolated from P34 mice labeled with FITC tagged-peanut lectin (*green*) to visualize the acrosome, mitotracker (*red*) to label the mitochondria, and DAPI (*blue*) to label the DNA. Scale bar: 20 μm . (b) At P21, in the Golgi phase, vesicles from the trans-Golgi network fuse at one pole of the nucleus (*blue*) to form a single large vesicle that attaches to the nucleus. At P23, in the cap phase, the acrosomal vesicle flattens over the nuclear membrane, forming a semi-circular cap-like structure around the spermatid head. At P34, in the acrosome phase, the cap-like structure stretches over the spermatid [47] [88]. (c) Testis cross-sections from P21, P23, and P34 wild-type (+/+) and GBA2 knockout-mice (-/-) labeled with peanut-lectin to label the acrosome (*green*), an anti-beta tubulin antibody (*red*), and DAPI to visualize DNA (*blue*). Scale bar: overview: 50 μm ; zoom-in: 20 μm .

In summary, accumulation of GlcCer in Sertoli and germ cells in the absence of GBA2 disturbs cytoskeletal structures during sperm development. In turn, this seems to impair acrosome and sperm-head formation resulting in globozoospermia.

4.10. Dermal fibroblasts as a model system

Next, I wanted to investigate the molecular mechanisms underlying the cytoskeletal defects during accumulation of GlcCer. However, isolated germ and Sertoli cells are difficult to culture and manipulate, rendering a detailed analysis of cytoskeletal dynamics difficult. However, GBA2 is also expressed in the skin [30], and dermal fibroblasts from adult mice are easy to maintain and manipulate in culture. Therefore, I tested whether dermal fibroblasts could be used as a model system to study cytoskeletal dynamics.

Western-blot analysis of protein lysates from wild-type fibroblasts showed a GBA2-specific band, which was absent in protein lysates from GBA2 knockout-fibroblasts, demonstrating that GBA2 is expressed in dermal fibroblasts (Figure 16a). Using thin layer chromatography (TLC) (conducted by Sophie Schonauer, caesar), we could demonstrate that GlcCer accumulated in GBA2 knockout-fibroblasts (Figure 16b, c). Most importantly, GBA2 knockout-fibroblasts also displayed cytoskeletal defects: organization of the microtubule and actin cytoskeleton was dramatically altered, resulting in a change in morphology compared to wild-type fibroblasts (Figure 16d). Thus, dermal fibroblasts from adult mice qualify as a good model system to study the effects of GlcCer accumulation on cytoskeletal dynamics.

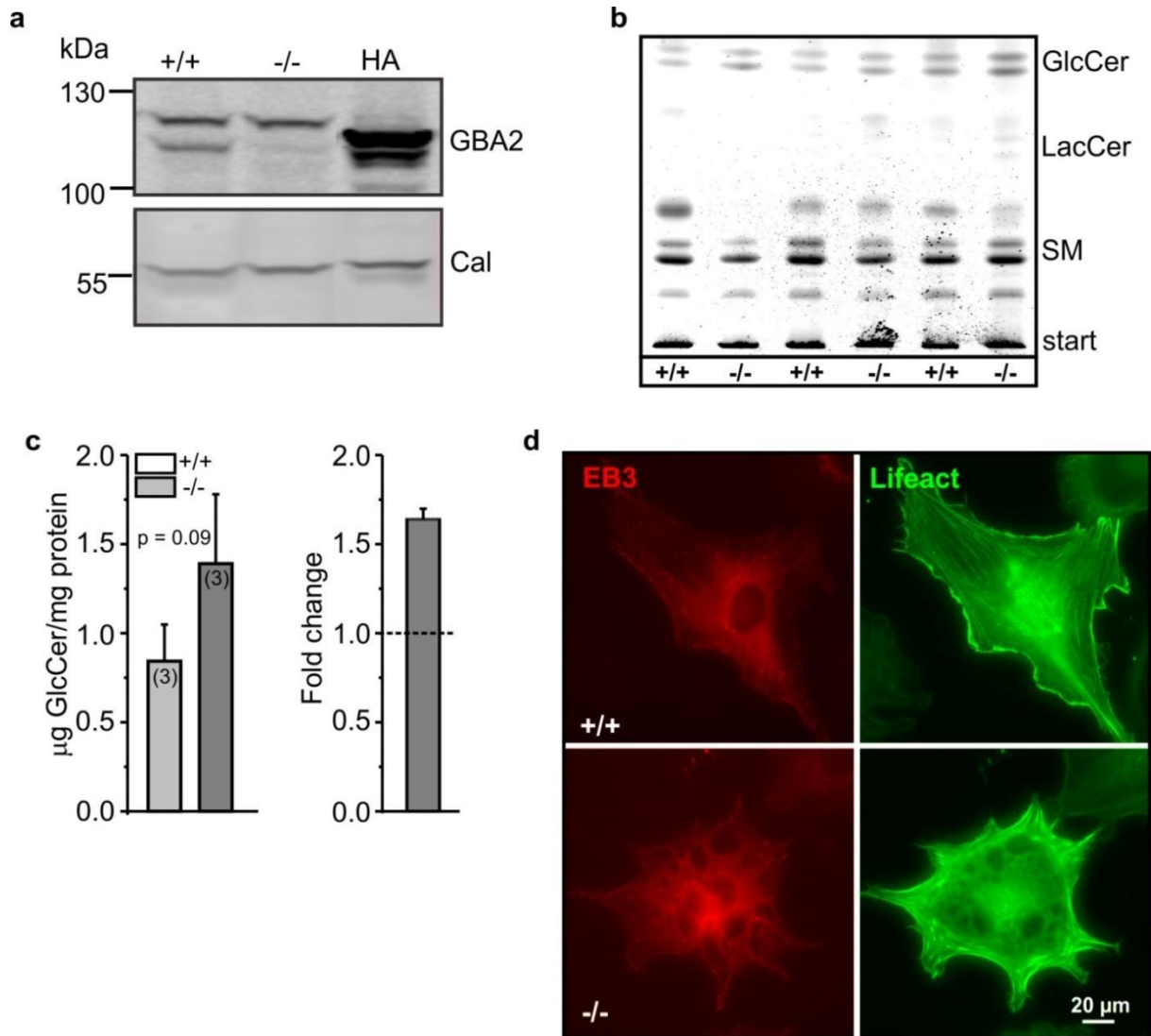


Figure 16. Mouse dermal fibroblasts as a model system. (a) Western-blot analysis of wild-type (+/+) and GBA2 knockout-fibroblasts (-/-). The blot was probed with the GBA2-specific 2F8 antibody. Protein lysates from HEK293 cells expressing GBA2-HA (HA) were used as a positive control and calnexin (Cal) served as a loading control. **(b)** Thin layer chromatograph of wild-type (+/+) and GBA2 knockout-fibroblasts (-/-). Levels of glucosylceramide (GlcCer), lactosylceramide (LacCer), and sphingomyelin (SM) have been analyzed. **(c)** Left: quantification of GlcCer in wild-type (+/+) and GBA2

knockout-fibroblasts (-/-). Right: relative change in GlcCer levels in GBA2 knockout compared to wild-type fibroblasts (indicated by the dotted line). **(d)** Fluorescent labeling of the cytoskeleton in dermal fibroblasts isolated from wild-type (+/+) and GBA2 knockout-mice (-/-). Cells were transfected with lifeact-GFP (*green*) to label actin and EB3-mcherry (*red*) to label the plus-tips of microtubules. Scale bar: 20 μ m. All data are presented as mean \pm S.D.; n numbers and p values calculated using One-way ANOVA are indicated.

4.11. GlcCer accumulation in the absence of GBA2 affects actin dynamics

To analyze how accumulation of GlcCer in the absence of GBA2 affects cytoskeletal dynamics, I first analyzed the actin dynamics. Since dermal fibroblasts in culture are morphologically heterogeneous, comparative analysis of their cytoskeleton is difficult. Therefore, wild-type and GBA2 knockout-fibroblasts were forced to acquire a specific morphology by seeding them onto glass-slides with fibronectin-coated micro-patterns. Four different shapes of micro-patterns were used: disc, cross-bow, dumb-bell, and Y (Figure 17a).

Immunofluorescent labelling of F-actin revealed dramatic differences: the F-actin network in GBA2 knockout-fibroblasts was more extensive and showed protruding F-actin structures (filopodia and lamellipodia) at the periphery. This effect was more pronounced on the cross-bow and disc micro-patterns (Figure 17a). Quantification of filopodia and lamellipodia revealed that GBA2 knockout-fibroblasts contain more filopodia and lamellipodia per cell compared to the wild-type fibroblasts. While wild-type fibroblasts contained 0.99 ± 0.3 filopodia and 1.76 ± 0.41 lamellipodia per cell, GBA2 knockout-fibroblasts contained 1.62 ± 0.47 filopodia and 3.08 ± 0.20 lamellipodia per cell (Figure 17b).

The formation of filopodia and lamellipodia depends upon actin polymerization [89] [90]. Therefore, the turnover rate of G-actin to F-actin in wild-type and GBA2 knockout-fibroblasts was determined as a measure of actin

polymerization. The ratio of F-actin to G-actin was higher in GBA2 knockout-fibroblasts (Figure 17c), indicating that an increase in actin polymerization underlies the increase in filopodia and lamellipodia formation. In principle, this assay can be applied to every cell type or tissue. Thus, I tested whether a difference in actin polymerization also underlies the cytoskeletal defects observed in GBA2 knockout-testis. However, the ratio of G-actin to F-actin was not different between wild-type and GBA2 knockout-testis, which could be due to the cellular heterogeneity in testis (Figure 17d).

Members of the Rho family of GTPases have been shown to be crucial for controlling actin dynamics. Cdc-42 and Rac1 regulate the formation of filopodia and lamellipodia, respectively [91] [92] [93] [94]. To investigate if a change in the expression level of Cdc42 or Rac1 underlies the increase in filopodia and lamellipodia formation observed in GBA2 knockout-fibroblasts, I first determined their mRNA expression levels using quantitative real-time PCR. The mRNA levels for both *Cdc-42* and *Rac1* were increased in GBA2 knockout compared to wild-type fibroblasts (*Cdc-42*: 1.24 ± 0.15 ; *Rac1*: 1.22 ± 0.11) (Figure 17e). However, this change was not translated to a change in protein expression - Cdc-42 and Rac1 protein expression-levels were similar between wild-type and GBA2 knockout-fibroblasts (Figure 17g, h). Hence, a change in protein expression of the key regulators, the Rho GTPases Cdc-42 and Rac1, does not seem to underlie the increase in filopodia and lamellipodia formation in GBA2 knockout-fibroblasts.

In testis, Rho GTPases regulate the cytoskeletal dynamics at the ectoplasmic specialization [95]. In GBA2 knockout-mice, formation of the apical ectoplasmic specialization is impaired (Figure 12a). Thus, I also analyzed mRNA expression levels of *Cdc-42* and *Rac1* in testis. However, no change in the expression of *Cdc-42* and *Rac1* was observed in GBA2 knockout compared to wild-type mice (Figure 17f). Nectin 2 has also been shown to control actin dynamics at the ectoplasmic specialization [70]. However, its mRNA expression level was also not different between wild-type and GBA2 knockout-testis (Figure 17f). Thus, changes in

expression of *Cdc-42*, *Rac1* or *nectin 2* do not seem to underlie the defects in the actin cytoskeleton of GBA2 knockout-testis.

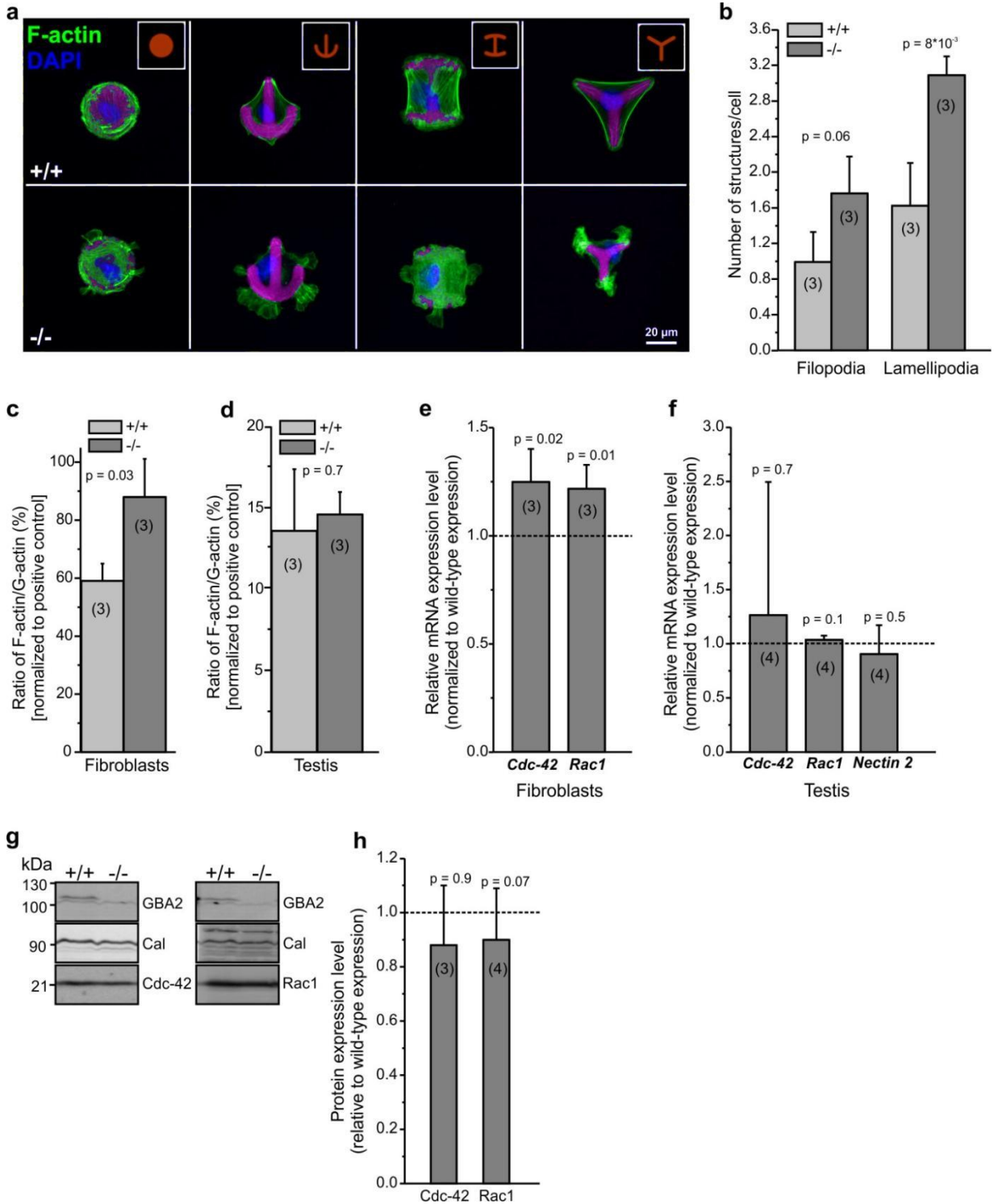


Figure 17. Analysis of the molecular mechanism underlying the defects in the actin cytoskeleton in GBA2 knockout-mice. (a) Immunofluorescent labeling of F-actin using phalloidin (*green*) in wild-type (+/+) and GBA2 knockout-fibroblasts (-/-) seeded on disc, crossbow, dumb-bell, and Y-shaped micropatterns coated with fluorescently-labeled fibronectin (*purple*). The DNA has been labeled using DAPI (*blue*). Scale bar: 20 μm . **(b)** Average numbers of filopodia and lamellipodia per cell in wild-type (+/+) and GBA2 knockout-fibroblasts (-/-). **(c)** Quantification of G-actin to F-actin turnover in wild-type (+/+) and GBA2 knockout-fibroblasts (-/-) by Western-blot analysis. **(d)** See (c) for testis. **(e)** mRNA expression levels of *Cdc-42* and *Rac1* in GBA2 knockout-fibroblasts relative to wild-type fibroblasts (indicated by black dotted line). **(f)** mRNA expression levels of *Cdc-42*, *Rac1*, and *Nectin 2* in GBA2 knockout-testis relative to wild-type testis (indicated by black dotted line). **(g)** Protein expression-levels of *Cdc-42* and *Rac1* in wild-type (+/+) and GBA2 knockout-fibroblasts (-/-) using Western-blot analysis. Calnexin (Cal) was used as a loading control. **(h)** Quantification of protein expression-levels of *Cdc-42* and *Rac1* in GBA2 knockout-fibroblasts relative to wild-type fibroblasts (indicated by black dotted line). All data are represented as mean \pm S.D. 'n' numbers and p values determined using One-way ANOVA are indicated.

4.12. GlcCer accumulation in the absence of GBA2 affects microtubule dynamics

Since microtubules in the sperm manchette of GBA2 knockout-mice persisted longer than in wild-type mice (Figure 18b, c), the microtubule dynamics of wild-type and GBA2 knockout-fibroblasts were studied in greater detail using live-cell imaging. To visualize growing microtubules, fibroblasts were transfected with a fluorescently-tagged EB3 probe. EB3 binds to the plus-ends of growing microtubules, which allows to determine the growth rate and persistence of microtubules using the Metamorph image-analysis software [96] (Figure 18a). While the microtubule growth-rate was similar between wild-type and GBA2 knockout-fibroblasts

(+/+: $16.4 \pm 6.3 \mu\text{m}/\text{min}$; -/-: $19.7 \pm 6.9 \mu\text{m}/\text{min}$), microtubule persistence in GBA2 knockout-fibroblasts was increased (+/+: $13.3 \pm 5.6 \mu\text{m}$; -/-: $16.1 \pm 6.9 \mu\text{m}$) (Figure 18b, c). These results indicate that accumulation of GlcCer in the absence of GBA2 prolongs the persistence of microtubules in dermal fibroblasts.

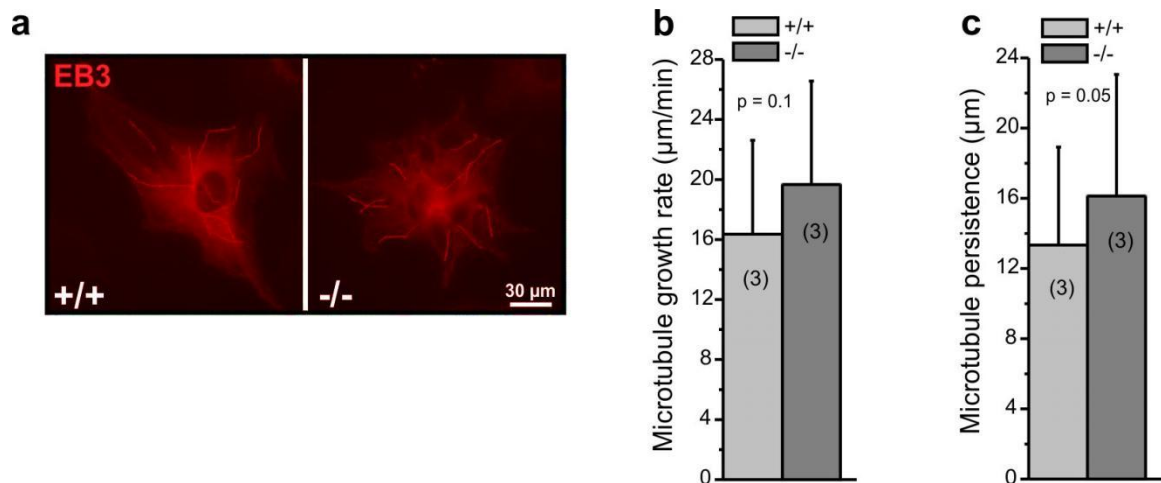


Figure 18. Microtubule dynamics in GBA2 knockout-fibroblasts. (a) Expression of mcherry-tagged EB3 (red) in wild-type (+/+) and GBA2 knockout-fibroblasts (-/-). EB3 labels the plus-tips of growing microtubules. Representative microtubule tracks (red) that were used to quantify microtubule dynamics are marked. Scale bar: 30 μm (b) Quantification of microtubule growth rate in wild-type (+/+) and GBA2 knockout-fibroblasts (-/-). Per genotype, 3 animals were used and at least 7 cells per animal were analyzed. (c) See (b) for microtubule persistence. All data are represented as mean ± S.D. n numbers and p values determined using One-way ANOVA are indicated.

4.13. GlcCer accumulation augments lipid stacking in the plasma membrane

Glycosphingolipids in the membrane are organized in microdomains that possess specialized signaling functions [97] [98]. GlcCer is incorporated into the inner leaflet of the plasma membrane [99]. I hypothesized that in the absence of GBA2, accumulation of GlcCer alters the stacking of lipids in the plasma membrane, thereby affecting the function of proteins that control cytoskeletal dynamics. To analyze lipid stacking, giant plasma-membrane vesicles (GPMV) were isolated from wild-type and GBA2 knockout-fibroblasts and the phase separation was spectrophotometrically measured using Laurdan. Laurdan is a fluorescent membrane dye that displays spectral sensitivity to solvent relaxation effects [100]. A red shift in the emission spectrum occurs when the membrane has a liquid-crystalline (disordered) phase, whereas the emission is shifted to the blue range when the membrane has a gel-like (ordered) phase (Figure 19a) [101]. GPMVs isolated from wild-type fibroblasts displayed a laurdan emission peak at 460 nm, whereas GPMVs from GBA2 knockout-fibroblasts showed an emission peak around 440 nm (Figure 19b). Changes in the emission spectrum can be quantified by the generalized polarization (GP) index [102]. The GP value for GBA2 knockout-fibroblasts was significantly higher than for wild-type fibroblasts (+/+ : 0.12 ± 0.03 ; -/- : 0.24 ± 0.03 ; Figure 19c). These observations demonstrate that the accumulation of GlcCer in GBA2 knockout-fibroblasts results in a highly ordered lipid stacking in the plasma membrane. This, in turn, could affect the function of proteins in the plasma membrane, e.g. of proteins that control cytoskeletal dynamics.

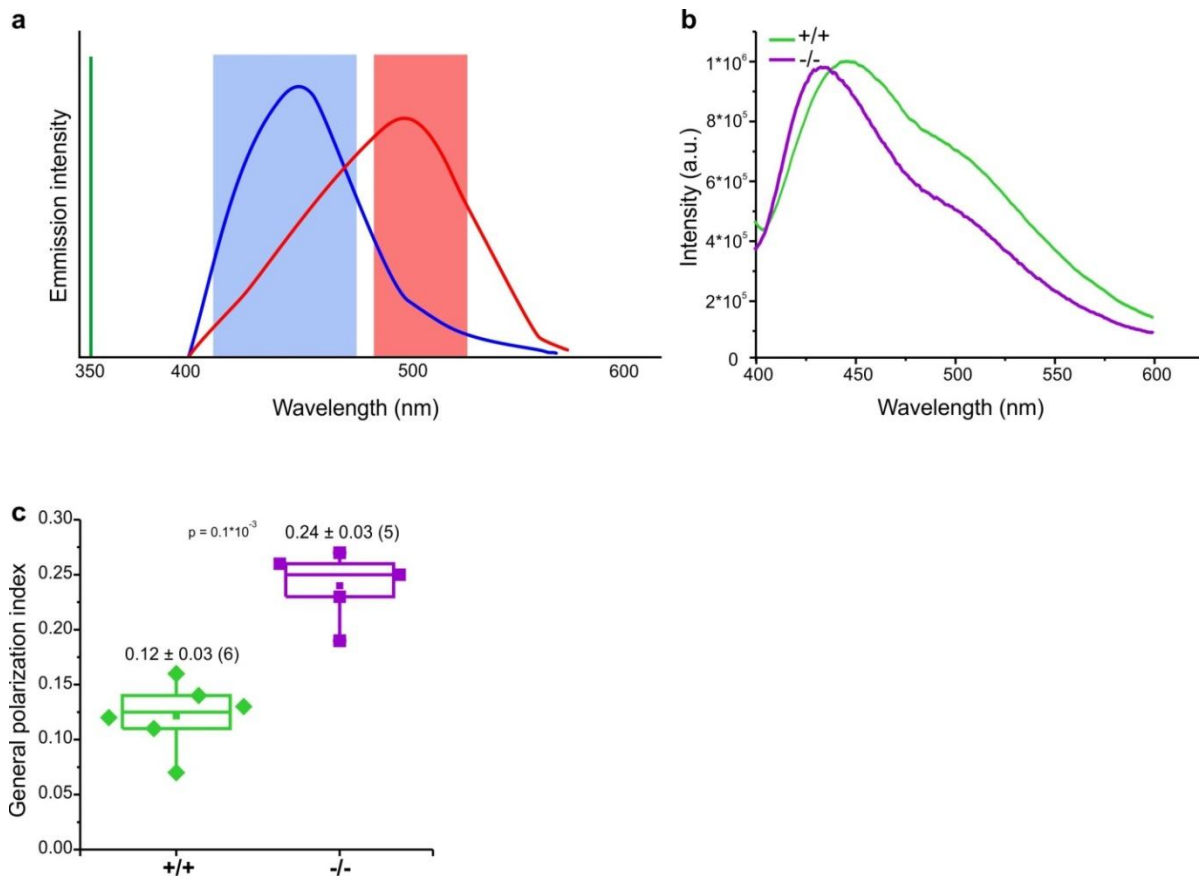


Figure 19. GlcCer accumulation leads to a highly ordered lipid stacking in the plasma membrane. (a) Schematic representation of the fluorescence properties of Laurdan. The dye is excited at 350 nm (indicated by the *green* line), and emission peaks at around 450 nm (*blue*), when residing in the ordered phospholipid phase and shifts to around 500 nm (*red*) when the dye resides in a more disordered phospholipid phase [103]. **(b)** Representative emission spectra of Laurdan measured in GPMVs isolated from wild-type (+/+; *green*) and GBA2 knockout-fibroblasts (-/-; *purple*). **(c)** Generalized polarization index calculated from Laurdan measurements presented in (b); wild-type: +/+; green, GBA2 knockout-fibroblasts: -/-; purple. Individual data points are represented along with the mean \pm S.D.; n numbers and p value determined by One-way ANOVA are also indicated.

4.14. GlcCer accumulation in the absence of GBA2 alters cellular behavior

Changes in the cytoskeleton affect cellular physiology. GlcCer has been proposed to induce proliferation [104]. Thus, I analyzed the proliferation rate of fibroblasts using bromodeoxyuridine (BrdU). BrdU is a thymidine analogue, which is incorporated into newly synthesized DNA strands of proliferating cells [105]. Fibroblasts were labeled with an anti-BrdU antibody and the rate of proliferation was determined by calculating the ratio of proliferating cells over the total number of cells (Figure 20a). The rate of BrdU incorporation was not significantly different between wild-type and GBA2 knockout-fibroblasts, indicating that increased GlcCer levels in GBA2 knockout-fibroblasts do not alter cellular proliferation (Figure 20b).

GBA2 knockout-fibroblasts display a higher number of lamellipodia (Figure 17b). Lamellipodia formation is a hallmark of migrating cells [106]. Thus, I analyzed cell migration of wild-type and GBA2 knockout-fibroblasts using a simple wound-healing assay (Figure 20c) [107]. The assay revealed that GBA2 knockout-cells migrated faster than wild-type fibroblasts, especially between 2-4 hours after starting the assay (Figure 20d).

These results indicate that the accumulation of GlcCer in the absence of GBA2 changes cellular cytoskeletal dynamics, and, thereby, cell behavior, as shown by an increase in cell migration.

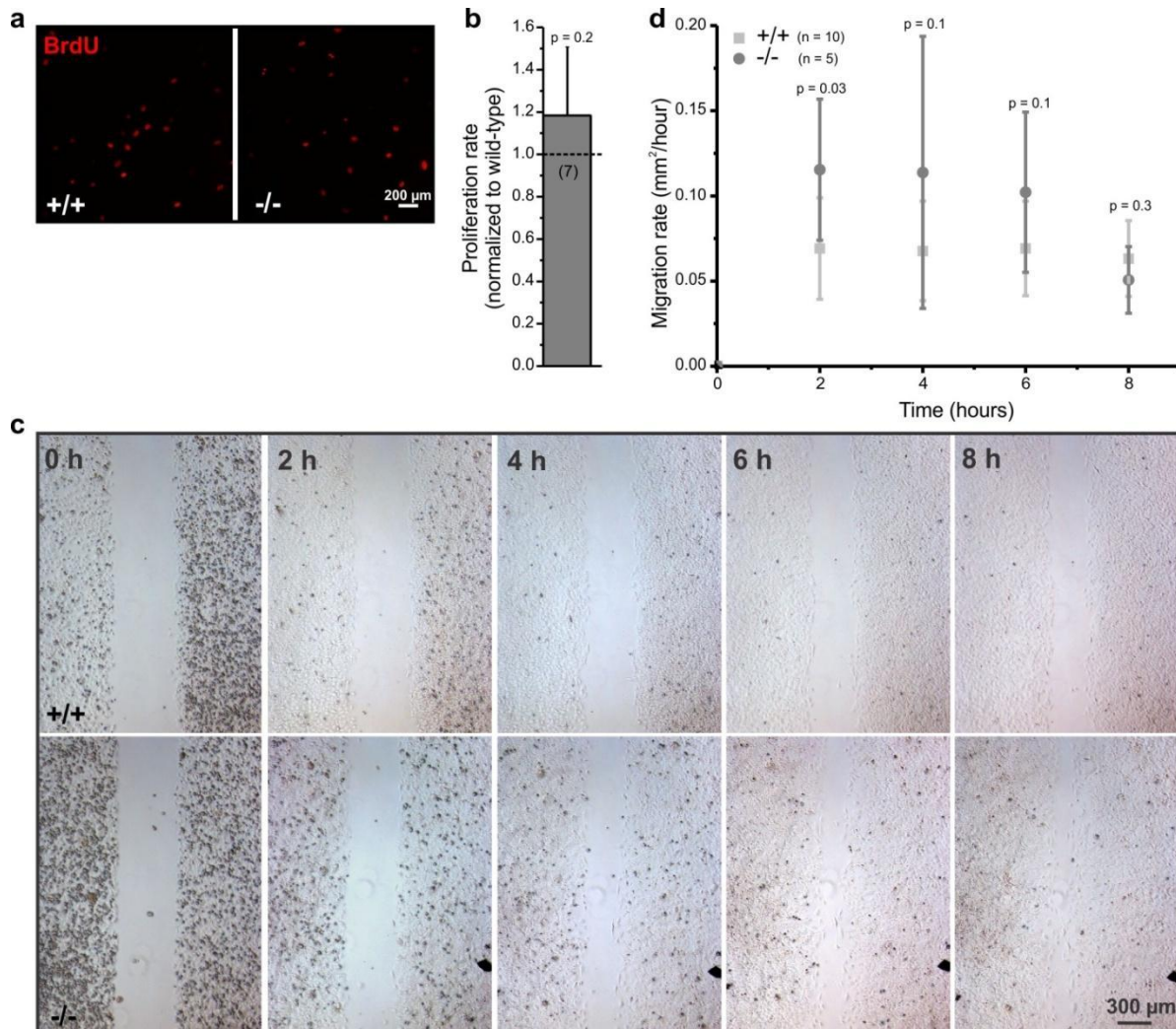


Figure 20. Analysis of cell proliferation and migration. (a) Wild-type (+/+) and GBA2 knockout-fibroblasts (-/-) were treated with BrdU for 8 hours and were labeled with an anti-BrdU antibody (red). Scale bar: 200 μ m. (b) Quantification of cellular proliferation determined by the rate of BrdU incorporation. The proliferation rate has been normalized to wild-type (indicated by black dotted line). (c) Representative images of wild-type (+/+) and GBA2 knockout-fibroblasts (-/-) in the wound-healing assay. (d) Quantification of migration rates of wild-type (+/+) and GBA2 knockout-fibroblasts (-/-) at the indicated time points. All data are represented as mean \pm S.D. n numbers and p values determined using One-way ANOVA are indicated.

4.15. NB-DNJ-mediated inhibition of GBA2 activity induces a similar cellular phenotype as observed in GBA2 knockout-fibroblasts

To verify whether the cellular defects observed in GBA2 knockout-fibroblasts are solely due to the loss of GBA2 and the consequent accumulation of GlcCer, the contribution of GBA2 in controlling cytoskeletal dynamics was independently assessed using *N*-butyldeoxynojirimycin (NB-DNJ), a blocker for GBA2 [108]. Wild-type fibroblasts were treated with 2 μ M NB-DNJ for 48 hours. Analysis of the enzyme activity showed that this treatment completely inhibited GBA2 activity, while the activity of GBA1 remained unchanged (Figure 21a). TLC analysis revealed that NB-DNJ treatment resulted in the accumulation of GlcCer (Figure 21a, b; experiments performed by Sophie Schonauer, caesar). Immunofluorescent labeling of the actin cytoskeleton demonstrated that the treated cells, similar to GBA2 knockout-fibroblasts, contained more actin protrusions compared to untreated wild-type cells (Figure 21c). Furthermore, NB-DNJ-treated fibroblasts also migrated faster than the untreated cells (Figure 21d). To determine if the NB-DNJ treatment also altered the plasma membrane stacking, Laurdan spectra were measured and GP values were calculated from GPMVs isolated from control and NB-DNJ-treated wild-type cells. The shift in the Laurdan spectrum of treated cells was similar to the shift in GBA2 knockout-fibroblasts. While the GP value for the untreated controls was 0.15 ± 0.06 , the treated wild-type cells displayed a GP value of 0.26 ± 0.07 (Figure 21e).

These results demonstrate that inhibition of GBA2 activity by NB-DNJ results in a similar cellular phenotype as observed in GBA2 knockout-fibroblasts. This emphasizes my earlier finding that loss of GBA2 leading to accumulation of GlcCer alters cytoskeletal dynamics in fibroblasts.

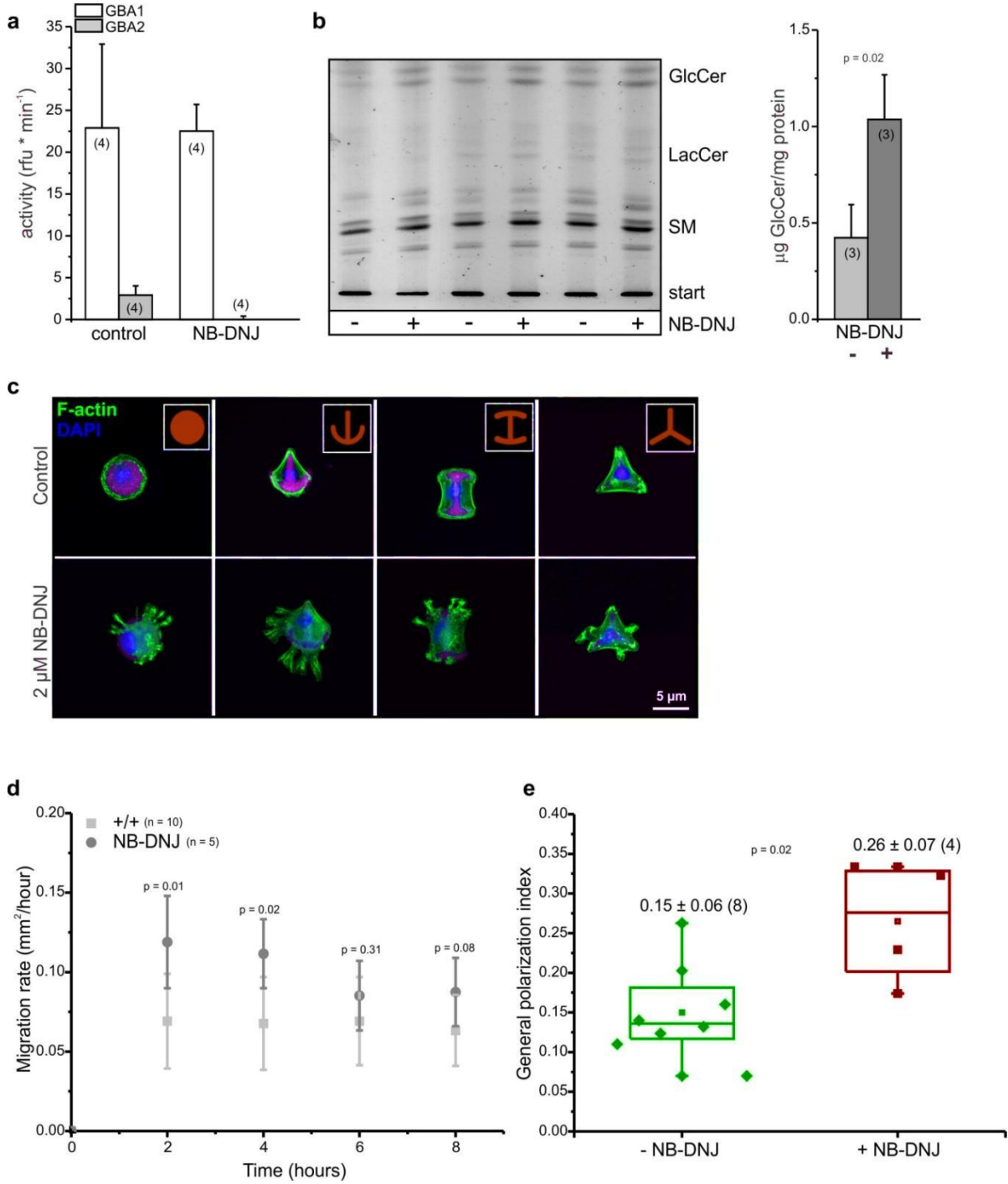


Figure 21. NB-DNJ treated wild-type fibroblasts display a GBA2 knockout-phenotype. **(a)** Beta-glucocerebrosidase activity of GBA1 (pH 4.0) and GBA2 (pH 6.0) in wild-type fibroblasts treated with 2 μ M NB-DNJ for 48 hours and untreated control cells. **(b)** Left: thin-layer chromatograph of wild-type fibroblasts treated with 2 μ M NB-DNJ (+) and the corresponding untreated controls (-). Levels of sphingomyelin (SM), lactosylceramide (LacCer), and glucosylceramide (GlcCer) have been analyzed. Right: quantification of GlcCer from left. **(c)** Immunofluorescent labeling of F-actin (phalloidin, *green*) and DNA (DAPI, *blue*) in untreated and NB-DNJ-treated (2 μ M) wild-type fibroblasts. Scale bar: 5 μ m. **(d)** Quantification of migration rates of NB-DNJ-treated wild-type fibroblasts (2 μ M; *NB-DNJ*) and untreated controls (+/+) at different time points in wound-healing assay. **(e)** Generalized polarization index calculated from laurdan emission spectra of wild-type fibroblasts treated with 2 μ M NB-DNJ for 48 hours: + NB-DNJ, untreated control fibroblasts: - NB-DNJ. Individual data points are represented along with the mean \pm S.D.; 'n' numbers and p values determined by One-way ANOVA are indicated.

In summary, my results demonstrate that GBA2 is expressed in Sertoli cells. In the absence of GBA2, GlcCer accumulates in Sertoli cells, germ cells, and sperm. This alters the cytoskeletal dynamics of F-actin at the apical ES in Sertoli cells and the microtubule manchette in spermatids. Furthermore, using dermal fibroblasts as a model system, my results provide a mechanistic insight into how accumulation of non-lysosomal GlcCer in the absence of GBA2 affects cytoskeletal dynamics. Accumulation of GlcCer leads to a highly ordered lipid packaging in the plasma membrane, which could influence protein function in the plasma membrane. In particular, proteins controlling cytoskeletal dynamics seem to be sensitive to this change in the lipid environment, resulting in a defect in the actin and microtubule cytoskeleton. This could also feed-back on vesicle fusion in developing germ cells, leading to deformed acrosomes responsible for globozoospermia in GBA2 knockout-mice.

5. Discussion

My work demonstrates that in the absence of GBA2, GlcCer accumulates leading to a highly ordered lipid stacking in the plasma membrane. This in turn seems to affect the function of membrane proteins that regulate cytoskeletal dynamics. This effect is most prominent in the testis of GBA2 knockout-mice, where the cytoskeletal structures that shape the sperm head are disturbed causing globozoospermia and, thereby, a defect in fertility.

5.1. Implications of the subcellular localization of GBA2 and GlcCer

To understand the physiological function of GBA2, it is important to analyze its subcellular localization. Our results demonstrate that GBA2 is not a transmembrane protein, but rather associated with the Golgi and the ER membrane from the cytosolic side [26]. What is the impact of this localization for GBA2 function? GlcCer is synthesized at the cytosolic side of the *cis*-Golgi and transported to the Golgi lumen and ER by GLTP/FAPP2 [8] [9]. Within the Golgi lumen, GlcCer is converted to LacCer and consequently to higher order glycosphingolipids [8]. The localization of GBA2 at the cytosolic side of the Golgi implies that GlcCer is degraded close to where it is synthesized. Hence, GBA2 could function as a fine tuner to regulate the level of GlcCer that is available for higher order glycosphingolipid synthesis.

An interesting observation is that in both GBA2 knockout-mice and mice treated with NB-DNJ the levels of sphingomyelin, LacCer, and higher order glycosphingolipids were not altered – only GlcCer levels were increased [30] [109]. Moreover, our lipid analyses underlined these results and revealed that also the levels of ceramide in GBA2 knockout-mice remained unchanged. Thus, an increase in GlcCer level does not change the levels of other glycosphingolipids or ceramide

although GlcCer serves as one of the main building blocks for higher order glycosphingolipids. These results suggest that lipid synthesis remains constant independent of the substrate availability. However, it could also mean that GlcCer, when it is accumulating, is not transported to the side of glycosphingolipid synthesis. Therefore, it is important to analyze where GlcCer accumulates in the cell. Does it accumulate at the place of degradation or is it transported to the plasma membrane and accumulate there? My results indicate that GlcCer accumulation in GBA2 knockout-cells causes a more ordered lipid stacking in the plasma membrane. This implies that GlcCer is incorporated into the plasma membrane. Using two-photon imaging, our lab is currently setting-up a technique to visualize, whether the change in lipid stacking occurs uniformly within the plasma membrane or if micro domains are formed. Furthermore, this imaging technique will also allow us to analyze, whether lipid stacking of intracellular membranes is also affected by accumulation of GlcCer. In addition, we are studying the subcellular localization of GlcCer accumulation in GBA2 knockout-cells using immunogold-labelling in combination with electron microscopy [110] [111] [112]. Our final goal is to visualize GlcCer accumulation and the changes in the membrane composition not only in single cells, but also in testis sections. This will allow us to further determine how GlcCer controls cellular function.

5.2. How does GlcCer accumulation in GBA2 knockout-mice lead to globozoospermia?

One of the main questions that I wanted to answer during my PhD thesis was how GlcCer accumulation affects cytoskeletal dynamics, in particular in the testis. Does the altered lipid stacking at the plasma membrane directly influence the underlying cytoskeleton or does it disturb signaling cascades controlling cytoskeletal dynamics? The assembly, stability, and function of membrane proteins relies on protein-lipid interactions in the bilayer. The chain length of the lipids in the bilayer and the density of their packing controls the activity of membrane proteins [113]. This has been shown for different proteins. Activity of the Ca^{2+} -ATPase, a calcium pump in skeletal muscle cells that transports Ca^{2+} ions across the ER membrane upon ATP hydrolysis, was low when the fatty acid acyl chains of the phospholipids surrounding the purified protein were shorter (C14) or longer (C20) than C16 – C18, the required chain length for optimal activity [114]. Furthermore, the activity was highest in the ordered phase of phospholipid packing and lower in the disordered phase [114]. The function of certain membrane proteins can be stimulated or inhibited by lipids acting as cofactors [115]. For the Ca^{2+} -ATPase, binding of phosphatidylinositol-4-phosphate to the inner region of the transmembrane domain results in doubling of the ATPase activity [116], whereas binding of phosphatidylserine inhibits the ATPase activity [117].

Glycosphingolipids have a propensity to form micro domains, which function as specialized signaling platforms [3]. The lipid raft hypothesis was proposed to explain the preferential segregation of glycosphingolipids to the apical region in polarized cells [18]. Lipid rafts are formed by the non-random assembly of membrane components such as cholesterol, proteins, and sphingolipids to form dynamic clusters also known as micro domains (Figure 22). Lipid rafts have been proposed to determine cell polarity, regulate signal transduction, sorting and trafficking of proteins through the secretory and endosomal pathway, to form platforms for adhesion of the

extracellular matrix and tethering of intracellular cytoskeletal proteins to the plasma membrane, and they also serve as entry points for viruses, bacteria, toxins, etc. [118] [119].

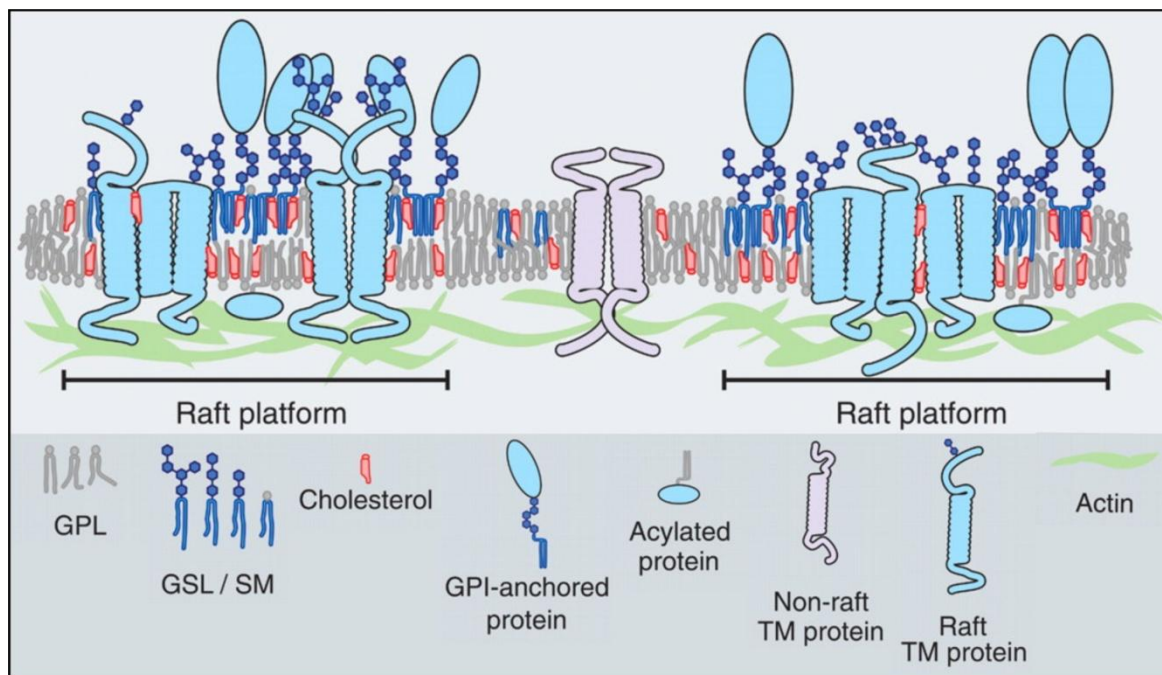


Figure 22. Lipid-raft formation. Schematic representation of a lipid-bilayer membrane. The lipid raft domains contain tightly packed glycerophospholipids (GPL), glycosphingolipids (GSL), sphingomyelin (SM), membrane-anchored proteins, and transmembrane proteins (TM). The formation and maintenance of the rafts is also supported by the underlying actin cytoskeleton. Image taken from [120].

How do glycosphingolipids control membrane-protein function? The activation of rafts for signal transduction involves protein-lipid interactions and a change in the membrane order within the lipid rafts (Figure 22) [120]. The function of growth factor receptor-associated protein kinases is modulated by gangliosides, complex glycosphingolipids that form a part of the rafts [121]. It has been shown that a change in membrane-lipid packing causes a direct interaction of the neuraminic acid in the

head group of the ganglioside GM3 (monosialodihexosylganglioside) with the membrane-proximal lysine of the epidermal growth factor (EGF) receptor kinase domain, thereby, inhibiting autophosphorylation of the intracellular tyrosine residues of the EGF receptor. This prevents receptor dimerization, rendering it inactive, thereby, attenuating uncontrolled signaling in the absence of the ligand. In contrast, the EGF receptor can be activated by autophosphorylation when cholesterol is depleted from the membrane [122]. Furthermore, in B16 mouse melanoma cells, increasing GM3 levels augments the activity of the focal adhesion kinase (FAK) and binding of GTP to Rho and Ras signaling molecules. As a consequence, B16 melanoma cells spread and migrate faster [123]. Hence, the lipid environment plays a significant role in the regulation of membrane protein-function.

How do membrane lipids and the cytoskeleton communicate? It is known that actin filaments can be directly bound to the plasma membrane via proteins like ERM (ezrin, radixin, and moesin) proteins, cellular prion protein, CIP4 (Cdc-42 interacting protein-4), IRSp53 (insulin receptor substrate protein-53kDa), caveolin-1, and filamin A [124] [125] [126] [119]. Furthermore, flotillin/reggie and TSPN7 (tetraspannin-7) recruit actin-binding proteins to the plasma membrane that bind to the plasma membrane and also interact with the actin cytoskeleton [127] [119]. A prominent example for how changes in the lipid composition of the plasma membrane control cell function through the cytoskeleton is the activation and migration of T lymphocytes. Upon antigen binding to the T cell receptors, lipids in the membrane reorganize and lead to clustering of the receptors with cholesterol and glycosphingolipids, thereby forming part of the immunological synapse [128]. In turn, adhesion molecules and junctional proteins are recruited to the synapse, including proteins that control the actin cytoskeleton such as talin, vinculin, and ERM proteins. This initiates lymphocyte migration [128] [119]. Reciprocally, the actin cytoskeleton assists in reorganizing membrane lipids. The actin-binding protein filamin A which is also recruited to the immunological synapse controls reorganization of membrane lipids [129]. Hence, there seems to be a cross-talk between the lipids and proteins in membrane rafts and the cytoskeleton.

The actin cytoskeleton responds to stimuli by localized polymerization or depolymerization [126]. Actin is a globular protein (G-actin) with an ATP binding-site in the center of the molecule [130]. Dimerization or trimerization of G-actin serves as a site for nucleation and growth of the actin filament [131]. Actin filaments polymerize at the plus-end whereas depolymerization occurs at the minus end [131], a process known as actin treadmilling. Several classes of actin-binding proteins control the polymerization and depolymerization of F-actin. For example, profilin is a promoter of actin polymerization. It binds to G-actin, thereby, attracting more G-actin monomers and accelerating nucleation [132]. In contrast, actin-severing proteins, such as gelsolin and cofilin, clip existing F-actin filaments, causing depolymerization of actin filaments to regulate their length [133] [134]. Actin capping-proteins bind to the free ends of F-actin filaments to protect them from depolymerization [135]. Hence, actin dynamics are controlled via the activity of actin binding-proteins.

But how does GlcCer control actin dynamics? Which signaling pathways are affected by accumulation of GlcCer? Lipidomics revealed that in GBA2 knockout-mice, glycosphingolipids with the C16 carbon-chain length were more abundant (Figure 11d, e). C16 ceramide has been shown to increase cell migration in embryonic stem cells by increasing actin polymerization [136]. C16 ceramide regulates PKC-dependent phosphorylation of FAK and paxillin, which leads to complex formation of Cdc-42, neural Wiskott-Aldrich syndrome protein (N-WASP), and the actin-related protein (ARP 2/3). This complex increases the interaction of the actin polymerizing proteins cofilin-1 and alpha-actinin-1/-4 with F-actin, thereby, facilitating F-actin elongation [136]. However, the authors did not examine whether the increase in C16 ceramide levels also increased the intracellular levels of GlcCer. Thus, these effects could also be due to an increase in C16 GlcCer levels. My results demonstrate that in particular the C16 GlcCer levels are increased in GBA2 knockout-mice and that fibroblasts from GBA2 knockout-mice migrate faster. Thus, future studies will show, whether FAK activity and complex formation of N-WASP, Cdc-42, and ARP 2/3 is affected in GBA2 knockout-mice. Indeed, I have shown that

actin polymerization in GBA2 knockout-fibroblasts is increased, leading to the formation of filopodia and lamellipodia.

The formation of filopodia and lamellipodia is controlled by the Rho GTPases Cdc-42 and Rac1, respectively, which locally activate actin polymerization [137] [91]. Filopodia are important for sensing the environment, axon guidance, and the formation of epithelial cell–cell contacts [138]. As described above Cdc-42 induces actin polymerization via N-WASP/ARP 2/3 complex formation [137]. However, Cdc-42 also induces actin polymerization via mDia2 (mammalian diaphanous protein 2), a member of the formin protein family [139]. Independent of Cdc-42 and Rac1, bundling of polymerized F-actin to form filopodia is mediated by fascin, an actin cross-linking protein [126]. Lamellipodia form the leading edge of migrating cells and actin polymerization at the lamellipodium is thought to drive membrane protrusion [140]. Rac1 mediates lamellipodia formation by inducing ARP 2/3 complex formation via WAVE (WASP-family verprolin-homologous protein) or mDia [91]. Rac proteins also regulate actin polymerization by increasing the availability of free F-actin ends either by removing the capping proteins or by severing actin filaments via cofilin and gelsolin [141]. Regulation of cofilin levels also replenishes the supply of actin monomers, thereby, facilitating actin polymerization [142]. Therefore, the temporal and spatial regulation of Rho GTPase activity is crucial for actin dynamics. In addition, it has been shown that effectors of Rho GTPases such as mDia stabilize microtubules in the leading edge of migrating cells [143]. Hence, interfering with the actin cytoskeleton can also have an impact on the microtubule cytoskeleton.

Lipids have been shown to regulate Rho GTPase signaling [119]. Stimulation of dendritic cells with lipopolysaccharide (LPS) reorganizes the plasma membrane, thereby, recruiting Rac1 to lipid rafts [144]. Similarly, Cdc-42 is recruited to lipid rafts resulting in a rearrangement of the actin cytoskeleton, which controls cellular morphology and conditions dendritic cells to efficiently stimulate CD8+ receptors on T cells [144]. Also, it is known that phosphatidylinositol (3,4,5)-triphosphate (PIP₃) generated by phosphoinositide 3-kinase (PI3K) activates Rac1 via Rac-GEFs [145]

and phosphatidylinositol (4,5)-diphosphate (PIP₂) directly interacts with Cdc-42 and RhoA to stimulate the release of GDP [146]. My results indicate that the more ordered lipid packaging in the plasma membrane influences the activity of signaling molecules that regulate cytoskeletal dynamics. However, further experiments need to be performed to elucidate, whether the activity of Rho GTPases is affected in GBA2 knockout-mice.

Depending on the cell type, cytoskeletal defects in GBA2 knockout-mice have a different impact on cell function. Whereas in GBA2 knockout-fibroblasts, augmented actin polymerization and a higher microtubule persistence results in faster cell migration, in GBA2 knockout-testis, sperm-head formation is disturbed, reducing fertility. Sertoli and germ cells lack structures like lamellipodia and filopodia [95] [147] [148] [149]. However, during sperm development, the developing germ cells are transported towards the lumen of the seminiferous tubule with the help of Sertoli cells [150]. Here, the cytoskeleton plays an important role. The first check point is the BTB, a tight junction set up by adjacent Sertoli cells consisting of a dynamic network of actin filaments that undergo rapid bundling and debundling to facilitate the 'opening' and 'closing' of the BTB. Thus, spermatocytes can pass and are transported towards the lumen [151] [152]. The next check point is the apical ES, an adherence junction which has a slightly different protein composition compared to the BTB [40] [151] [153]. It has been proposed that the regulation of actin dynamics at the BTB and the apical ES relies on the activation of Rac1 and Cdc-42 [154]. Furthermore, Cdc-42 and Rac1 together with the N-cadherin-beta-catenin complex maintain the integrity of the adherence junction [113] [155]. Germ cell release from Sertoli cells into the lumen is initiated by the activation of RhoB GTPase through integrins at the apical ES. The following downstream activation of ROCK1 (Rho-associated protein kinase 1), LIMK1 (LIM kinase 1), and cofilin disrupts the actin cytoskeleton at the apical ES resulting in germ cell release [95]. It has been shown that the function of integrins is different in ordered and disordered membrane phases [156]. Furthermore, changes in lipid environment also prevented formation of

the cadherin-catenin complex, compromising the function of the adherence junction [157].

My results demonstrate that BTB integrity and function in GBA2 knockout-mice is not affected because germ cells are not prematurely released into the lumen. Rather the structure of the apical ES is severely compromised (Figure 13). We have shown that GBA2 is attached to the membranes of the ER, which in the Sertoli cells, forms a part of the apical ES [57]. Thus, GBA2 could regulate GlcCer levels at the interface between Sertoli and germ cells. In turn, in GBA2 knockout-mice, GlcCer might accumulate in the membranes at the ES, causing a more ordered lipid stacking and, thereby, affecting signaling in the ES, e.g. the function of Rho GTPases or the N-cadherin-beta-catenin complex (to mention a few examples). Consequently, the tightly regulated process of recruitment and activation of actin-binding proteins at the ES is impaired, resulting in misalignment of actin filaments around the sperm heads. This would explain how actin dynamics at the ES are altered when GlcCer accumulates.

Furthermore, in the sperm manchette of GBA2 knockout-mice microtubule persistence is augmented. This could be due to a mis-regulation of the signaling molecules that control both the actin and microtubule cytoskeleton. GlcCer has also been shown to control vesicle transport and fusion [18]. My results underline this finding, demonstrating that accumulation of GlcCer during spermatogenesis hinders vesicle fusion and, thereby, acrosome formation, generating sperm with a round head and devoid of a well-formed acrosome (Figure 23). Future experiments will reveal, which signaling molecules are affected by GlcCer.

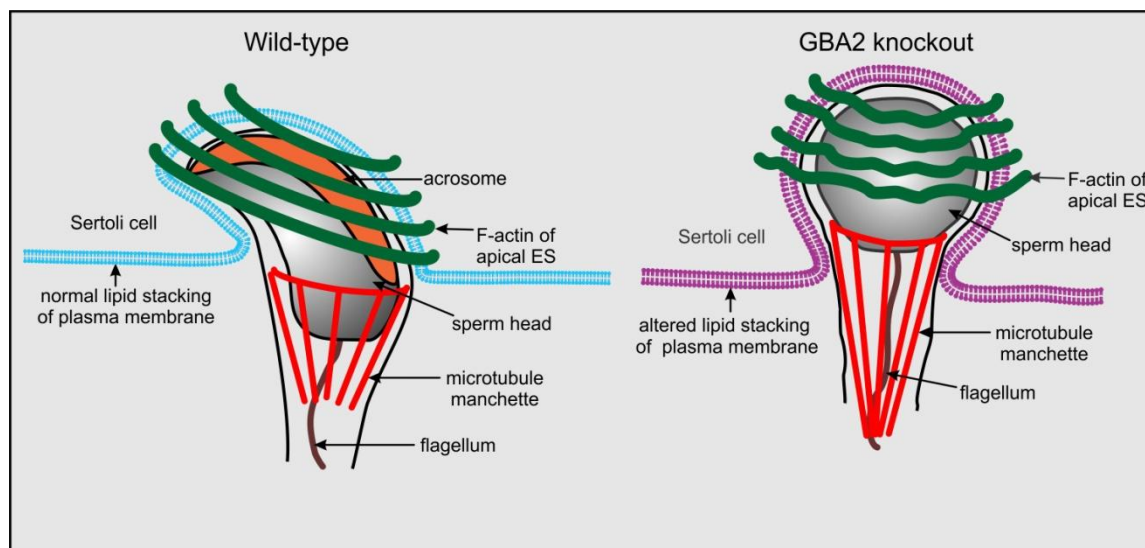


Figure 23. Sperm-head shaping in wild-type and GBA2 knockout-mice. Left: Schematic representation of the apical junction (ES) between a wild-type sperm head and a Sertoli cell. F-actin at the apical ES (*green*) from the Sertoli cell and the microtubule manchette (*red*) from the spermatid jointly shape the sperm head. As a result, sperm heads are sickle-shaped with a well formed acrosome (*orange*). The nucleus and the flagellum are indicated in *grey* and *brown* respectively. Right: see left for GBA2 knockout-sperm. Accumulation of GlcCer levels alters the lipid stacking at the ES (*purple*) which disrupts F-actin alignment and renders the microtubules of the manchette more persistent. Thereby, the sperm head is deformed causing globozoospermia.

5.3. Novel role for GlcCer

Apart from the known functions of GlcCer mentioned in chapter 1.2, my work demonstrates for the first time that GlcCer controls cytoskeletal dynamics and, thereby regulates, spermatogenesis in mice. Recently, it was reported that patients carrying a mutations in the *GBA2* gene are infertile due to bilateral testicular hypertrophy with severe sperm-head deformation and motility defects [35]. However, the main clinical symptoms of these patients were cerebellar ataxia and severe hereditary spastic paraplegia with varying degrees of cerebellar and corpus callosum atrophies [158] [35]. So far we have not observed major neurological defects in *GBA2*

knockout-mice, although GBA2 is highly expressed in the brain. Studies performed by a master student in our lab revealed that the mutations found in patients with cerebellar ataxia and severe hereditary spastic paraplegia are dead mutants (Master thesis, Carina Marx). Thus, we analyzed locomotor function of GBA2 knockout-mice in more detail using behavioral studies. Preliminary results suggest that muscle strength in GBA2 knockout-mice is severely impaired (Master thesis, Carina Marx). Similarly, a study in zebrafish demonstrated that down-regulation of GBA2 expression affected locomotion and reduced axon outgrowth of motor neurons [35]. Axon growth crucially relies on actin and microtubule function [159]. In future studies, we will investigate if GlcCer also accumulates in motor neurons of GBA2 knockout-mice, thereby, affecting cytoskeletal dynamics and axon growth.

6. References

1. van Meer, G., J. Wolthoorn, and S. Degroote, *The fate and function of glycosphingolipid glucosylceramide*. *Philos Trans R Soc Lond B Biol Sci*, 2003. **358**(1433): p. 869-73.
2. Yamashita, T., et al., *A vital role for glycosphingolipid synthesis during development and differentiation*. *Proc Natl Acad Sci U S A*, 1999. **96**(16): p. 9142-7.
3. Degroote, S., J. Wolthoorn, and G. van Meer, *The cell biology of glycosphingolipids*. *Semin Cell Dev Biol*, 2004. **15**(4): p. 375-87.
4. van Meer, G., D.R. Voelker, and G.W. Feigenson, *Membrane lipids: where they are and how they behave*. *Nat Rev Mol Cell Biol*, 2008. **9**(2): p. 112-24.
5. Hanada, K., et al., *Molecular machinery for non-vesicular trafficking of ceramide*. *Nature*, 2003. **426**(6968): p. 803-9.
6. Jeckel, D., et al., *Glucosylceramide is synthesized at the cytosolic surface of various Golgi subfractions*. *J Cell Biol*, 1992. **117**(2): p. 259-67.
7. Lannert, H., *Functional Organization of the Golgi Apparatus in Glycosphingolipid Biosynthesis. LACTOSYLCERAMIDE AND SUBSEQUENT GLYCOSPHINGOLIPIDS ARE FORMED IN THE LUMEN OF THE LATE GOLGI*. *Journal of Biological Chemistry*, 1998. **273**(5): p. 2939-2946.
8. Halter, D., et al., *Pre- and post-Golgi translocation of glucosylceramide in glycosphingolipid synthesis*. *J Cell Biol*, 2007. **179**(1): p. 101-15.
9. Metz, R.J. and N.S. Radin, *Glucosylceramide uptake protein from spleen cytosol*. *J Biol Chem*, 1980. **255**(10): p. 4463-7.
10. Jennemann, R., et al., *Integrity and barrier function of the epidermis critically depend on glucosylceramide synthesis*. *J Biol Chem*, 2007. **282**(5): p. 3083-94.
11. Sando, G.N., E.J. Howard, and K.C. Madison, *Induction of Ceramide Glucosyltransferase Activity in Cultured Human Keratinocytes. CORRELATION WITH CULTURE DIFFERENTIATION*. *Journal of Biological Chemistry*, 1996. **271**(36): p. 22044-22051.

12. Ichikawa, S. and Y. Hirabayashi, *Glucosylceramide synthase and glycosphingolipid synthesis*. Trends Cell Biol, 1998. **8**(5): p. 198-202.
13. Schwarz, A. and A.H. Futerman, *Distinct roles for ceramide and glucosylceramide at different stages of neuronal growth*. J Neurosci, 1997. **17**(9): p. 2929-38.
14. Boldin, S. and A.H. Futerman, *Glucosylceramide synthesis is required for basic fibroblast growth factor and laminin to stimulate axonal growth*. J Neurochem, 1997. **68**(2): p. 882-5.
15. Dotti, C.G., R.G. Parton, and K. Simons, *Polarized sorting of glypiated proteins in hippocampal neurons*. Nature, 1991. **349**(6305): p. 158-61.
16. Datta, S.C. and N.S. Radin, *Stimulation of liver growth and DNA synthesis by glucosylceramide*. Lipids, 1988. **23**(5): p. 508-10.
17. Shayman, J.A., et al., *Modulation of renal epithelial cell growth by glucosylceramide. Association with protein kinase C, sphingosine, and diacylglycerol*. J Biol Chem, 1991. **266**(34): p. 22968-74.
18. van Meer, G. and K. Simons, *Lipid polarity and sorting in epithelial cells*. J Cell Biochem, 1988. **36**(1): p. 51-8.
19. Tewes, B.J. and H.J. Galla, *Lipid polarity in brain capillary endothelial cells*. Endothelium, 2001. **8**(3): p. 207-20.
20. de Graaf, M., et al., *Cloning and characterization of human liver cytosolic beta-glycosidase*. Biochem J, 2001. **356**(Pt 3): p. 907-10.
21. Henrissat, B., *A classification of glycosyl hydrolases based on amino acid sequence similarities*. Biochem J, 1991. **280 (Pt 2)**: p. 309-16.
22. Day, A.J., et al., *Deglycosylation of flavonoid and isoflavonoid glycosides by human small intestine and liver beta-glucosidase activity*. FEBS Lett, 1998. **436**(1): p. 71-5.
23. van Weely, S., et al., *Demonstration of the existence of a second, non-lysosomal glucocerebrosidase that is not deficient in Gaucher disease*. Biochim Biophys Acta, 1993. **1181**(1): p. 55-62.
24. Hayashi, Y., et al., *Klotho-related protein is a novel cytosolic neutral beta-glycosylceramidase*. J Biol Chem, 2007. **282**(42): p. 30889-900.

25. Dinur, T., et al., *Human acid beta-glucosidase: isolation and amino acid sequence of a peptide containing the catalytic site*. Proc Natl Acad Sci U S A, 1986. **83**(6): p. 1660-4.
26. Korschen, H.G., et al., *The non-lysosomal beta-glucosidase GBA2 is a non-integral membrane-associated protein at the endoplasmic reticulum (ER) and Golgi*. J Biol Chem, 2013. **288**(5): p. 3381-93.
27. Schulze, H., T. Kolter, and K. Sandhoff, *Principles of lysosomal membrane degradation: Cellular topology and biochemistry of lysosomal lipid degradation*. Biochim Biophys Acta, 2009. **1793**(4): p. 674-83.
28. Brady, R.O., J.N. Kanfer, and D. Shapiro, *Metabolism of Glucocerebrosides. II. Evidence of an Enzymatic Deficiency in Gaucher's Disease*. Biochem Biophys Res Commun, 1965. **18**: p. 221-5.
29. Cox, T.M., *Gaucher disease: understanding the molecular pathogenesis of sphingolipidoses*. J Inherit Metab Dis, 2001. **24 Suppl 2**: p. 106-21; discussion 87-8.
30. Yildiz, Y., et al., *Mutation of β -glucosidase 2 causes glycolipid storage disease and impaired male fertility*. The Journal of Clinical Investigation, 2006. **116**(11): p. 2985-2994.
31. Overkleeft, H.S., et al., *Generation of Specific Deoxynojirimycin-type Inhibitors of the Non-lysosomal Glucosylceramidase*. Journal of Biological Chemistry, 1998. **273**(41): p. 26522-26527.
32. Boot, R.G., et al., *Identification of the non-lysosomal glucosylceramidase as beta-glucosidase 2*. J Biol Chem, 2007. **282**(2): p. 1305-12.
33. Gonzalez-Carmona, M.A., et al., *Beta-glucosidase 2 knockout mice with increased glucosylceramide show impaired liver regeneration*. Liver Int, 2012. **32**(9): p. 1354-62.
34. Votsi, C., et al., *A novel GBA2 gene missense mutation in spastic ataxia*. Ann Hum Genet, 2014. **78**(1): p. 13-22.
35. Martin, E., et al., *Loss of function of glucocerebrosidase GBA2 is responsible for motor neuron defects in hereditary spastic paraplegia*. Am J Hum Genet, 2013. **92**(2): p. 238-44.

36. Clermont, Y. and M. Trott, *Duration of the cycle of the seminiferous epithelium in the mouse and hamster determined by means of 3H-thymidine and radioautography*. Fertil Steril, 1969. **20**(5): p. 805-17.
37. Vogl, A.W., et al., *Unique and multifunctional adhesion junctions in the testis: ectoplasmic specializations*. Arch Histol Cytol, 2000. **63**(1): p. 1-15.
38. Cheng, C.Y. and D.D. Mruk, *The blood-testis barrier and its implications for male contraception*. Pharmacol Rev, 2012. **64**(1): p. 16-64.
39. Francavilla, F., et al., *Naturally-occurring antisperm antibodies in men: interference with fertility and clinical implications. An update*. Front Biosci, 2007. **12**: p. 2890-911.
40. Cheng, C.Y. and D.D. Mruk, *A local autocrine axis in the testes that regulates spermatogenesis*. Nat Rev Endocrinol, 2010. **6**(7): p. 380-395.
41. Clermont, Y., *Kinetics of spermatogenesis in mammals: seminiferous epithelium cycle and spermatogonial renewal*. Physiol Rev, 1972. **52**(1): p. 198-236.
42. Russell, L., *Observations on rat Sertoli ectoplasmic ('junctional') specializations in their association with germ cells of the rat testis*. Tissue Cell, 1977. **9**(3): p. 475-98.
43. Maronpot, R.R., G.A. Boorman, and B.W. Gaul, *Pathology of the Mouse: Reference and Atlas*. 1999: Cache River Press.
44. Sen, C.G.S., A.F. Holstein, and C. Schirren, *Über die Morphogenese rundköpfiger Spermatozoen des Menschen*. Andrologia, 1971. **3**(3): p. 117-125.
45. Dam, A.H., et al., *Globozoospermia revisited*. Hum Reprod Update, 2007. **13**(1): p. 63-75.
46. Kang-Decker, N., et al., *Lack of acrosome formation in Hrb-deficient mice*. Science, 2001. **294**(5546): p. 1531-3.
47. Abou-Haila, A. and D.R. Tulsiani, *Mammalian sperm acrosome: formation, contents, and function*. Arch Biochem Biophys, 2000. **379**(2): p. 173-82.
48. Yao, R., et al., *Lack of acrosome formation in mice lacking a Golgi protein, GOPC*. Proc Natl Acad Sci U S A, 2002. **99**(17): p. 11211-6.

49. Xiao, N., et al., *PICK1 deficiency causes male infertility in mice by disrupting acrosome formation*. The Journal of Clinical Investigation, 2009. **119**(4): p. 802-812.
50. Paiardi, C., et al., *Failure of acrosome formation and globozoospermia in the wobbler mouse, a Vps54 spontaneous recessive mutant*. Spermatogenesis, 2011. **1**(1): p. 52-62.
51. Lin, Y.N., et al., *Loss of zona pellucida binding proteins in the acrosomal matrix disrupts acrosome biogenesis and sperm morphogenesis*. Mol Cell Biol, 2007. **27**(19): p. 6794-805.
52. Pierre, V., et al., *Absence of Dpy19l2, a new inner nuclear membrane protein, causes globozoospermia in mice by preventing the anchoring of the acrosome to the nucleus*. Development, 2012. **139**(16): p. 2955-65.
53. Berruti, G., M. Ripolone, and M. Ceriani, *USP8, a regulator of endosomal sorting, is involved in mouse acrosome biogenesis through interaction with the spermatid ESCRT-0 complex and microtubules*. Biol Reprod, 2010. **82**(5): p. 930-9.
54. Quenneville, N.R., et al., *Domains within the GARP subunit Vps54 confer separate functions in complex assembly and early endosome recognition*. Mol Biol Cell, 2006. **17**(4): p. 1859-70.
55. Mori, E., et al., *Purification and characterization of a 38-kDa protein, sp38, with zona pellucida-binding property from porcine epididymal sperm*. Biochem Biophys Res Commun, 1993. **196**(1): p. 196-202.
56. Dooher, G.B. and D. Bennett, *Abnormal microtubular systems in mouse spermatids associated with a mutant gene at the T-locus*. Journal of Embryology and Experimental Morphology, 1974. **32**(3): p. 749-761.
57. Kierszenbaum, A.L. and L.L. Tres, *The acrosome-acroplaxome-manchette complex and the shaping of the spermatid head*. Arch Histol Cytol, 2004. **67**(4): p. 271-84.
58. Cole, A., et al., *Nuclear and manchette development in spermatids of normal and azh/azh mutant mice*. Biol Reprod, 1988. **38**(2): p. 385-401.

59. Cherry, L.M. and T.C. Hsu, *Antitubulin immunofluorescence studies of spermatogenesis in the mouse*. *Chromosoma*, 1984. **90**(4): p. 265-74.
60. Vogl, A.W. and L.J. Soucy, *Arrangement and possible function of actin filament bundles in ectoplasmic specializations of ground squirrel Sertoli cells*. *J Cell Biol*, 1985. **100**(3): p. 814-25.
61. Guttman, J.A., P. Janmey, and A.W. Vogl, *Gelsolin--evidence for a role in turnover of junction-related actin filaments in Sertoli cells*. *J Cell Sci*, 2002. **115**(Pt 3): p. 499-505.
62. Braun, A., et al., *Genomic organization of profilin-III and evidence for a transcript expressed exclusively in testis*. *Gene*, 2002. **283**(1-2): p. 219-25.
63. O'Donnell, L., et al., *An essential role for katanin p80 and microtubule severing in male gamete production*. *PLoS Genet*, 2012. **8**(5): p. e1002698.
64. Kierszenbaum, A.L., E. Rivkin, and L.L. Tres, *Molecular biology of sperm head shaping*. *Soc Reprod Fertil Suppl*, 2007. **65**: p. 33-43.
65. Akhmanova, A., et al., *The microtubule plus-end-tracking protein CLIP-170 associates with the spermatid manchette and is essential for spermatogenesis*. *Genes Dev*, 2005. **19**(20): p. 2501-15.
66. Smith, L.B., et al., *KATNAL1 Regulation of Sertoli Cell Microtubule Dynamics Is Essential for Spermiogenesis and Male Fertility*. *PLoS Genet*, 2012. **8**(5): p. e1002697.
67. Berruti, G. and C. Paiardi, *The dynamic of the apical ectoplasmic specialization between spermatids and Sertoli cells: the case of the small GTPase Rap1*. *Biomed Res Int*, 2014. **2014**: p. 635979.
68. Russell, L.D., et al., *The consequences of actin disruption at Sertoli ectoplasmic specialization sites facing spermatids after in vivo exposure of rat testis to cytochalasin D*. *Biol Reprod*, 1988. **39**(1): p. 105-18.
69. Gliki, G., et al., *Spermatid differentiation requires the assembly of a cell polarity complex downstream of junctional adhesion molecule-C*. *Nature*, 2004. **431**(7006): p. 320-324.
70. Mueller, S., et al., *Loss of nectin-2 at Sertoli-spermatid junctions leads to male infertility and correlates with severe spermatozoan head and midpiece*

- malformation, impaired binding to the zona pellucida, and oocyte penetration.* Biol Reprod, 2003. **69**(4): p. 1330-40.
71. Lorenz, H., D.W. Hailey, and J. Lippincott-Schwartz, *Fluorescence protease protection of GFP chimeras to reveal protein topology and subcellular localization.* Nat Methods, 2006. **3**(3): p. 205-10.
72. Sezgin, E., et al., *Elucidating membrane structure and protein behavior using giant plasma membrane vesicles.* Nat Protoc, 2012. **7**(6): p. 1042-51.
73. Livak, K.J. and T.D. Schmittgen, *Analysis of relative gene expression data using real-time quantitative PCR and the 2(-Delta Delta C(T)) Method.* Methods, 2001. **25**(4): p. 402-8.
74. Reichelt, J., et al., *Loss of keratin 10 is accompanied by increased sebocyte proliferation and differentiation.* Eur J Cell Biol, 2004. **83**(11-12): p. 747-59.
75. Yildiz, Y., et al., *Functional and genetic characterization of the non-lysosomal glucosylceramidase 2 as a modifier for Gaucher disease.* Orphanet J Rare Dis, 2013. **8**: p. 151.
76. Wewer, V., et al., *Quantification of sterol lipids in plants by quadrupole time-of-flight mass spectrometry.* J Lipid Res, 2011. **52**(5): p. 1039-54.
77. Ginkel, C., et al., *Ablation of neuronal ceramide synthase 1 in mice decreases ganglioside levels and expression of myelin-associated glycoprotein in oligodendrocytes.* J Biol Chem, 2012. **287**(50): p. 41888-902.
78. Lorenz, H., O. Windl, and H.A. Kretzschmar, *Cellular phenotyping of secretory and nuclear prion proteins associated with inherited prion diseases.* J Biol Chem, 2002. **277**(10): p. 8508-16.
79. Heuser, J., *The production of 'cell cortices' for light and electron microscopy.* Traffic, 2000. **1**(7): p. 545-52.
80. Lewis, S.A. and N.J. Cowan, *Complex regulation and functional versatility of mammalian alpha- and beta-tubulin isoforms during the differentiation of testis and muscle cells.* J Cell Biol, 1988. **106**(6): p. 2023-33.
81. Myers, M., et al., *Atypical development of Sertoli cells and impairment of spermatogenesis in the hypogonadal (hpg) mouse.* J Anat, 2005. **207**(6): p. 797-811.

82. Auharek, S.A. and L.R. de Franca, *Postnatal testis development, Sertoli cell proliferation and number of different spermatogonial types in C57BL/6J mice made transiently hypo- and hyperthyroidic during the neonatal period*. J Anat, 2010. **216**(5): p. 577-88.
83. Retterstol, K., et al., *Metabolism of very long chain polyunsaturated fatty acids in isolated rat germ cells*. Lipids, 2001. **36**(6): p. 601-6.
84. Beckman, J.K. and J.G. Coniglio, *The metabolism of polyunsaturated fatty acids in rat Sertoli and germinal cells*. Lipids, 1980. **15**(6): p. 389-94.
85. Rabionet, M., et al., *Male Germ Cells Require Polyenoic Sphingolipids with Complex Glycosylation for Completion of Meiosis: A LINK TO CERAMIDE SYNTHASE-3*. Journal of Biological Chemistry, 2008. **283**(19): p. 13357-13369.
86. Furland, N.E., et al., *Very long-chain polyunsaturated fatty acids are the major acyl groups of sphingomyelins and ceramides in the head of mammalian spermatozoa*. J Biol Chem, 2007. **282**(25): p. 18151-61.
87. Mortimer, D., E.F. Curtis, and R.G. Miller, *Specific labelling by peanut agglutinin of the outer acrosomal membrane of the human spermatozoon*. J Reprod Fertil, 1987. **81**(1): p. 127-35.
88. Funaki, T., et al., *The Arf GAP SMAP2 is necessary for organized vesicle budding from the trans-Golgi network and subsequent acrosome formation in spermiogenesis*. Mol Biol Cell, 2013. **24**(17): p. 2633-44.
89. Mattila, P.K. and P. Lappalainen, *Filopodia: molecular architecture and cellular functions*. Nat Rev Mol Cell Biol, 2008. **9**(6): p. 446-54.
90. Ridley, A.J., *Life at the leading edge*. Cell, 2011. **145**(7): p. 1012-22.
91. Heasman, S.J. and A.J. Ridley, *Mammalian Rho GTPases: new insights into their functions from in vivo studies*. Nat Rev Mol Cell Biol, 2008. **9**(9): p. 690-701.
92. Krugmann, S., et al., *Cdc42 induces filopodia by promoting the formation of an IRSp53:Mena complex*. Curr Biol, 2001. **11**(21): p. 1645-55.

93. Ridley, A.J. and A. Hall, *The small GTP-binding protein rho regulates the assembly of focal adhesions and actin stress fibers in response to growth factors*. Cell, 1992. **70**(3): p. 389-99.
94. Hall, A., *Rho GTPases and the Actin Cytoskeleton*. Science, 1998. **279**(5350): p. 509-514.
95. Lui, W.Y., W.M. Lee, and C.Y. Cheng, *Sertoli-germ cell adherens junction dynamics in the testis are regulated by RhoB GTPase via the ROCK/LIMK signaling pathway*. Biol Reprod, 2003. **68**(6): p. 2189-206.
96. Komarova, Y., et al., *EB1 and EB3 control CLIP dissociation from the ends of growing microtubules*. Mol Biol Cell, 2005. **16**(11): p. 5334-45.
97. Wang, T.-Y. and J.R. Silvius, *Sphingolipid Partitioning into Ordered Domains in Cholesterol-Free and Cholesterol-Containing Lipid Bilayers*. Biophysical Journal, 2003. **84**(1): p. 367-378.
98. Hakomori, S.I., *Cell adhesion/recognition and signal transduction through glycosphingolipid microdomain*. Glycoconj J, 2000. **17**(3 -4): p. 143-51.
99. Warnock, D.E., et al., *Transport of newly synthesized glucosylceramide to the plasma membrane by a non-Golgi pathway*. Proc Natl Acad Sci U S A, 1994. **91**(7): p. 2708-12.
100. Harris, F.M., K.B. Best, and J.D. Bell, *Use of laurdan fluorescence intensity and polarization to distinguish between changes in membrane fluidity and phospholipid order*. Biochim Biophys Acta, 2002. **1565**(1): p. 123-8.
101. Parasassi, T., et al., *Quantitation of lipid phases in phospholipid vesicles by the generalized polarization of Laurdan fluorescence*. Biophysical Journal, 1991. **60**(1): p. 179-189.
102. Parasassi, T., et al., *Phase fluctuation in phospholipid membranes revealed by Laurdan fluorescence*. Biophys J, 1990. **57**(6): p. 1179-86.
103. Owen, D.M., et al., *Quantitative imaging of membrane lipid order in cells and organisms*. Nat Protoc, 2012. **7**(1): p. 24-35.
104. Marsh, N.L., P.M. Elias, and W.M. Holleran, *Glucosylceramides stimulate murine epidermal hyperproliferation*. J Clin Invest, 1995. **95**(6): p. 2903-9.

105. Kee, N., et al., *The utility of Ki-67 and BrdU as proliferative markers of adult neurogenesis*. J Neurosci Methods, 2002. **115**(1): p. 97-105.
106. Theriot, J.A. and T.J. Mitchison, *Actin microfilament dynamics in locomoting cells*. Nature, 1991. **352**(6331): p. 126-31.
107. Rodriguez, L.G., X. Wu, and J.L. Guan, *Wound-healing assay*. Methods Mol Biol, 2005. **294**: p. 23-9.
108. Platt, F.M., et al., *N-butyldeoxynojirimycin is a novel inhibitor of glycolipid biosynthesis*. J Biol Chem, 1994. **269**(11): p. 8362-5.
109. Walden, C.M., et al., *Accumulation of glucosylceramide in murine testis, caused by inhibition of beta-glucosidase 2: implications for spermatogenesis*. J Biol Chem, 2007. **282**(45): p. 32655-64.
110. D'Angelo, G., et al., *Glycosphingolipid synthesis requires FAPP2 transfer of glucosylceramide*. Nature, 2007. **449**(7158): p. 62-7.
111. Pfeiffer, S., et al., *High-pressure freezing provides new information on human epidermis: simultaneous protein antigen and lamellar lipid structure preservation. Study on human epidermis by cryoimmobilization*. J Invest Dermatol, 2000. **114**(5): p. 1030-8.
112. Vielhaber, G., et al., *Localization of ceramide and glucosylceramide in human epidermis by immunogold electron microscopy*. J Invest Dermatol, 2001. **117**(5): p. 1126-36.
113. Lee, A., *Lipid-protein interactions in biological membranes: a structural perspective*. Biochimica et Biophysica Acta (BBA) - Biomembranes, 2003. **1612**(1): p. 1-40.
114. Starling, A.P., J.M. East, and A.G. Lee, *Separate effects of long-chain phosphatidylcholines on dephosphorylation of the Ca(2+)-ATPase and on Ca2+ binding*. Biochem J, 1996. **318 (Pt 3)**: p. 785-8.
115. Lee, A.G., *How lipids interact with an intrinsic membrane protein: the case of the calcium pump*. Biochim Biophys Acta, 1998. **1376**(3): p. 381-90.
116. Starling, A.P., J.M. East, and A.G. Lee, *Phosphatidylinositol 4-phosphate increases the rate of dephosphorylation of the phosphorylated Ca(2+)-ATPase*. J Biol Chem, 1995. **270**(24): p. 14467-70.

117. Dalton, K.A., et al., *Interaction of phosphatidic acid and phosphatidylserine with the Ca²⁺-ATPase of sarcoplasmic reticulum and the mechanism of inhibition*. Biochem J, 1998. **329 (Pt 3)**: p. 637-46.
118. Brown, D.A. and E. London, *Functions of lipid rafts in biological membranes*. Annu Rev Cell Dev Biol, 1998. **14**: p. 111-36.
119. Head, B.P., H.H. Patel, and P.A. Insel, *Interaction of membrane/lipid rafts with the cytoskeleton: impact on signaling and function: membrane/lipid rafts, mediators of cytoskeletal arrangement and cell signaling*. Biochim Biophys Acta, 2014. **1838(2)**: p. 532-45.
120. Lingwood, D. and K. Simons, *Lipid rafts as a membrane-organizing principle*. Science, 2010. **327(5961)**: p. 46-50.
121. Weis, F.M. and R.J. Davis, *Regulation of epidermal growth factor receptor signal transduction. Role of gangliosides*. J Biol Chem, 1990. **265(20)**: p. 12059-66.
122. Coskun, U., et al., *Regulation of human EGF receptor by lipids*. Proc Natl Acad Sci U S A, 2011. **108(22)**: p. 9044-8.
123. Iwabuchi, K., et al., *GM3-enriched Microdomain Involved in Cell Adhesion and Signal Transduction through Carbohydrate-Carbohydrate Interaction in Mouse Melanoma B16 Cells*. Journal of Biological Chemistry, 1998. **273(15)**: p. 9130-9138.
124. Fehon, R.G., A.I. McClatchey, and A. Bretscher, *Organizing the cell cortex: the role of ERM proteins*. Nat Rev Mol Cell Biol, 2010. **11(4)**: p. 276-87.
125. Brouckova, A. and K. Holada, *Cellular prion protein in blood platelets associates with both lipid rafts and the cytoskeleton*. Thromb Haemost, 2009. **102(5)**: p. 966-74.
126. Sit, S.T. and E. Manser, *Rho GTPases and their role in organizing the actin cytoskeleton*. J Cell Sci, 2011. **124(Pt 5)**: p. 679-83.
127. Otto, G.P. and B.J. Nichols, *The roles of flotillin microdomains--endocytosis and beyond*. J Cell Sci, 2011. **124(Pt 23)**: p. 3933-40.
128. Viola, A. and N. Gupta, *Tether and trap: regulation of membrane-raft dynamics by actin-binding proteins*. Nat Rev Immunol, 2007. **7(11)**: p. 889-96.

129. Tavano, R., et al., *CD28 interaction with filamin-A controls lipid raft accumulation at the T-cell immunological synapse*. Nat Cell Biol, 2006. **8**(11): p. 1270-6.
130. Kinosian, H.J., et al., *Nucleotide binding to actin. Cation dependence of nucleotide dissociation and exchange rates*. J Biol Chem, 1993. **268**(12): p. 8683-91.
131. Winder, S.J. and K.R. Ayscough, *Actin-binding proteins*. J Cell Sci, 2005. **118**(Pt 4): p. 651-4.
132. Suetsugu, S., H. Miki, and T. Takenawa, *The essential role of profilin in the assembly of actin for microspike formation*. EMBO J, 1998. **17**(22): p. 6516-26.
133. Sun, H.Q., et al., *Gelsolin, a Multifunctional Actin Regulatory Protein*. Journal of Biological Chemistry, 1999. **274**(47): p. 33179-33182.
134. Zhao, R., et al., *Actin depolymerization factor/cofilin activation regulates actin polymerization and tension development in canine tracheal smooth muscle*. J Biol Chem, 2008. **283**(52): p. 36522-31.
135. Weeds, A. and S. Maciver, *F-actin capping proteins*. Current Opinion in Cell Biology, 1993. **5**(1): p. 63-69.
136. Park, S.S., et al., *C(16)-Ceramide-induced F-actin regulation stimulates mouse embryonic stem cell migration: involvement of N-WASP/Cdc42/Arp2/3 complex and cofilin-1/alpha-actinin*. Biochim Biophys Acta, 2013. **1831**(2): p. 350-60.
137. Snapper, S.B., et al., *N-WASP deficiency reveals distinct pathways for cell surface projections and microbial actin-based motility*. Nat Cell Biol, 2001. **3**(10): p. 897-904.
138. Gupton, S.L. and F.B. Gertler, *Filopodia: the fingers that do the walking*. Sci STKE, 2007. **2007**(400): p. re5.
139. Peng, J., et al., *Disruption of the Diaphanous-Related Formin Drf1 Gene Encoding mDia1 Reveals a Role for Drf3 as an Effector for Cdc42*. Current Biology, 2003. **13**(7): p. 534-545.
140. Mendoza, M.C., et al., *ERK-MAPK drives lamellipodia protrusion by activating the WAVE2 regulatory complex*. Mol Cell, 2011. **41**(6): p. 661-71.

141. Jaffe, A.B. and A. Hall, *Rho GTPases: biochemistry and biology*. Annu Rev Cell Dev Biol, 2005. **21**: p. 247-69.
142. Wang, C.Q. and C.Y. Cheng, *A seamless trespass: germ cell migration across the seminiferous epithelium during spermatogenesis*. J Cell Biol, 2007. **178**(4): p. 549-56.
143. Palazzo, A.F., et al., *mDia mediates Rho-regulated formation and orientation of stable microtubules*. Nat Cell Biol, 2001. **3**(8): p. 723-9.
144. Jaksits, S., et al., *Lipid Raft-Associated GTPase Signaling Controls Morphology and CD8+ T Cell Stimulatory Capacity of Human Dendritic Cells*. The Journal of Immunology, 2004. **173**(3): p. 1628-1639.
145. Welch, H.C.E., et al., *Phosphoinositide 3-kinase-dependent activation of Rac*. FEBS Letters, 2003. **546**(1): p. 93-97.
146. Zheng, Y., et al., *Phosphatidylinositol 4,5-bisphosphate provides an alternative to guanine nucleotide exchange factors by stimulating the dissociation of GDP from Cdc42Hs*. J Biol Chem, 1996. **271**(39): p. 23815-9.
147. Cheng, C.Y. and D.D. Mruk, *Regulation of spermiogenesis, spermiation and blood-testis barrier dynamics: novel insights from studies on Eps8 and Arp3*. Biochem J, 2011. **435**(3): p. 553-62.
148. Cheng, C.Y. and D.D. Mruk, *Actin binding proteins and spermiogenesis: Some unexpected findings*. Spermatogenesis, 2011. **1**(2): p. 99-104.
149. Tang, E.I., D.D. Mruk, and C.Y. Cheng, *MAP/microtubule affinity-regulating kinases, microtubule dynamics, and spermatogenesis*. J Endocrinol, 2013. **217**(2): p. R13-23.
150. Xiao, X., et al., *Germ Cell Transport Across the Seminiferous Epithelium During Spermatogenesis*. Vol. 29. 2014. 286-298.
151. Lie, P.P., et al., *Restricted Arp3 expression in the testis prevents blood-testis barrier disruption during junction restructuring at spermatogenesis*. Proc Natl Acad Sci U S A, 2010. **107**(25): p. 11411-6.
152. Su, W., et al., *Filamin A is a regulator of blood-testis barrier assembly during postnatal development in the rat testis*. Endocrinology, 2012. **153**(10): p. 5023-35.

153. Qian, X., et al., *Palladin is a regulator of actin filament bundles at the ectoplasmic specialization in adult rat testes*. *Endocrinology*, 2013. **154**(5): p. 1907-20.
154. Ip, C.K. and A.S. Wong, *p70 S6 kinase and actin dynamics: A perspective*. *Spermatogenesis*, 2012. **2**(1): p. 44-52.
155. Fukata, M., et al., *Cdc42 and Rac1 Regulate the Interaction of IQGAP1 with - Catenin*. *Journal of Biological Chemistry*, 1999. **274**(37): p. 26044-26050.
156. Hussain, N.F., et al., *Bilayer asymmetry influences integrin sequestering in raft-mimicking lipid mixtures*. *Biophys J*, 2013. **104**(10): p. 2212-21.
157. Marquez, M.G., et al., *Changes in membrane lipid composition cause alterations in epithelial cell-cell adhesion structures in renal papillary collecting duct cells*. *Biochim Biophys Acta*, 2012. **1818**(3): p. 491-501.
158. Hammer, M.B., et al., *Mutations in GBA2 cause autosomal-recessive cerebellar ataxia with spasticity*. *Am J Hum Genet*, 2013. **92**(2): p. 245-51.
159. Conde, C. and A. Caceres, *Microtubule assembly, organization and dynamics in axons and dendrites*. *Nat Rev Neurosci*, 2009. **10**(5): p. 319-32.

7. Appendix

```

1  M V T C V P A S E Q V G C A E R D S Q V Y C E D T G G T E A V R V T D C G S P E D S G P Q D E P S
Y
51  C N S E D S G Q L M A S Y E G K A R G Y Q V P P F G W R I C L A H E F A E K R R P F Q A N N I S L
S
101 N L V K H L G M G L R Y L K W W Y R K T H V E K K T P F I D M L N S L P L R Q I Y G C P L G G I G
G
151  G T I T R G W R G Q F C R W Q L N P G M Y Q H Q T V I A D Q F I V C L R R D G R T V Y Q Q V L S L
E
201  L P N V L R S W N W G L C G Y F A F Y H A L Y P R A W T V Y Q L P G Q N V T L T C R Q V T P I L P
H
251  D Y Q D S S L P V G V F V W D V E N E G D E T L D V S I T F S M R N G L G G E D D A A G S L W N E
P
301  F R L E Q G G T T V Q G L L L H H P T P P N P Y T M A V A A R C T A D T T V T H T T A F D P N G T
G
351  Q Q V W Q D L L Q D G Q L D S P A G Q S T P T Q K G E G I A G A V C V S S K L L P R S R C C L E F
S
401  L A W D M P K I M F G A K S Q V H Y R R Y T R F F G S D G D V A P A L S H Y A L C H Y A D W E D R
I
451  S A W Q N P V L D D R T L P A W Y K S A L F N E L Y F L A D G G T V W L E V P A D S L P E G L G G
S
501  M R Q L R S T L Q D Y G R E G Y L E G Q E Y R M Y N T Y D V H F Y A S F A L V M L W P K L E L S L
Q
551  Y D M A L A T L K E D L T R R R Y L M S G V V A P V K R R N V I P H D I G D P D D E P W L R V N A
Y
601  L I H D T A D W K D L N L K F V L Q I Y R D Y Y L T G D Q G F L E D M W P V C L A V M E S E M K F
D
651  K D Q D G L I E N G G Y A D Q T Y D A W V T T G P S A Y C G G L W L A A V A V M V Q M A V L C G A
Q
701  D V Q E R F A S I L C R G R E A Y E R L L W N G R Y Y N Y D S S S H P Q S R S I M S D Q C A G Q W
F
751  L R A C G L G E G D T E V F P T L H V V R A L Q T I F E L N V Q A F A G G A M G A V N G M H P H G
V
801  P D R S S V Q S D E V W V G V Y G L A A T M I Q E G L T W E G F R T A E G C Y R T V W E R L G L
A
851  F Q T P E A Y C Q Q Q V F R S L A Y M R P L S I W A M Q L A L Q Q Q H K K S R R P S V T Q G T G
L
901  S T Q P E C G P K R S L A N L N S E
    
```

Figure 24. Mass spectrometric detection of GBA2 in testis of mouse. Five different peptides from the GBA2 protein-sequence were chosen and using mass spectrometry their presence in the testis and Sertoli cells was detected. Four of the chosen peptides were present in testis (indicated in blue) and 2 peptides appeared in the Sertoli cells. However, 1 peptide was present in both testis and Sertoli cells (indicated in red and blue).

Peptide 1

```

1  MVTCVPASEQVGCAERDSQVYC-EDTGGTEAVRVTDCGSPEDSGPQDEPSYCNSEDSGQL 59
60 MASYEGKARGYQVPPFGWRICLAHEFAEKRRPFQANNISLSNLVKHLGMGLRRLKWWYR 119
120 THVEKKTFFIDMLNSLPLRQIYGCPPLGGIGGGTITRGWRGQFCRWQLNPGMYQHQTVIAD 179
180 QFIVCLRRDGRTVYQQVLSLELPNVLRSWNWGLCGYFAFYHALYPRAWTVYQLPGQNVT 239
240 TCRQVTPILPHDYQDSSSLPVGVFVWDVENEGDETLDVSIITFSMRNGLGGEDDAAGSLWNE 299
    
```

300 **PFRLEQGGTTVQGLLLHHPTPPNPYTMVAARCTADTTVTHTTAFDPNGTGQQVWQDL**LQ**** 359
Peptide 2
360 **DGQLDSPAGQSTPTQKGEGIAGAVCVSSKLLPRSRCCLEFSLAWDMPKIMFGAKSQVHYR** 419
420 **RYTRFFGSDGDVAPALSHYALCHYADWEDRISAWQNPVLDDDRTLPAWYKSALFNELYFLA** 479
Peptide 3
480 **DGGTVWLEVPADSLPEGLGGSMRQL**RSTLQDYGRFGYLEGQEYRMNTYD**VHIFYASFALV** 539
540 MLWPKLELSLQYDMALATLKEDLTRRRYLMSGVVAPVKRRNVI PHDIGDPDDEPWLRVNA 599
600 YLIHDTADWKDLNLKFVLQIYRDYYLTGDQGFLEDMWPVCLAVMESEMKFDDKQDGLIEN 659
660 GGYADQTYDAWVTTGPSAYCGGLWLAAVAVMVQMAVLCGAQDVQERFASILCRGREAYER 719
Peptide 4
720 **LLWNGRYNYDSSSH**PQRS**IMS**DQC**AGQWFLRACGLGEGDTEVFPTLHVVRALQTIFEL 779
780 NVQAFAGGAMGAVNGMHPHGV PDRSSVQSDEVWVG VVYGLAATMIQEGLTWEGFRTAEGC 839
840 YRTVWERLGLAFQTPEAYCQQQVFRSLAYMRPLSIWAMQLALQQQQHKKSRRPSVTQGTG 899
900 LSTQPECGPKRSLANLNSE 918**

Figure 25. Mouse GBA2 protein-sequence with epitopes for the generation of antibodies indicated. The four peptides that were used to generate monoclonal antibodies are indicated in *red* and the epitope used to generate a polyclonal antibody is indicated in black.

I consider myself fortunate to have received the unmatched guidance of Dr. Dagmar Wachten throughout my doctoral work. Among many things she has helped in shaping the way I think about science and also life in general. Moreover, her patience and thoughtfulness will never be forgotten. She also helped me immensely with writing. I cannot thank her enough for all the support.

I would like to thank Prof. U. Benjamin Kaupp for giving me the opportunity to work in this group. He has been a source of inspiration. I also thank Prof. Dr. Frank Bradke and Prof. Dr. Christoph Thiele for their early inputs into my project.

I would like to thank all my past and present colleagues from caesar for the pleasure and experience of having worked with them. I have had a good time with the members of our close-knit Minerva research group - Sophie Schonauer, Jens Henning Krause, and Hussein Hamzeh. I am thankful for their help with experiments for the paper and also for a good laugh! A very special thanks to David-Leon for the invaluable support and my friends from the MNS group Fabio, Shatanik, Vera, David, Meggie, and others for their much appreciated help and a good time; and Kevin Flynn for introducing me into the interesting aspects of live imaging of the cytoskeleton. I thank Kathie Mauel and Daniella Müller for their indispensable help with cell culture. I also thank Heike Krause and Anja Reike (in the initial months) for taking care of the administrative details.

I also thank the Sonderforschungsbereich (SFB-645) of the Deutsche Forschungsgemeinschaft for funding.

I am deeply grateful to my family. I could not have made it without their support.

Name: Diana Nancy Raju

Date of Birth: March 25, 1986

Address: Kölnstraße 57, 53111 Bonn, Germany

Nationality: Indian

Email: diana.raju@caesar.de

Education:

1992 – 2002	High School, St. Francis Xavier's Girls High School, Bangalore, India.
2002 - 2004	Pre-University education: Mount Carmel College, Bangalore, India.
2004 – 2007	Bachelor in Science, Mount Carmel College, Bangalore, India.
2007 – 2009	Master of Science (Biotechnology), Mount Carmel College, Bangalore, India.
2009 – 2010	Research assistant, Indian Institute of Science, Bangalore, India.
2011 – present	PhD student, centre for advanced european studies and research (caesar), Bonn, Germany.

Publications:

Heinz G. Körschen, Yildiz Yildiz, **Diana Nancy Raju**, Sophie Schonauer, Wolfgang Bönigk, Vera Jansen, Elisabeth Kremmer, U. Benjamin Kaupp, and Dagmar Wachten. *The non-lysosomal beta-glucosidase GBA2 is a non-integral membrane-associated protein at the endoplasmic reticulum (ER) and Golgi.* Journal of Biological Chemistry, 2013. 288(5): p. 3381-93.

Diana Nancy Raju, Sophie Schonauer, Hussein Hamzeh, Kevin C. Flynn, Frank Bradke, Katharina vom Dorp, Peter Dörmann, Yildiz Yildiz, Christain Trötschel, Ansgar Poetsch, Bernadette Breiden, Konrad Sandhoff, Heinz G. Körschen, Dagmar Wachten. *Accumulation of GlcCer in the absence of the beta-glucosidase GBA2 alters cytoskeletal dynamics*. PLOS Genetics.